THE INFLUENCE OF NONSTRUCTURAL PARTITIONS ON THE STATIC AND DYNAMIC BEHAVIOR OF BUILDINGS

by

Ayoub Farahyar

Project submitted to the Faculty of the

Virginia Polytechnic Institute and State University

in partial fulfillment of the requirements for the degree of

MASTER OF ENGINEERING

in

Civil Engineering

APPROVED:

A. E. Somers, Chairman

R. M. Barker

T. Kuppusamy

May, 1983

Blacksburg, Virginia

ACKNOWLEDGMENTS

This is to gratefully acknowledge the help and support of the many individuals in the Civil Engineering Department and Engineering Science Mechanics who assisted me in my graduate studies. I especially thank Dr. Richard (S.U.N.Y. at Buffalo) for his initial inspiration which influenced my decision to continue the graduate work. Also, I thank Dr. Heller and Dr. Walker for their support and guidance during my studies. My special thanks goes to Dr. Somers for his help and ideas during the writing of this project.

TABLE OF CONTENTS

Chapter 1

INTRODUCTION

1.1 Introduction

The walls of buildings may be part of the structure or they may be purely for architectural effect, nonstructural in nature. Nonstructural walls are called filler walls or partitions. The term, nonstructural partition, is something of a misnomer because all partitions have some structural properties, i.e., stiffness and energy dissipation capacity. Traditionally, the term nonstructural partition has been used to imply that the integrity of the structure does not depend upon its strength. Any strength realized by the partition is considered an added margin of safety to the structure.

In static analysis, it is conventional to ignore the effect of nonstructural partitions. However, partition stiffnesses have considerable influence on lateral response of the structure and alter the respective bare frame natural periods, natural mode shapes, and viscous damping ratios. Also, the investigation of high rise buildings and the tests of full scale structures have shown that the presence of filler walls and partitions change the critical point. Thus, certain critical sections may be inadvertently neglected in the design of the structure, indicating that partitions should be considered in the analyses for lateral load.

One particular analysis problem is the discontinuity that occurs between the wall and frame resulting from low strength of grout, prior

motion of the building due to wind or ground motions, and poor construction techniques. The presence of gaps have a significant effect on the lateral response of the structure. With small displacements, the gaps are open and the frame does not contact the walls. Consequently the structure behaves as a relatively flexible frame structure. However, as the displacements increase sufficiently, the gaps will begin to close and the structure will become stiffer.

A linear elastic analysis should be used if the frame and filler wall are monolithic (no gaps between the frame and wall) or the gaps are sufficiently large so that the frame and panels do not contact. However, if gaps exist and displacement is sufficient to open and close the gaps, then the structure should be analyzed by nonlinear elastic techniques that account for the opening and closing of gaps.

1.2 Objective

This study considers the influence of nonstructural partitions on the overall response characteristics of the struture, namely the natural periods, natural mode shapes, viscous damping ratios, and lateral stiffness. The prime objective of this study is to review the correlation of analyses and experiments that have been done in order to demonstrate the degree to which the analytical solutions reproduce behavior as determined from tests, and to review and verify the assumptions which were necessary in the formulation of the analytical scheme.

It has been observed that the bare frame deflections, periods, and damping ratios are not constant, but vary significantly with age

and vibration history. Therefore, it is necessary to discuss and review in depth the properties and theoretical modeling for the bare frame.

The types of partitions in this study are:

- Gypsum board on metal studs,
- Plywood on wooden studs,
- Unreinforced hollow concrete block,
- Unreinforced masonry.

1.3 Theoretical Modeling of Bare Frames

All bare frame mathematical models considered in this study are based on the following assumptions. First, only two dimensional models have been considered. This assumption implies that there is no coupling between motions in two principal horizontal directions and that these two motions may be treated independently. For symmetric structures, this does not introduce errors. However, for asymmetric structures, torsional coupling may cause the actual response to differ greatly from the predicted response, warranting the use of a three-dimensional model.

The second assumption is that the floor diaphrams are rigid in their own planes. It is also assumed that base is fixed. However, in some cases consideration of the flexibility of the foundation material may significantly affect the predicted structural response. Specifically, the elasticity of the foundation must be considered when the relative stiffness of the structure is larger than the stiffness of the foundation. Also, the mass of a structure is assumed to be

concentrated at the floor levels.

A number of other physically rational assumptions can be made which may significantly affect the response of structure.

1.4 Previous Investigations

This is a brief discussion of previous investigations in the general subject area of this project. This discussion is directed towards rectangular building frame, as contrasted with general three-dimensional frames.

1.4.1 Frame with Filler Walls

The importance of the influence of filler walls on response is generally recognized, and has been pointed out by several authors [2,18,31,32]. Various approaches have been used to model the effects of filler walls on the frame; one such approach is the equivalent brace or strut method [18,31,32]. In this method, the wall is replaced by a diagonal strut in the frame. Formulae based partly on test data and partly on analytical studies to determine the stiffness of the equivalent strut have been presented by Smith [31].

Details of tests of eight scale models of reinforced concrete frames with filler walls were presented by Fiorato, Sozen, and Gamble [12]. These authors also presented their knee-braced frame model for the analyses of these frames. In this model, after initial cracking, the partition is assumed to act as a knee brace on the frame.

The development of the finite element method has had a considerable impact on the field of structural engineering, and a logical application of the method is to model the effect of filler walls on

the response of building frames.

The application of the finite element method to the analysis of infilled frames has been briefly discussed by Karamanski [21]. His work was intended primarily to state the ideas of the finite element rather than to propose assumptions for the analysis of infilled frames. He assumed that the frame elements carry only axial forces and are flexible in a direction perpendicular to the frame axis, that the tie between the frame and wall is not distributed, and that the frame and infill wall are of a fully elastic material.

Lamar and Fortoul [23] have shown that filler walls have a significant influence on the mode shapes of the framed structure when the structural system is assumed to be linearly elastic.

Natarajan and Wen [26] described static and dynamic analyses of frames with filler walls. The nonlinearity of the frame members was taken into account by assuming an elastic-perfectly plastic moment-curvature relationship. The wall elements were rectangular. An initial crack was assumed to occur in the wall when principal tensile stress exceeded a prescribed value. After initial cracking, the stiffness characteristics of the wall element were computed based on a reduced modulus.

Kost [22] developed an analytical model and computer program to perform nonlinear analyses of a plane frame with filler panels. The source of nonlinearity was the presence of gaps between the sides and tops of the panels and the frame. He also developed a program for the analysis of a plane frame with monolithic panels, that is, no gaps.

1.4.2 Properties of Filler Walls

Several authors have reported on testing to determine the properties of filler walls. The material of these walls can be concrete block, brick masonry, clay tile, plywood, gypsum wall board, or plaster. The tests reported in the literature are generally static tests with load increasing monotonically up to the failure of panel. Cyclic tests are generally not available except for certain of the above material categories.

Report of 27 tests of reinforced concrete frames with masonry filler walls were presented by Fiorato, Sozen, and Gamble [12]. These tests also were static tests with monotonically increasing lateral loads applied to the structures. These authors observed that when cracks form in the filler walls, they usually follow paths through the mortar joints of the masonry. The cracks can be idealized as occurring in the columns in which there are tensile forces, between the frame and wall in the regions of tensile stress, and roughly diagonally across the frame. Because of the loading schemes, no data are available from these tests regarding the cyclic nature of the load-deflection curves.

A testing program to determine the threshold of damage to partitions due to relative story displacements and to determine force-deformation characteristics has been performed by Blume [4,5], and Freeman [14]. These reports describe cyclic load tests of partitions constructed of wood or metal studs and faced with gypsum board. These tests generally consisted of five cycles of 1/32-inch displacement, followed by five cycles of 1/16-inch displacement, etc.

The displacement was progressively increased until a maximum of 1-1/4 inch was achieved. During the tests, it was generally observed that the first noise was heard at about 1/16 to 1/4 inch displacement, louder noise and popping sounds were heard at 1/4 to 3/4 inch displacement, first noticeable damage occurred at 1/16 to 1/2 inch displacement, adn substantial damage occurred at and above 1/2 inch displacement.

1.4.3 Experimental Data from Tests of Full Scale Structures

The experimental data in this study is obtained from reinforced concrete, four-story test structures located at the Nevada Atomic Energy Test Site [29], and tests of full sized reinforced concrete frames from the University of Illinois [12]. Detailed descriptions of these test structures and the experimental data used in this study are presented in the next chapters.

Chapter 2

STATIC ANALYSIS OF LINEAR ELASTIC STRUCTURE

2.1 Introduction

This chapter deals with the static analysis of linearly elastic structures, that is, frames with monolithic filler panel and without gaps. This classification includes those partitions which are mechanically fastened to the frame. For these it is assumed that the motions of the frame equal the partition motions everywhere on the boundary between frame and partition. Typical partitions of this type include gypsum board, plaster, plywood partitions, and unreinforced masonry with gaps.

The static analysis of linearly elastic frame structures has been well documented in numerous papers, texts, and reports [8,9,16,25], and will not be discussed in detail.

2.2 Frames with Filler Walls

There has been a considerable amount of research, both analytical and experimental, done on the behavior of frames with filler walls.

Benjamin and Williams [2] studied the behavior of full-scale infilled frames. Both steel and reinforced concrete were used in combination with either reinforced concrete or masonry filler walls. Brick walls without a bounding frame were also tested. They gave tentative formulas for predicting the stiffness and ultimate strength of infilled frames. They concluded that any exact mathematical analysis of the problem was superfluous, considering the statistical

nature of concrete, and, consequently, based their stiffness prediction on a strength of materials approach. The panel was considered as a cantilever and, therefore, its shearing and bending properties were involved.

Thomas (33) described the results of a number of tests on brick walls and piers. Included were racking tests of one-story infilled frames. The specimens were made up of concrete encased steel frames with and without masonry filler walls. Only measured load-deflection results were reported. However, these curves indicated the influence of the frame-wall interaction.

Fiorato, Sozen, and Gamble [12] performed full scale tests on 26 structural models of reinforced concrete with masonry filler walls. The controlled variables included in the experimental program were height (or number of stories); number of bays; amount, quality, and arrangement of the frame reinforcement; magnitude of vertical load applied to the columns; and size, shape, and location of wall openings. Details of these structures are shown in Figs. 2.1 and 2.2. They are summarized in this study because they provide explicit evidence of frame-wall interaction in actual structures.

Fedorkiw [11] and Sozen developed a discrete physical model for analysis of reinforced concrete frame with masonry fillers. The entire analytical procedure has been programmed for solution by digital computer, and yields crack formation and load deflection response up to ultimate load. They are also used in this study to determine the influence of nonstructural-partitions on the structural response of buildings.

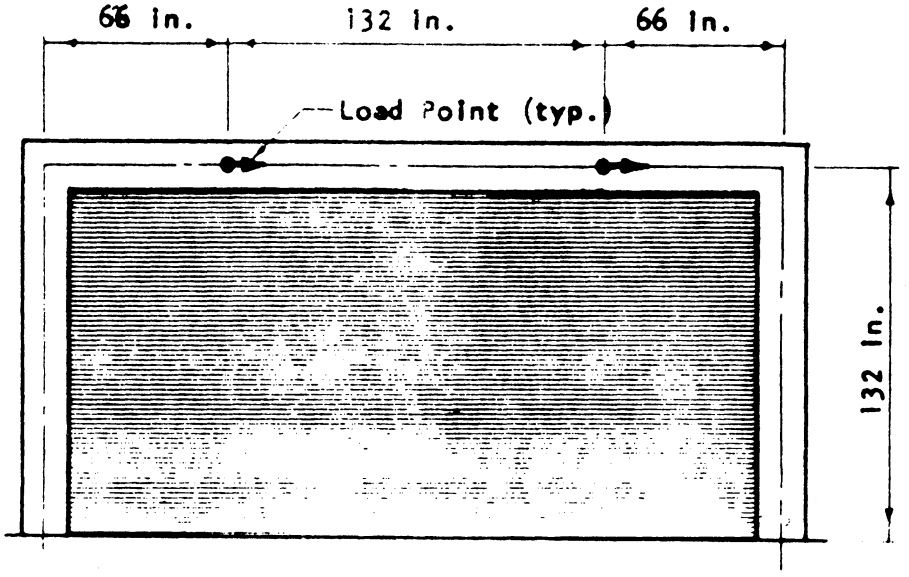

FIGURE 2.1 THE ONE-STORY STRUCTURE [Ref. No. 12]

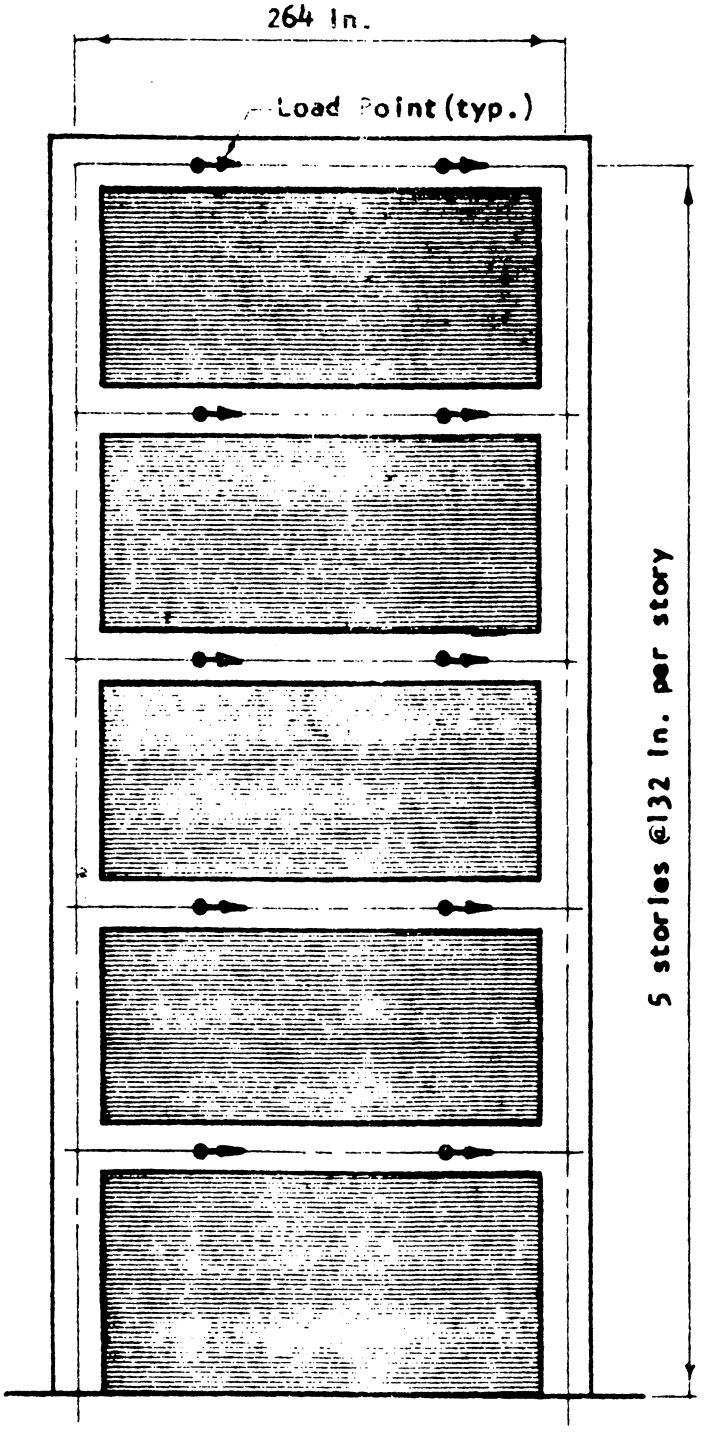

FIGURE 2.2 THE FIVE-STORY STRUCTURE
[Ref. No. 12]

2.3 Response and Assumed Basic Loading Conditions

The structure shown in Fig. 2.3 represents the system assumed as a basic unit for discussion of frame-wall composite. The moment, shear, and axial load may be caused by direct applied force or force transmitted from other parts of the structure.

Figure 2.4 shows the deflected shape of the frame alone, and wall alone subjected to lateral load. If the wall is flexible and the frame is stiff, the distorted shape of composite frame-wall approaches that of the frame alone. If the wall is stiff and the frame relatively flexible, the distorted shape approaches that of the wall alone. With frame and wall both in contact, both elements participate in transmitting the loads through the structure. An estimated amount of total shear distributed between the frame and wall can be obtained by considering the relative stiffnesses of the frame and wall.

Horizontal loads applied to the beam require shear and bending moment to be resisted by frame and partition across the base of the structure. The base shear is distributed between frame and filler. For the case of an unfilled frame, the frame alone must resist the total applied shear.

The flexural stiffness of a column with both ends fixed is

$$V_{col} = \frac{12E_c I_{col} a}{\ell_{col}^3} \qquad (2.1)$$

E_c = modulus of elasticity of concrete

I_c = moment inertia of uncracked transformed column cross section

a = deflection of column

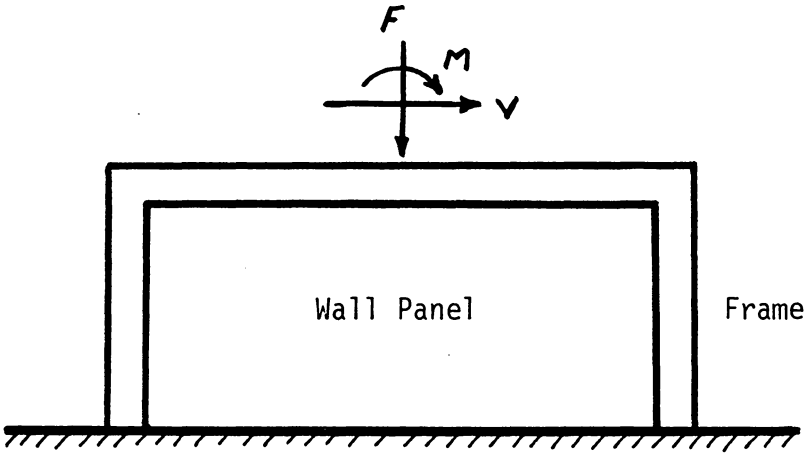

Figure 2.3 Frame Wall System

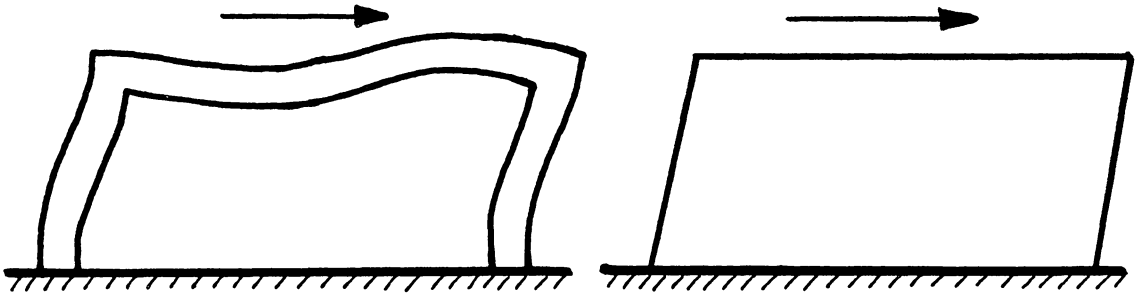

a) Frame Only b) Wall Only

Figure 2.4 Distorted Shape of Frame and Wall

ℓ_c = clear height of column

V_{col} = shear force in column

If it is assumed a value of 3.6×10^6 psi for the modulus of elasticity of the concrete frame, for a unit deflection, the total shear force in both columns (Fig. 2.1) is 190 kips. The shear stiffness of the wall alone can be represented as

$$V_w = \frac{A_w G_w a}{K \ell_w} \tag{2.2}$$

A_w = cross sectional area of the wall

G_w = shearing modulus of the wall material

a = deflection of the wall

ℓ_w = height of wall

K = coefficient dependent on the shape of cross section (the value of K was taken as unit assuming shear distribution on the rectangular cross-sectional area of the wall)

V_w = shear force in the wall

For simplicity, the filler is assumed to be a linearly elastic isotropic medium. This simplification for the behavior of a masonry type filler may be justified in the view of the nature of the desired results, where the determination of the overall structural behavior is of prime importance.

A shear force of 8400 kips is required to give a unit deflection of masonry wall, assuming a shearing modulus of 0.6×10^6 psi for the masonry wall. The distribution of total shear force in the frame-wall composite is estimated to be approximately 18% in the frame, and 82%

in the masonry wall. Table 2.1 shows the distribution of total shear force in the frame and different partitions (Poisson's ratio assumed to be zero).

Table 2.1 The distribution of total shear force in the frame and different partitions.

Partition Type	Partition Shearing Stiffness (psi)	Partition Elastic Modulus (psi)	Percent of Total Shear Carried by Frame	Percent of Total Shear Carried by Partition
Gypsum board	14500	29000	91	9
Plywood	15000	30000	90	10
Masonry	600000	1200000	18	82
Concrete block	968333	1936666	13	87

Fedorkiw [11] reported distributions of total shears from 0 to 95 percent in the wall depending on the modulus of elasticity for the filler wall. Figure 2.5, reproduced from Fedorkiw's report, shows the variation in the base shear distribution with the modulus of elasticity of the filler. It was assumed that the wall was isotropic and linearly elastic with Poisson's ratio equal to zero.

The resisting moment at the base of the structure consists of three components, base moment in the columns, the couple provided by axial loads in the column, and the resultant couple due to forces normal to the base of filler. Figure 2.6 reproduced from Fedorkiw's report, shows the relative values of these three components expressed

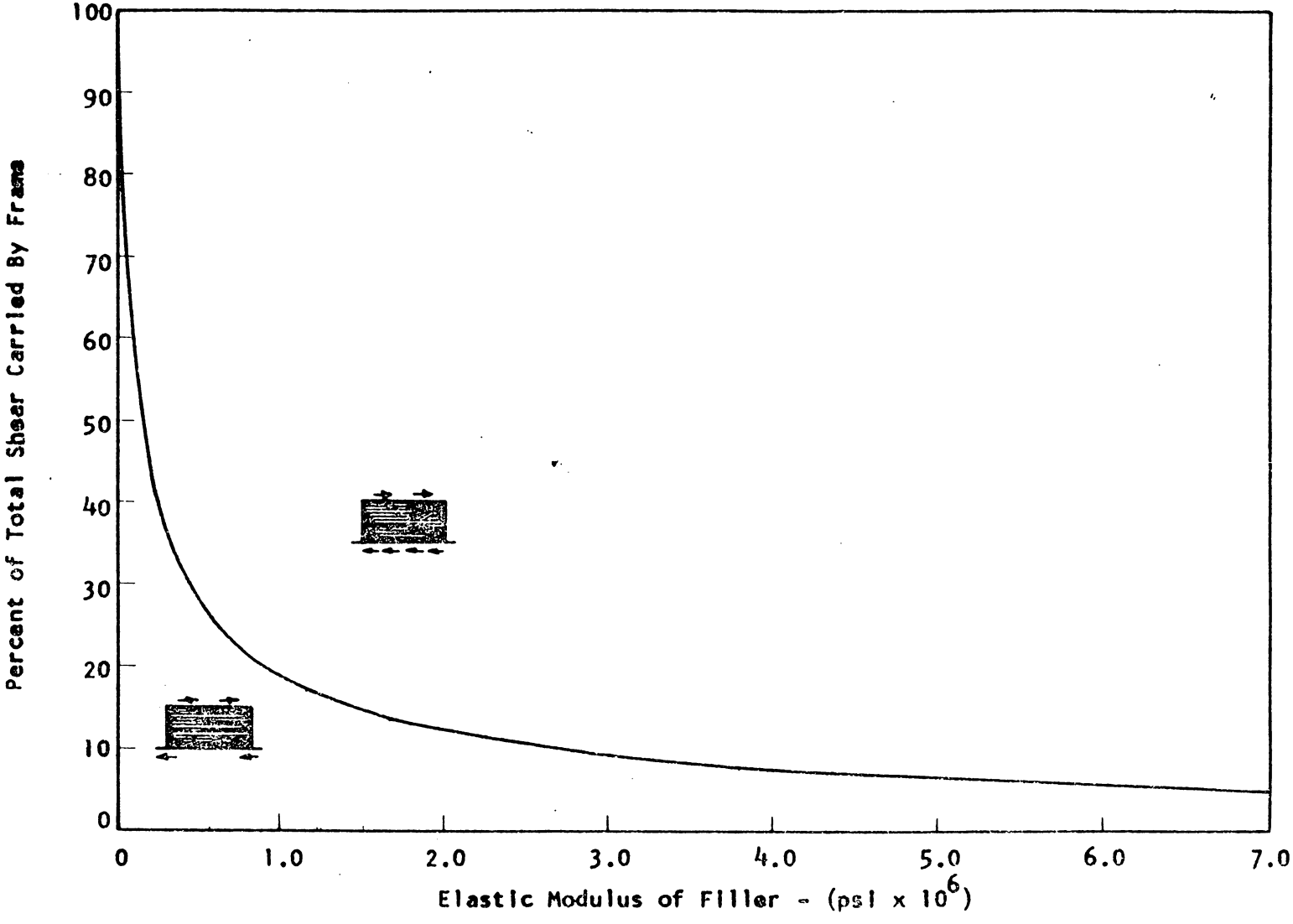

FIGURE 2.5 DISTRIBUTION OF BASE SHEAR BETWEEN FRAME AND FILLER, SINGLE-STORY STRUCTURE [Ref. No. 11]

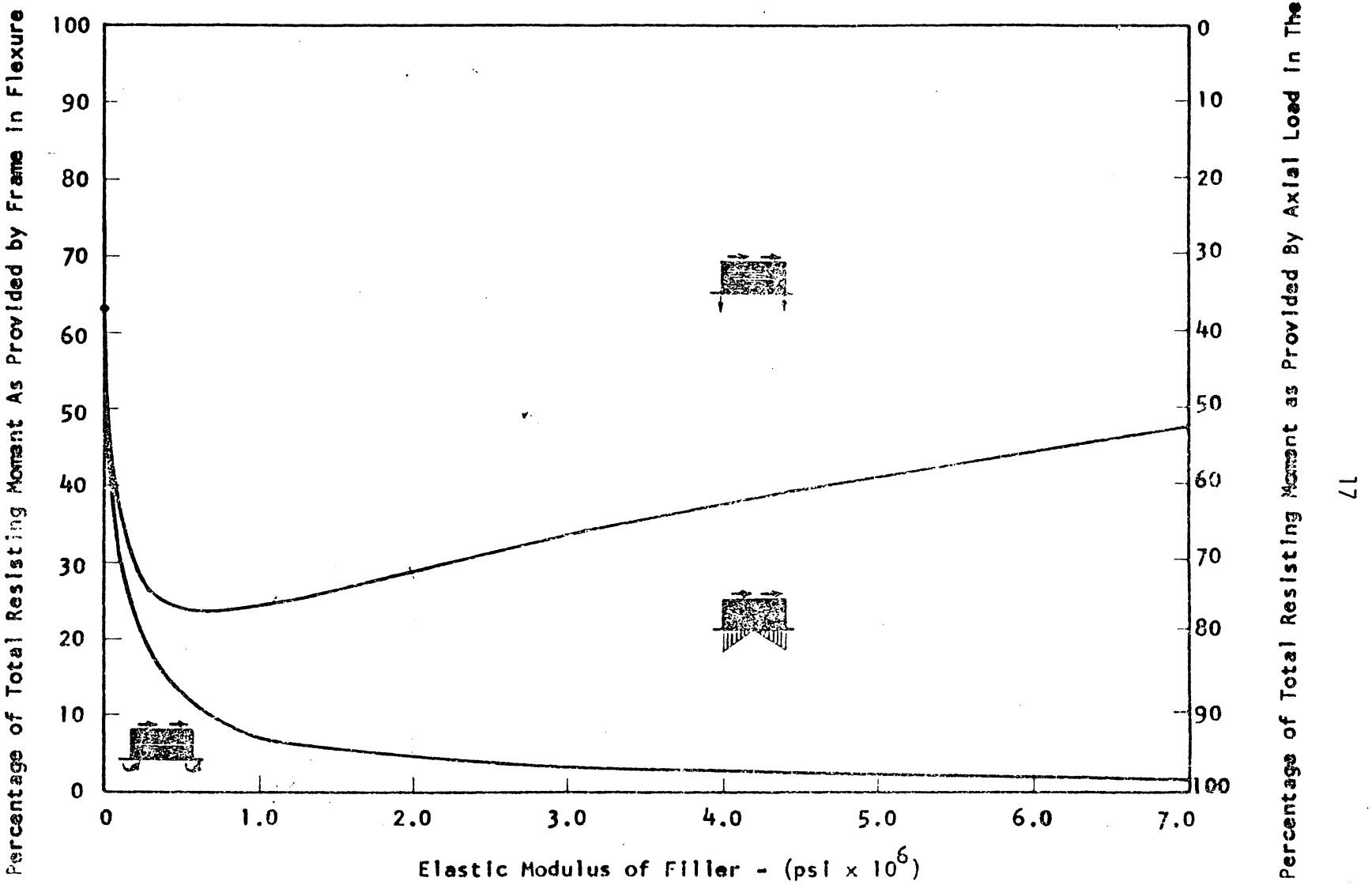

FIGURE 2.6 DISTRIBUTION OF RESISTING MOMENT IN THE BASE OF THE SINGLE-STORY STRUCTURE [Ref. No. 11]

as percentage of the total resisting moment. The figure is divided by two curves into three areas which correspond to the three components. The lower curve representing base moment in the columns is plotted with respect to the left side ordinate scale, whereas the upper curve, which represents the resisting couple from axial load in the columns, is plotted for the right side ordinate scale. The central region between the two curves thus represents the resisting moment as provided by normal force in the filler. For a given value of filler modulus, the ordinates to the curves define the contribution of three components in resisting the overturning moment. This mechanism and behavior is dependent on the relative frame-wall stiffness. For an unfilled frame, the resisting moment is provided by the combination of column base moments and the axial load couple. Figure 2.6 shows that base moment accounts for 63 percent of the total resisting moment. For values of filler modulus increasing from zero to 1,000,000 psi, the contribution of base moments decreases rapidly and continued to decrease for values above 1,000,000 psi but at a lower rate. The axial-load couple increased rapidly for low values of filler modulus and attained the maximum at approximately 600,000 psi. The resisting moment in the filler increased rapidly for values below 1,000,000 psi and thereafter continued to increase at a constant rate. In general, the effect of introducing a filler into a single-story structure served to suppress the flexural behavior of the frame and to increase the axial force in the columns. Except for the very low values of filler modulus, the resisting moment in the frame was mainly provided by axial load component.

The lateral deflection of the frame-wall structure is due to flexural distortion and shearing distortion which are dependent on the geometrical and material properties of the frame and wall. The lateral deflection at mid-height of top beam for one story structure can be calculated using this expression

$$a = \frac{V \ell_c^3}{3EI} + \frac{K V \ell_w}{A_w G_w} \qquad (2.3)$$

a = lateral deflection of the structure at the mid-height of top beam

V = total shear force on the structure

ℓ_c = distance from top of base beam to mid-height

E = modulus of elasticity of the frame-wall composite material

I = moment of inertia of the total frame-wall cross section

K = coefficient dependent on the shape of the cross section (the value was taken as unity assuming a uniform shear distribution on the rectangular cross-sectional area of the wall)

ℓ_w = height of wall

A_w = cross-sectional area of the wall

G_w = shearing modulus of the wall material

The first term in Eq. (2.3) represents the deflection due to bending distortion. It is assumed that total frame-wall cross section participates in resisting the applied bending. The second term represents the deflection due to shearing distortion. It is assumed that the wall alone resists the applied shear.

Figure 2.7, reproduced from Fedorkiw's report, shows the variation of deflection with respect to modulus of elasticity of the filler wall.

Figure 2.8 is reproduced from Fiarato, Sozen, and Gamble's report [12]. It shows the comparison between experimental results and the calculated deflection of a single story reinforced concrete structure with masonry partitions.

2.4 The Effect of Number of Stories

The basic difference between multi-story infilled frame and single story infilled frame, is the loading condition. The moment, shear, and axial load is transmitted from the upper stories. The change which the additional moment causes in the initial response of the single-story frame-wall are indicated by the lateral deflection of the system.

The lateral deflection of the first story of multi-story infilled frames is

$$a_1 = \frac{V \ell_c^3}{3EI} + \frac{K V_w}{A_w G_w} + \frac{M_1 \ell_c^2}{2EI} \qquad (2.4)$$

a_1 = lateral deflection of the structure at first story

V = total shear force on the structure

ℓ_c = distance from top of base beam to mid-height of first story beam

E = modulus of elasticity of the frame-wall composite material

I = moment of inertia of the total frame-wall cross section

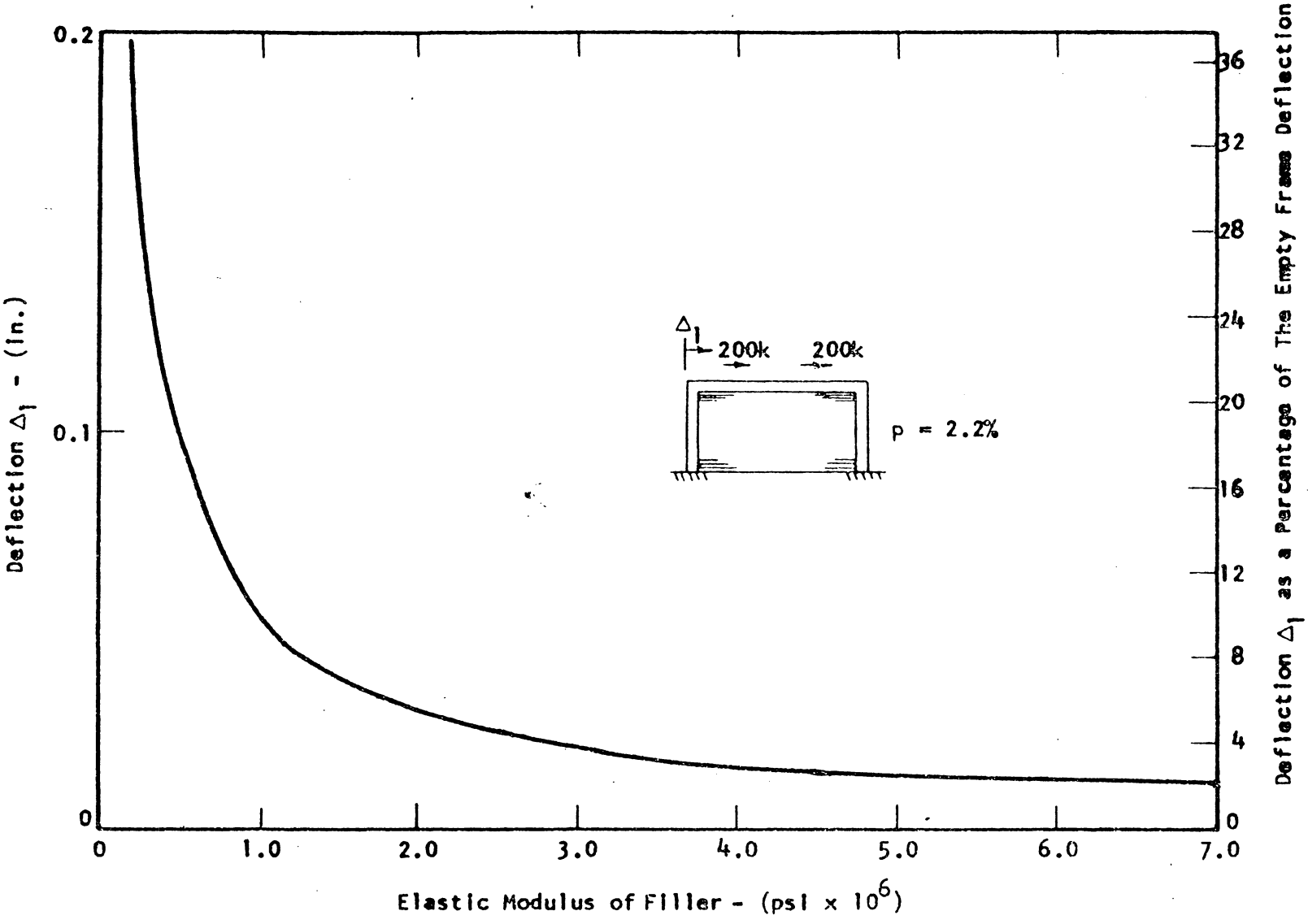

FIGURE 2.7 VARIATION OF DEFLECTION Δ_1 WITH ELASTIC MODULUS OF FILLER [Ref. No. 11]

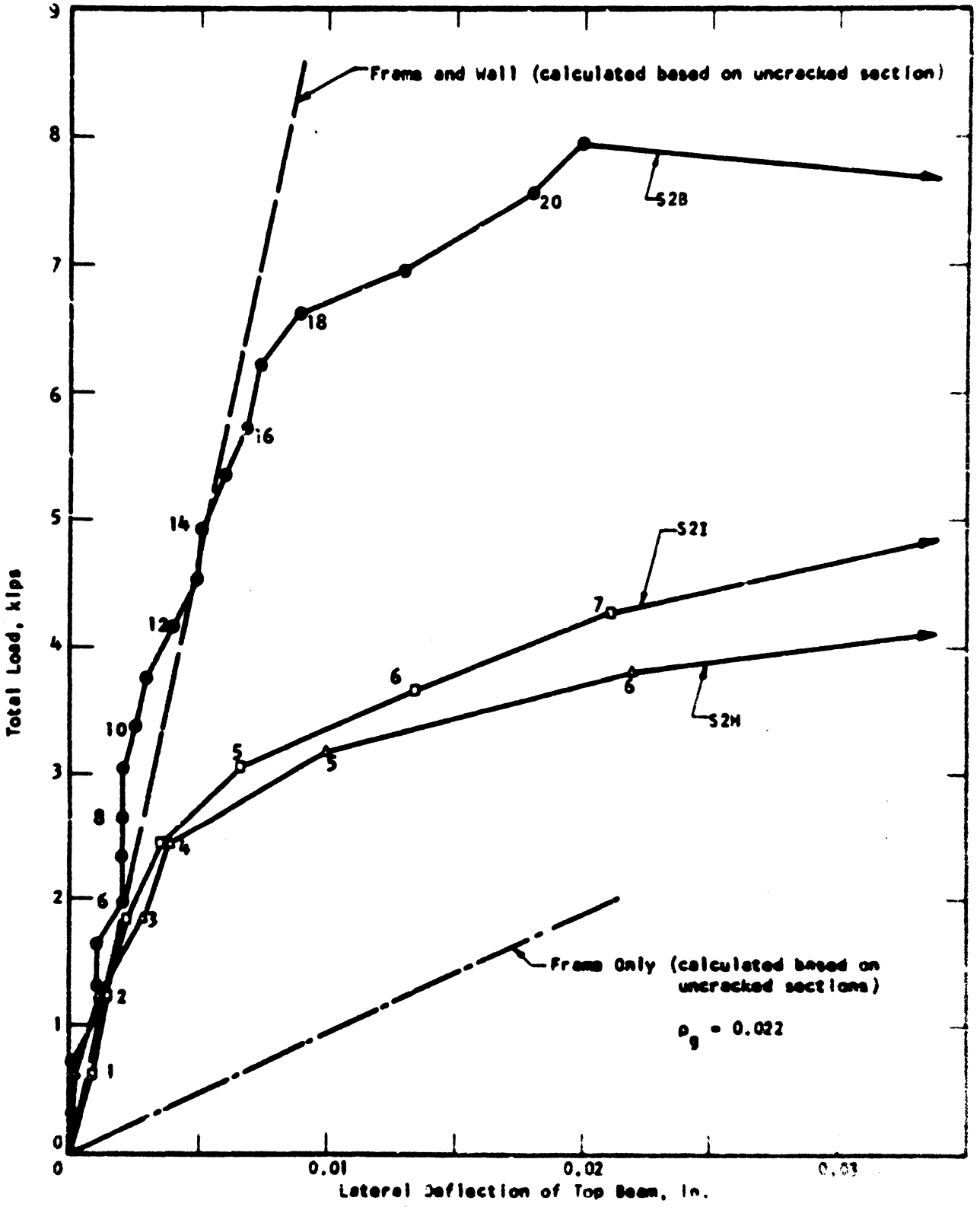

FIGURE 2.8 INITIAL RESPONSE OF SINGLE-STORY SPECIMENS S2B, S2M, AND S2I [Ref. No. 12].

M_1 = moment on the structure at the level of first story beam

K = coefficient dependent on the shape of the cross section (the value of K can be taken as unity assuming a uniform shear distribution on the rectangular cross sectional area of wall).

ℓ_w = height of the wall

A_w = cross sectional area of the wall

G_w = shearing modulus of the wall material

Except for the third term, Eq. (2.4) is identical to Eq. (2.3) used for single story specimens and the same assumptions apply. The third term represents the deflection due to flexural distortion caused by the moment transmitted from the upper stories. It is assumed that the total frame-wall complex resists the additional applied moment.

The calculated load-deflection relationship is shown in Fig. 2.9 (reproduced from Fiorato's report) along with the experimentally determined response for five story specimens with masonry filler in the initial range of loading. In the case of a five story frame filled with masonry, the flexural component represents 62 percent of total deflection at the fifth story but only 22 percent of the total at the first floor. In the multistory filler frame, the flexural distortion is significant at the upper story relative to the lower story.

2.5 Effect of Openings

The fundamental influence of openings on the frame-wall system is to decrease the amount of wall area resisting the loads on the

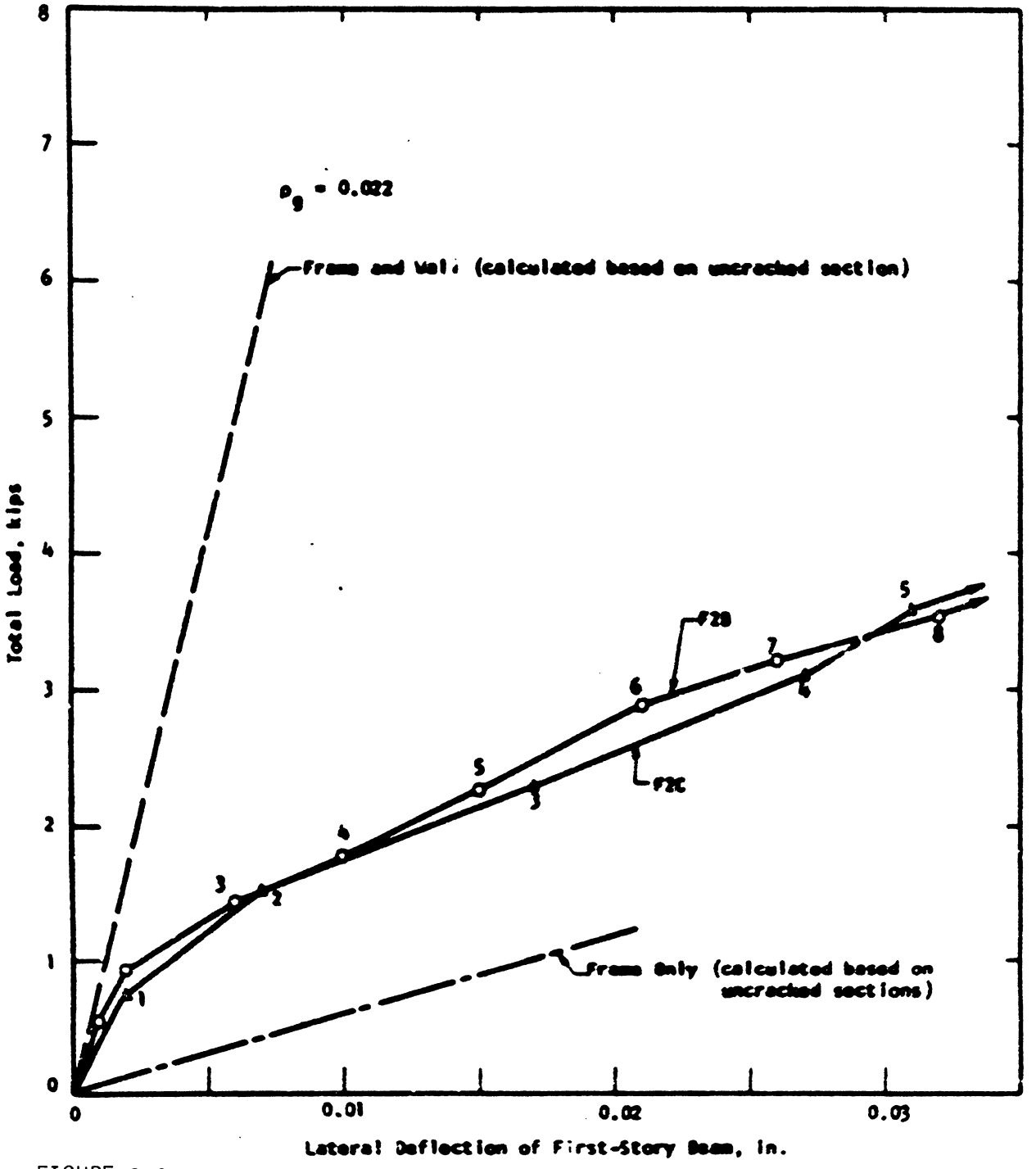

FIGURE 2.9 INITIAL RESPONSE OF FIVE-STORY SPECIMENS F2B AND F2C, FIRST-STORY BEAM DEFLECTION [Ref. No. 12]

system. The frame wall structure with openings should be more flexible than the system with openings. The effect of opening on the initial response of the frame-wall composite is described below for the one-story, and five story one-bay test specimens. Five one-story reinforced concrete structures with masonry filler and various types of openings were tested by Fiorato. Figures 2.10 through 2.13 show the initial portion of the load-deflection curves which were recorded in tests of the one-story specimens with openings. Also shown in the figures are the calculated load-deflection relationships. The calculated relationships are based on Eq. (2.3) with modification to account for reduced wall area. In the first term of Eq. (2.3), representing the flexural distortion of specimen, the moment of inertia was reduced according to the size and location of the opening. Because the reduced moment of inertia represented approximately 93 percent of the total moment of inertia for most cases and since the flexural distortion represented only a small part of the total deflection (eight percent for a specimen with no openings), the reduced moment of inertia was assumed over the full height of the specimen. For the second term in Eq. (2.3), representing the shearing distortion of the wall, the wall area was reduced at the sections where the openings were located.

Fiorato [12] also tested two five-story specimens with openings. The specimens were subjected to a constant vertical load of 2.5 kips per column during testing. The total load plotted vs the lateral deflection measured at the first story beam are shown in Fig. 2.14 and Fig. 2.15 (reproduced from Fiorato's report). Equation (2.4) was used for the load-deflection calculations with modifications to account for

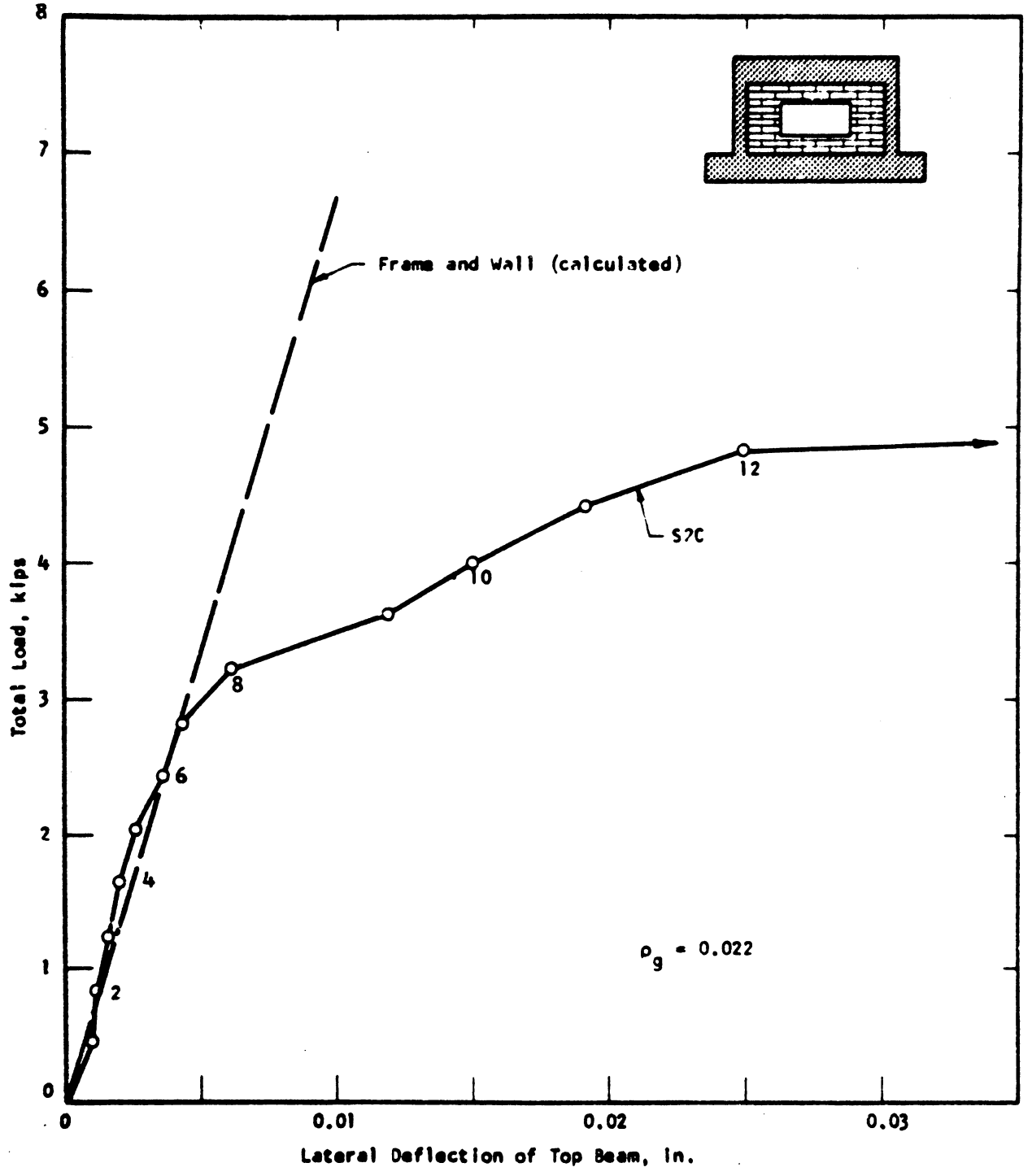

FIGURE 2.10 **INITIAL RESPONSE OF SINGLE-STORY SPECIMEN S2C** [Ref. No. 12]

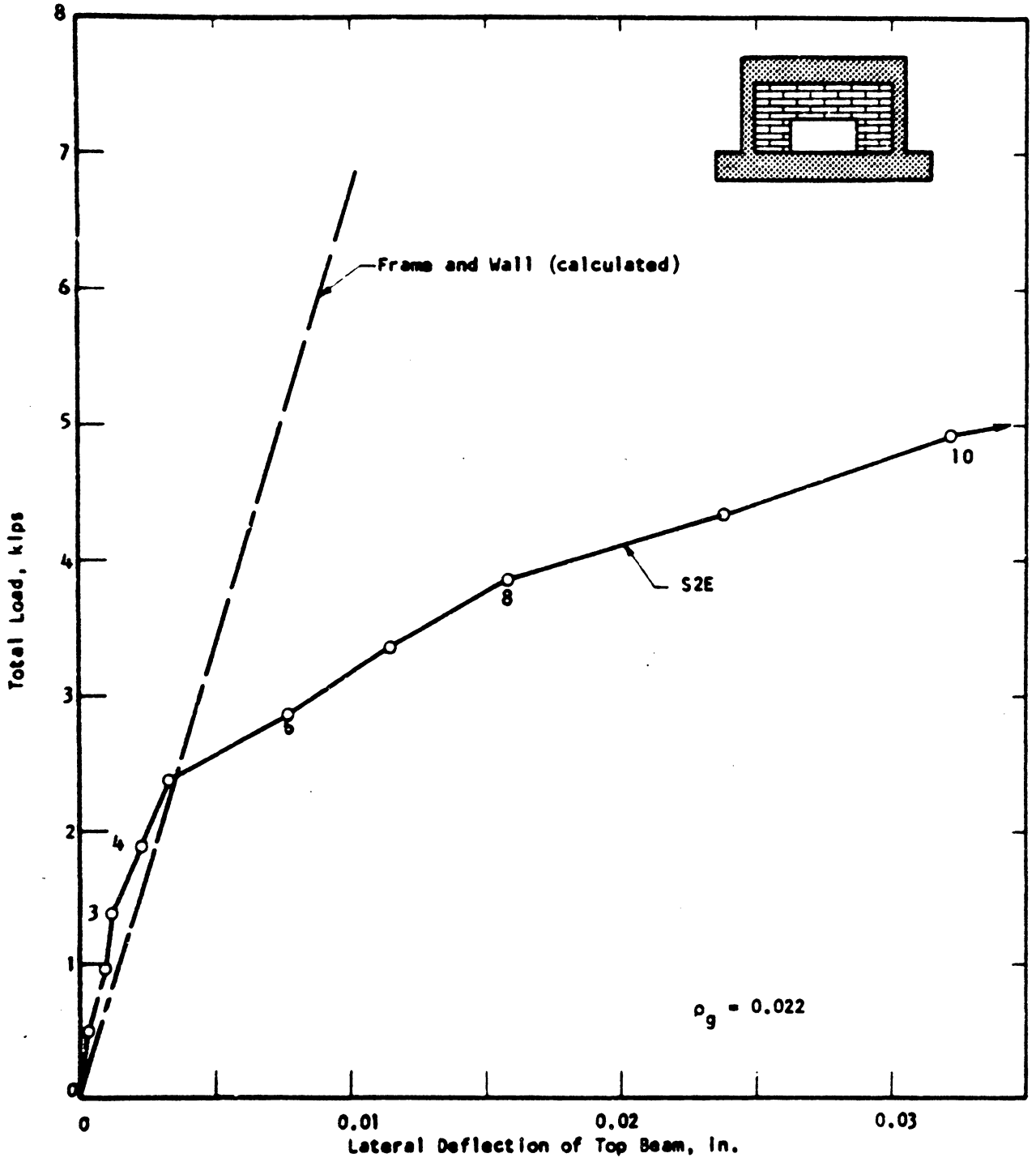

FIGURE 2.11 INITIAL RESPONSE OF SINGLE-STORY SPECIMEN S2E [Ref. No. 12]

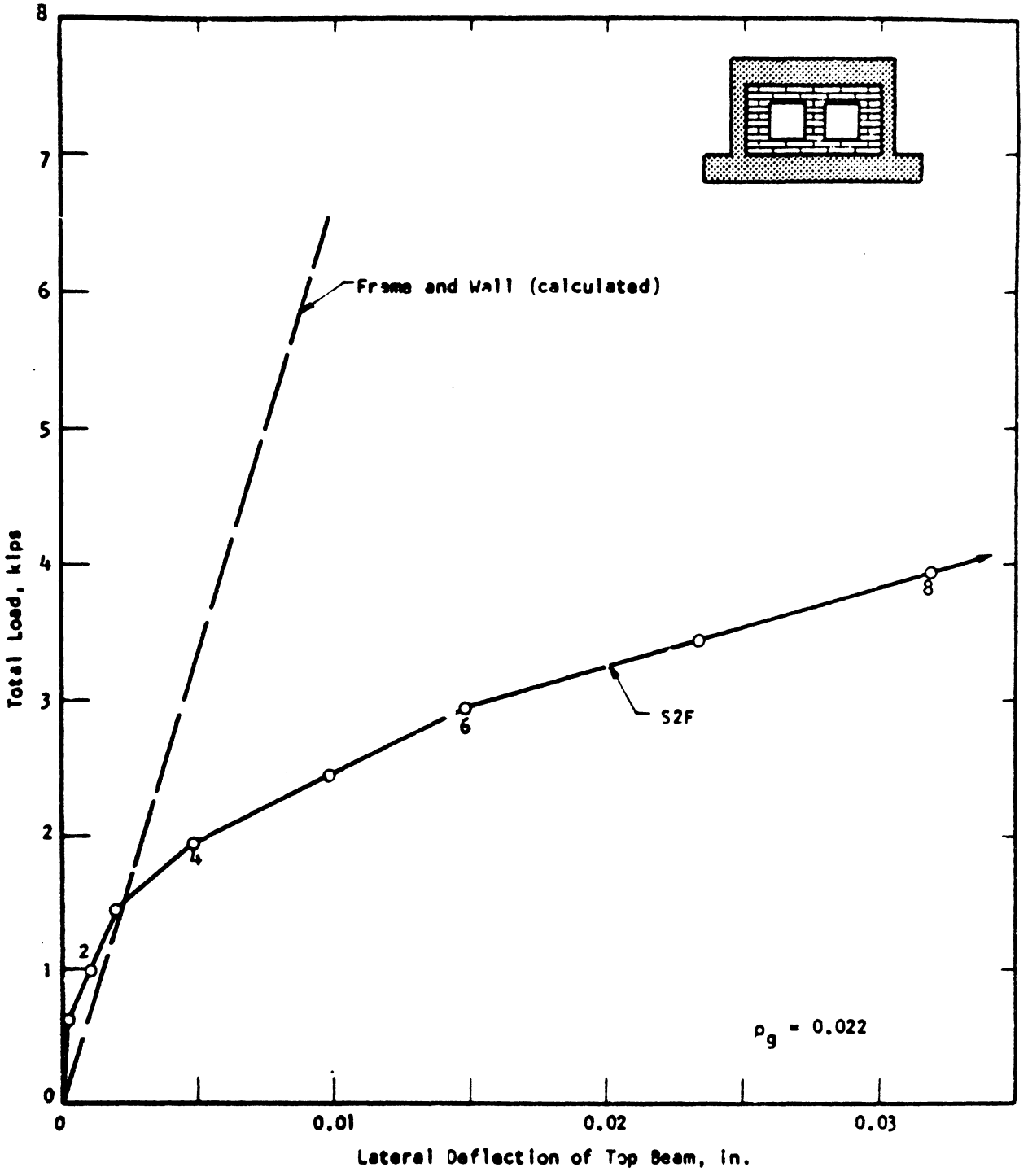

FIGURE 2.12 INITIAL RESPONSE OF SINGLE-STORY SPECIMEN S2F [Ref. No. 12]

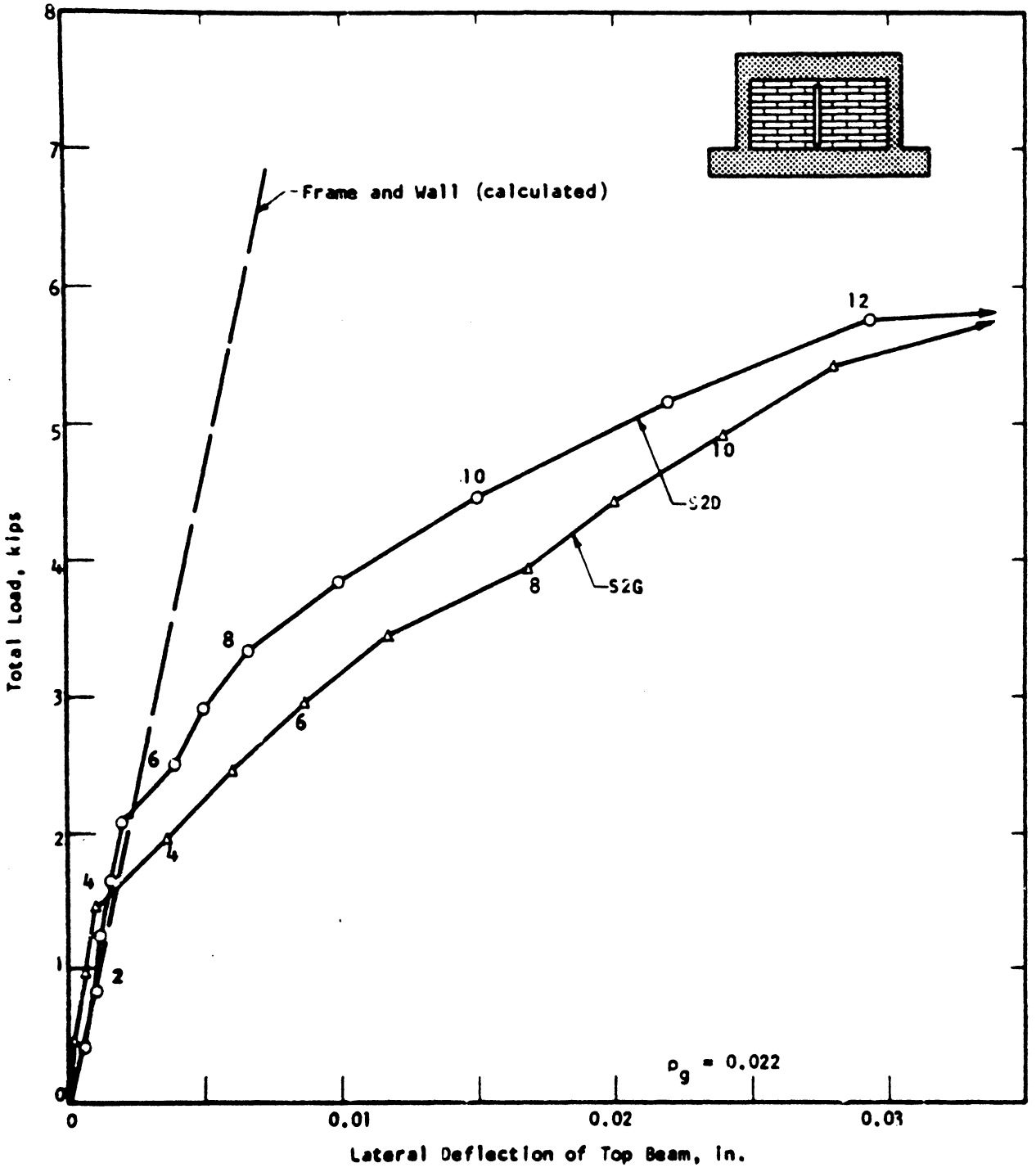

FIGURE 2.13 INITIAL RESPONSE OF SINGLE-STORY SPECIMENS S2D AND S2G [Ref. No. 12]

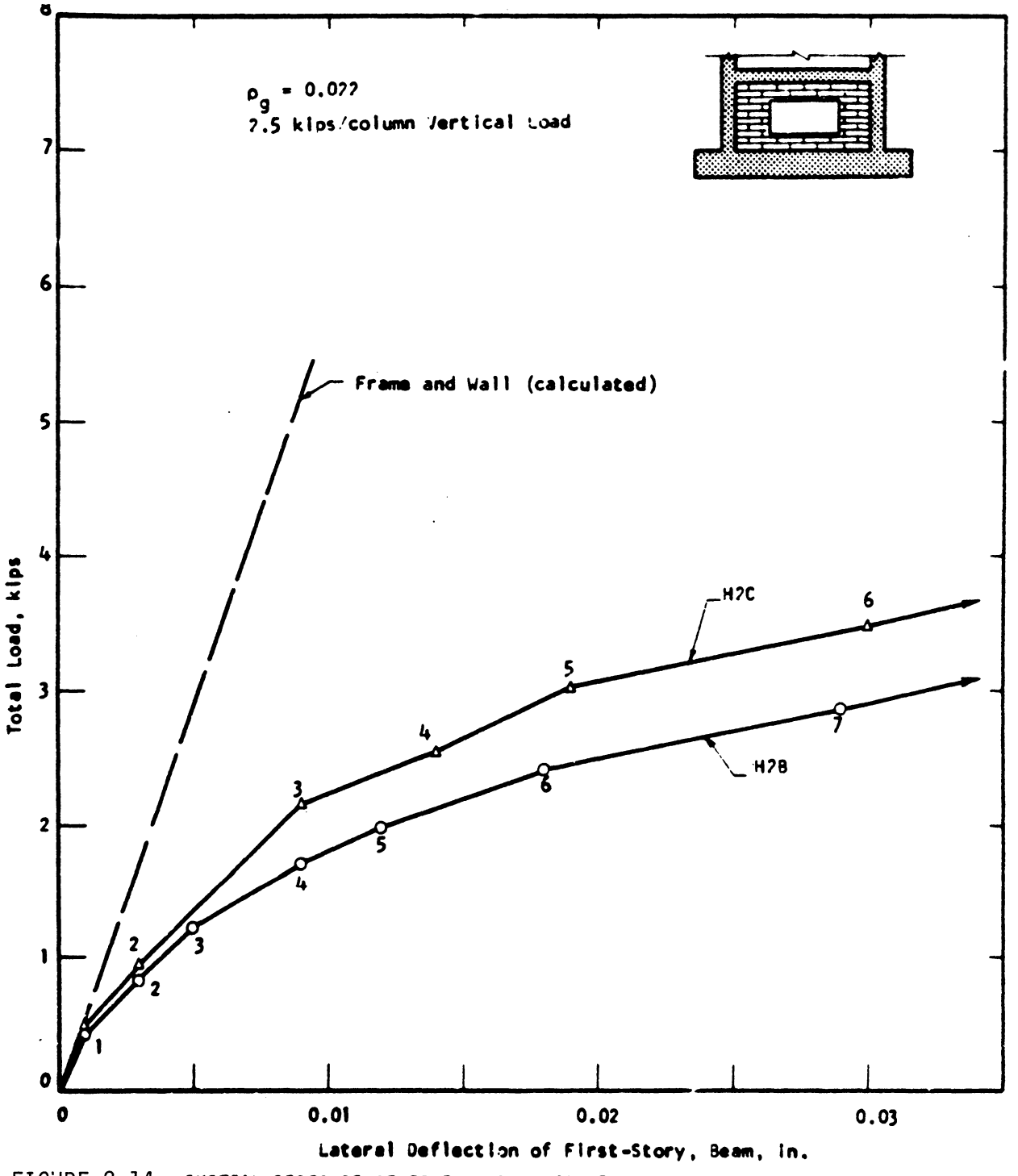

FIGURE 2.14 **INITIAL RESPONSE OF FIVE-STORY SPECIMENS H2B AND H2C, FIRST-STORY BEAM DEFLECTION** [Ref. No. 12]

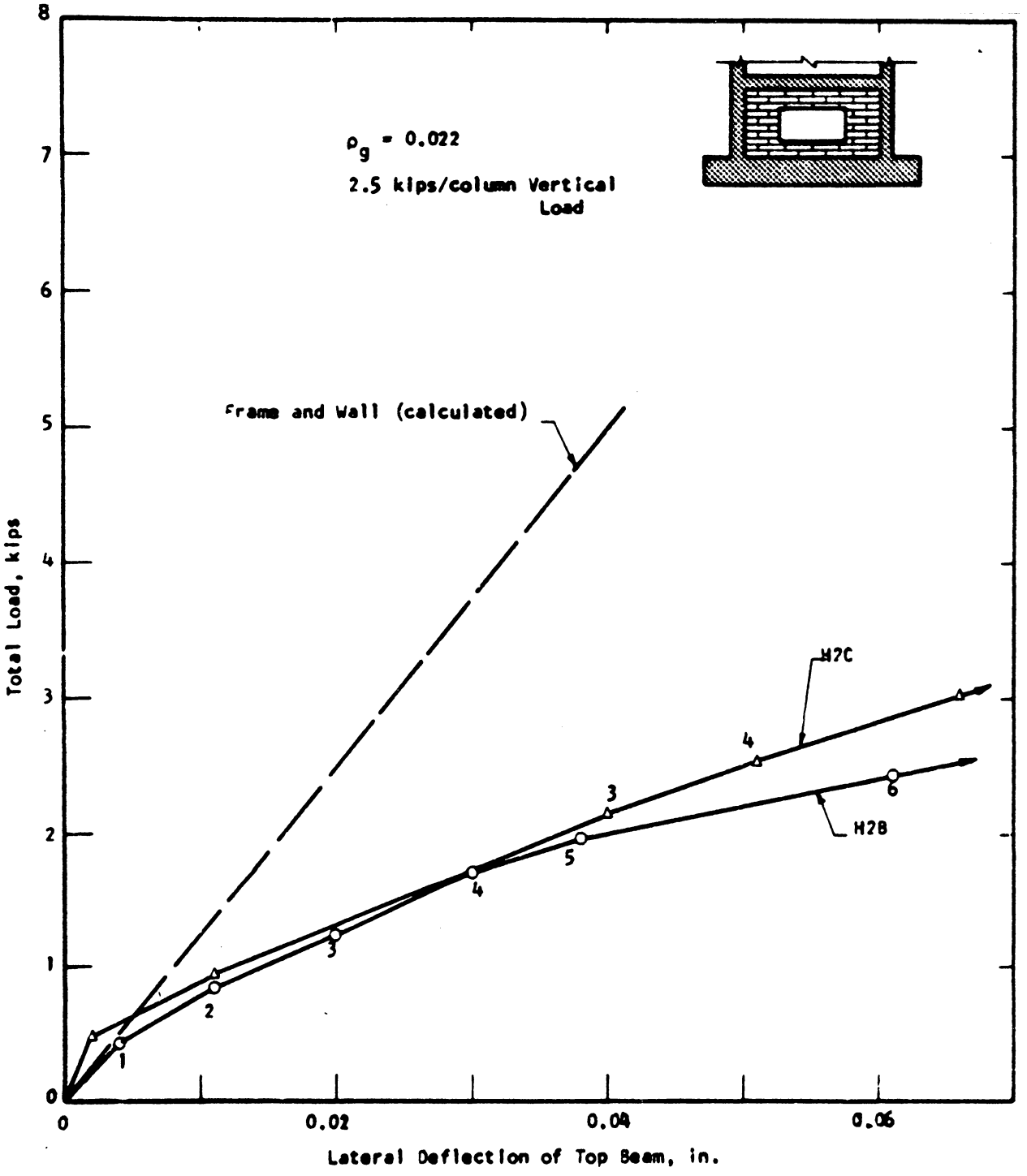

FIGURE 2.15 INITIAL RESPONSE OF FIVE-STORY SPECIMENS H2B AND H2C, TOP BEAM DEFLECTION [Ref. No. 12]

the reduced wall area.

Openings in the wall resulted in a more flexible system with a lower strength. However, the capacity of the structures was not reduced in proportion to the reduction in cross sectional area of the wall. Further research is needed to evaluate the effect of openings.

Chapter 3

DYNAMIC ANALYSIS OF LINEAR ELASTIC STRUCTURES

3.1 Introduction

This chapter deals with the dynamic analysis of linearly elastic structures, that is, frames with monolithic filler panels without gaps. The method of solution of the equilibrium equations for dynamic analysis is presented. The period and damping of the bare frame are discussed, then a practical method for estimating the damping and the period of a complete structure are discussed in detail. Several examples are summarized to illustrate the application of the techniques that are explained, and to illustrate the effects of varying certain parameters in the analyses.

3.2 The Method of Solution

The dynamic analysis of linearly elastic frame structures has been well documented in numerous publications [7,19,25,27,34] and will not be discussed in detail.

The equilibrium equations for a structure, including dynamic effects, may be written in the following form:

$$\underset{\sim}{M}\ddot{\underset{\sim}{r}}_a + \underset{\sim}{C}\dot{\underset{\sim}{r}} + \underset{\sim}{K}\underset{\sim}{r} = \underset{\sim}{P}(t) \qquad (3.1)$$

$\underset{\sim}{M}$ = mass matrix

$\underset{\sim}{C}$ = damping matrix

$\underset{\sim}{K} = \Sigma\, \underset{\sim}{K}_i$ = stiffness matrix

$\underset{\sim}{P}(t)$ = applied load, which may be variable with time

$\underset{\sim}{r}$ = displacement vector of deformation relative to support motion

$\ddot{\underset{\sim}{r}}_a$ = absolute acceleration vector

$\underset{\sim}{r}$ and $\underset{\sim}{r}_a$ are related in the following expression

$$\ddot{\underset{\sim}{r}}_a = \ddot{\underset{\sim}{r}}_g + \ddot{\underset{\sim}{r}} \qquad \text{and} \qquad \underset{\sim}{r}_a = \underset{\sim}{r}_g + \underset{\sim}{r}$$

where r_g is the vector of pseudo-static displacement due to support motion.

The solution of the undamped free vibration problem is given by

$$\underset{\sim}{M}\ddot{\underset{\sim}{r}} + \underset{\sim}{K}\underset{\sim}{r} = 0 \tag{3.2}$$

The eigenvalue problem to be solved is written as

$$\phi[\omega^2 M - K] = 0 \tag{3.3}$$

$\underset{\sim}{\phi}$ = mode shapes

$\underset{\sim}{\omega}$ = circular natural frequency

The mode shape can be normalized such that

$$\underset{\sim}{\phi}^T \underset{\sim}{M} \underset{\sim}{\phi} = 1 \tag{3.4}$$

Then also,

$$\underset{\sim}{\phi}^T \underset{\sim}{K} \underset{\sim}{\phi} = \omega^2 \tag{3.5}$$

In this study simple modal damping will be assumed in each principal mode. The damping can be expressed as a fraction of critical damping.

$$\phi^T C \phi = [2\xi_m \quad \omega_m] \tag{3.6}$$

where the ξ_m represents the damping of the mth mode. The actual displacements, r, are now expressed as a linear combination of the mode shapes.

$$[r] = [\phi_1, \phi_2, \phi_3, \quad , \phi_m] \begin{bmatrix} \eta_1(t) \\ \eta_2(t) \\ \\ \eta_m(t) \end{bmatrix} \tag{3.7}$$

where η_m represents the response of the mth mode, i.e.,

$$[r] = [\phi][\eta]$$

also

$$\begin{aligned} [\dot{r}] &= [\phi][\dot{\eta}] \\ [\ddot{r}] &= [\phi][\ddot{\eta}] \end{aligned} \tag{3.8}$$

$[\phi]$ = modal vector

$[\eta]$ = modal coordinate

In the following section, the damping and the stiffness of complete structure are discussed in detail. The complete structure consists of two major components: nonstructural partitions and a structural bare frame.

3.3 Damping and Stiffness of the Bare Frame

3.3.1 Steel Frame

The bare steel frame has an extremely low value of damping. In well-controlled laboratory tests, Cole [9] gives damping values from 0.036% - 0.15%. Lazan and Goodman [24] have also given damping ratios

for various steels and various mechanisms of internal damping. Generally, for steel, a damping ratio caused by thermoelastic effect is 0.05% for frequencies between 1 Hz and 10 Hz. Damping caused by magnetoelasticity may be a relatively high 0.75%, but only for a special 403 steel alloy. For stress well below the elastic limit, low carbon 1020 steel has a damping ratio about 0.25% due to microscopic plastic strain. Except for the magnetoelastic damping for the special 403 alloy, the highest material damping for steel alone from these two sources is 0.25%.

Damping of a full scale steel structure is difficult to ascertain. Cloud [6] has found damping ratio of 0.3% - 0.4% from pull-tests of welded steel. Hogan [17] reports for small amplitude motions, the completed John Hancock building in Chicago has a damping ratio of 0.5%.

Obviously, the damping ratio of a steel frame by itself depends to some extent on its structural configuration and perhaps to a greater extent on its connection details. It is also evident that for any configuration, the steel frame damping will be less than 1%. A reasonable average frame damping ratio, considering standard construction details, would seem to be 0.5%.

3.3.2 Reinforced Concrete

The damping ratio for laboratory controlled test specimens is remarkably low. Cole [9] states a value of 0.18% for a dry curved specimen independent of amplitude of motion, quality, and frequency of motion above 3 cps. For unreinforced cement, plaster, mortar, and concrete specimens, his results indicate that for frequencies less than

3 cps the damping ratio may increase, rising to approximately 0.25% at 1 cps.

Penzien [28] reports that for uncracked prestressed concrete beams the damping ratios, independent of prestress, were from 0.5% - 1.0%. The damping ratio did vary significantly, however, with development of cracking. Therefore, the damping ratio is indirectly related to the amount of prestress that governs the extent of cracking. For beams that were extensively cracked but still in the linear range of concrete behavior, the damping ratio varied from 1.0% - 2.0%.

Penzien's results compare favorably with damping ratios obtained from the pull-testing of full scale four story reinforced concrete frames (Fig. 3.1). Pull tests yielded damping ratios of approximately 1.5% - 2% for the bare frame, for motions approaching the design level, and for lower motions, the dead load effectively prestresses the cracks and prohibits extensive tension cracking, with a resulting decrease in the observed damping ratio. For very low motions, the damping ratio decreased to approximately 0.7%.

In light of experimental data and the normal condition of most reinforced concrete structures, a reasonable energy ratio to use for the reinforced concrete frame near design level stresses might be 1.5%. For low amplitude motions, a value of 10.7% might be more appropriate.

For a reinforced structure only, it has little meaning to speak of fundamental period for the structure. The period can assume a number of values between well defined limiting values. The limiting values are based upon the condition of the frame, i.e., whether the

frame is fresh and uncracked, or old, having fully developed hairline cracks throughout the tensile area in the concrete. On the basis of these assumptions, the limiting cases may be predicted with confidence using accepted structural theories. The condition of the actual structure between these two limiting cases can presently only be estimated, but it is obviously a function of age and vibration history.

3.4 Damping and Stiffness of the Frame with Partitions

The contributions to stiffness and damping by partitions are important because they influence the amplitude of structural response due to dynamic loads. In 1972 Blume [3] performed full-scale tests on two identical four-story buildings (Fig. 3.1). He used several different types of material as infilling for the frames. He showed the effects of each of these materials on the dynamic characteristics of the structure. Blume is one of the few researchers who has performed dynamic tests on full-scale buildings. The objective of the testing program was to determine thresholds for damage to partitions due to horizontal adjacent story displacement in high-rise buildings, and to gather data that can be used to determine the influence of non-structural partitions on the structural response. Raggett [29,30] and Freeman [13,14] also investigated the dynamic effects of wall panels on the structural response of buildings.

3.4.1 Period and Stiffness of Frame with Partitions

Freeman [13,14] suggested the following method for finding the period of the complete structure. The relative stiffness and period determinations are based on

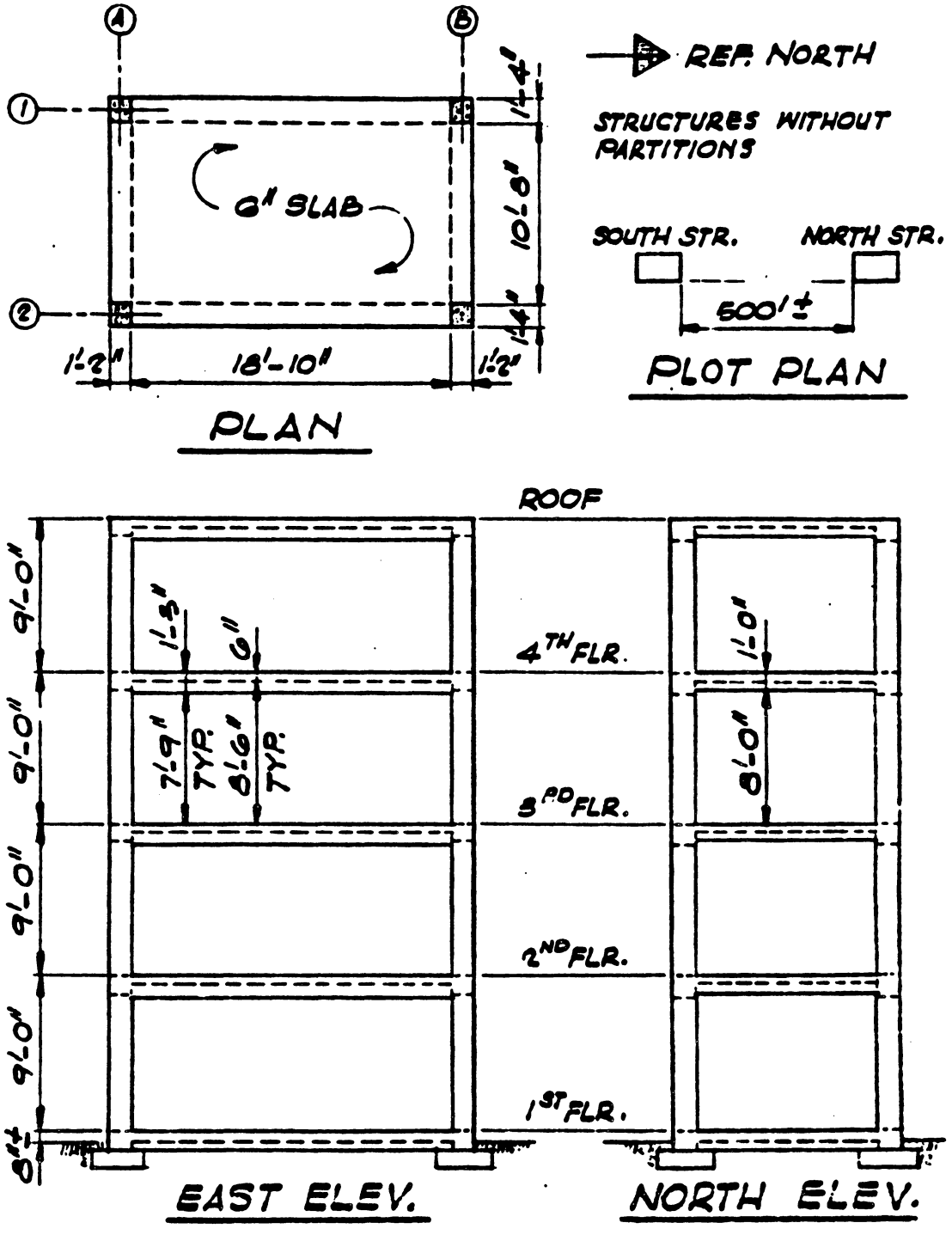

FIGURE 3.1 REINFORCED CONCRETE 4-STORY TEST STRUCTURE
[Ref. No. 29]

$$T = 2\pi\sqrt{\frac{M}{K}} \tag{3.9}$$

in which M = mass, K = stiffness, and T = period.

$$G_p = \frac{\text{shearing stress}}{\text{shearing strain}} = \frac{\text{load} \times h}{t \times \ell \times \Delta_n}$$

$$\text{Partition story stiffness} = K_p = \frac{\text{load}}{\Delta_n} = \frac{G_p \times t \times \ell}{h} \tag{3.10}$$

h = height;

G_p = modulus of rigidity of partitions;

t = thickness;

ℓ = length;

Δ_n = lateral interstory displacement between story n and story n+1

$$K = K_f + K_p$$

$$K = K_f + K_p = 1 \text{ (assumed)}$$

K_p = the relative partition stiffness

K_f = the relative frame stiffness

$$T_f = T\,\frac{\sqrt{K_f + K_p}}{\sqrt{K_f}} = \frac{T}{\sqrt{K_f}} \tag{3.11}$$

$$K_f = \left(\frac{T}{T_f}\right)^2 \qquad K_p = 1 - K_f$$

T = frame and partition period

T_f = frame period

Example 1

For the four-story reinforced concrete structure shown in Fig. 3.1, T_f is measured to be 0.4 sec, average story stiffness is estimated to be 460 kip/ ', partition effective length is 16 × 2 ft, h is 9 ft, thickness is 2 × 1/2 in, and modulus of rigidity is 14500 psi.

$$\text{Story stiffness} = \frac{G_p \times t \times \ell}{h}$$

$$= \frac{14500 \times 1 \times (16 \times 2 \times 12)}{9 \times 12} = 51.5 \text{ kip/ '}$$

The relative stiffness of the partition is

$$K_p = \frac{51.5}{460 + 51.5} = 0.10$$

$$K_f = 0.90$$

$$T = T_f\sqrt{K_f} = 0.39\sqrt{0.9} = 0.37 \text{ sec.}$$

Table 3.1 shows the comparisons between theoretical periods and measured periods of complete structure for different types of partitions.

3.4.2.1 Damping of Frame with Partitions

Little can be said theoretically about the effect of nonstructural partitions on the damping ratio of overall structure-partition combination because, at present, purely theoretical means of predicting the damping ratio for either the bare frame or the partitions do not exist. Damping ratios must presently be obtained empirically or experimentally for the structure in question.

Table 3.1 Comparisons between theoretical periods and measured periods of complete structure for different type of partitions.

Fundamental Mode Periods Measured for Frame (sec)	Partition Type	Partition Interstory Shearing Stiffness (psi)	Theoretical Fundamental Mode Periods for Frame and Partition	Fundamental Mode Periods Measured for Frame and Partition
0.39 (north)	Gypsum board	14500	0.37	0.35
0.37 (north)	Plywood	15000	0.36	0.34
0.5 (south)	Concrete block	968333	0.2	0.17

Measured by John Blume and associates. [Ref. No. 24].

Theoretical means do exist for predicting the increase in the total damping ratio of the structure due to partitions, given the static or dynamic energy dissipated during a complete loading cycle. This is the approximate method of obtaining an equivalent viscous damping ratio for a nonlinear system outlined by Jacobson [20]. The necessary energy dissipation data have been obtained in racking tests [4,14] for gypsum board and plywood partitions.

John D. Raggett [30] suggested a method for estimating the damping ratio of a structure composed of many structural and non-structural elements. This method is useful for low-amplitude non-damaging motion and requires the natural mode shape and frequencies of the structure and the energy ratios for the various building elements be given. Additional consideration must be given to large amplitude plastic behavior. Furthermore, it is suggested primarily for

application to structures whose component stiffnesses are parallel. Most structures fall into this category.

For steady-state resonant vibrations of single mode of a linear system, the total damping ratio may be expressed by

$$\xi_t = \frac{E_t}{4\pi\ U_t} \tag{3.12}$$

in which ξ_t = total viscous damping ratio,

E_t = total energy dissipated per cycle of motion,

U_t = total peak potential energy per cycle of motion for viscously damped system.

For a nonlinear system, the above equation defines an equivalent viscous damping ratio. Equivalent viscous damping ratios are usually amplitude-dependent and should be used with caution.

The total energy dissipated by a building made of many components can be expressed as follows:

$$E_t = \Sigma_i\ E_i$$

$E_i = 4\pi\ \lambda_i\ U_i$ (see Eq. (3.12)) (λ_i is component damping ratio)

$$E_t = \Sigma\ E_i = 4\pi\ \Sigma\ \lambda_i\ U_i = 4\pi\ \xi_t\ U_t \Rightarrow \xi_t = \Sigma\ \lambda_i\ \frac{U_i}{U_t} \tag{3.13}$$

(U_i is component peak potential energy per cycle of motion) which specifically states that the total modal damping ratio equals the sum of component damping ratios weighted by the respective ratio of component potential energy to total potential energy. Therefore, the component damping ratios and component potential energies should be estimated.

3.4.2.2 Component Damping Ratios (λ_i)

The damping ratios may be used directly if they are not highly frequency- or amplitude-dependent. An attempt is made herein to present realistic component damping ratios for those typical building components which are most familiar: a steel frame, monolithic poured-in-place reinforced concrete, and gypsum board on metal stud partition. Damping ratios of steel frame and poured-in-place reinforced concrete were discussed previously in Sections 3.3.1 and 3.3.2.

Stiffness and energy absorption properties of gypsum board partitions have been obtained from racking tests of 8 ft by 8 ft test panel (by John Blume and associate [5,14]). Upper and lower connection details have been designed to simulate a typical partition-concrete slab condition. Two types of partitions are reported by Freeman [14]. Type 1 partitions have 1/2-inch gypsum wallboard on both sides of 3-5/8 inch screwed metal studs. Type 2 partitions differ from type 1 partitions only in the sense that the studs are pop-riveted to the runners. An energy ratio for the type 2 partition is of the order of 7% - 8%, although some results from low amplitude motions are as high as 14%. Energy ratios for type 1 partitions start at about 14% and extend up to 30% - 40% for higher amplitude motion. For low-nondamaging motions, a value of 14% is reasonable. As shown in the next example, this value can be used consistently to estimate the damping of complete structures.

3.4.2.3 Component of Potential Energies (U_i)

For any component of structure, the peak potential energy is theoretically given by

$$U_i = \frac{1}{2} |[r]^T[K_i][r]|_{max} \tag{3.14}$$

[r] = a vector of displacement defining the mode shapes

$[K_i]$ = the associated component stiffness matrix

The total peak potential energy of the building is readily computed if the period of vibration for that mode is known. The total peak potential energy for mode of vibration

$$U_T = \frac{1}{2} |[r]^T[K_t][r]|_{max}$$

or, in modal coordinates

$$U_T = \frac{1}{2} [\phi]^T[K_T][\phi][\eta^2]_{max} \tag{3.15}$$

in which [U] is given by

$[r] = [\phi][\eta]$ $\quad$ $[\phi]$ = modal vector $\quad$ $[\eta]$ = modal coordinate

By definition,

$$\omega^2 = \frac{[\phi]^T[K_T][\phi]}{[\phi]^T[M][\phi]} \tag{3.16}$$

in which ω = natural frequency.

If the usual convention is used, the mode shape is normalized such that $[\phi]^T[M][\phi] = 1$ then

$$\omega^2 = [\phi]^T[K_T][\phi] \tag{3.17}$$

$$U_T = \frac{\omega^2}{2} |\eta^2|_{max} \tag{3.18}$$

or in terms of the period

$$U_T = 2\left(\frac{\pi}{T}\right)^2 |\eta^2|_{max} \tag{3.19}$$

Partitions are usually stressed by racking deflection alone. For an N-story structure, the peak partition potential energy is given by

$$U_p = \frac{1}{2} \sum_{N=1}^{N} K_{n-1}\, \ell_{n-1}\, (r_n - r_{n-1})^2_{max} \tag{3.20}$$

K_n = stiffness per linear foot of partition type on the nth floor,

ℓ_n = length of partition on the nth floor parallel to the plane of motion,

U_n = nth floor lateral displacement for that mode.

If the floor displacements are gain expressed in terms of modal coordinates, then the partition potential energy is

$$U_p = \frac{1}{2} |\eta^2|_{max} \sum_{n=1}^{N} K_{n-1}\, \ell_{n-1}\, (\phi_n - \phi_{n-1})^2 \tag{3.21}$$

For structures with nonstructural partitions, the total potential energy is simply summation of frame and the partition potential energies.

Example 2

For north reinforced concrete four-story test structure (Fig. 3.1) with gypsum wallboard partitions, the frame is assumed to have

1.5% damping and the gypsum wallboard partitions, 14%. The racking stiffness is assumed to be 17 kip/ft/lin ft of the 8 ft high partition.

Theoretical dynamic response characteristics for the first three modes of vibration are computed for this structure using the data presented in Table 3.2. Partitions are modeled as shear panels. The three natural periods are 0.353 sec, 0.111 sec, and 0.059 sec.

Experimental results obtained by Freeman [3] are used for comparison with theoretical value (Table 3.3), for low amplitude of motion (peak roof displacement of 0.02 cm), a fundamental mode damping of 3.9% was measured as was a fundamental period of 0.39 sec. Damping ratios for the higher modes of vibration were not obtained. An observation by Freeman [3] is that as the amplitude of vibration from the pull test increased, so did the period and damping ratio. For a peak roof displacement of 0.10 cm, the period was found to be 0.43 sec and the damping ratio, 4.8%. The increase in period is assumed to be due to extensive hairline cracking throughout the structural frame.

3.5 Experimental Data from Tests of Full Scale Structures

For verification of theoretical models, experimentally obtained periods and damping ratios for the fundamental mode are summarized from Raggett's report [29]. These experimental values have been obtained from pull tests, vibration generator tests, and underground nuclear event records. These data are presented for dynamic response characteristics for the four story reinforced concrete structure (Fig. 3.1). The periods and damping ratios are presented chronologically

Table 3.2 Calculated Mode Shapes for Example 2, Reinforced Concrete Building [Ref. No. 30].

Level	Floor Mass in $\frac{\text{kip-seconds}^2}{\text{ft}}$	Floor Height in ft	Partition Shearing Stiffness kip/ft/lin ft	Partition Length (ft)	First Mode Shape	Second Mode Shape	Third Mode Shape
Roof	1.01	8.5	17	32.33	0.6546	0.5755	0.3906
4th	1.14	8.5	17	32.33	0.5463	-0.0892	-0.5682
3rd	1.14	8.5	17	32.33	0.3680	-0.5899	-0.022
2nd	1.14	8.5	17	32.33	0.1533	-0.4298	0.6089

Table 3.3 Example 2 Energies and Damping Ratios [Ref. No. 30]

Mode	Dimensionless Total Peak Potential Energy, U_t (Eq. 3.19)	Dimensionless Partition Peak Potential Energy, U_p (Eq. 3.21)	Dimensionless Structure Peak Potential Energy, U_s ($U_t - U_p$)	Total Viscous Damping Ratio $_t$ (Eq. 3.13)
1	158.4	29.2	129.	3.8%
2	1602.	233.5	1368.5	3.3%
3	5670.5	513.76	5156.8	2.6%

for a period of approximately four years. Figures 3.6 through 3.8 give these periods and damping ratios.

The data presented here are for motions having maximum roof displacements between 0.1 centimeters and 2.5 centimeters. It is expected that for motions of this amplitude the assumption that the structure does behave linearly is quite accurate and independent of the amplitude of motion. It is recognized that non-linearities do affect the dynamic response characteristics significantly, but this variation is studied in the next chapter.

Shaded bands in the experimental data are simply showing the general trend in the data with age. The observed scatter in the data cannot be explained by measurement and data analysis errors alone. It is expected that experimental variations do not exceed plus or minus 5% of their true values. Therefore, most of the observed scatter in the data must be physical and must actually exist.

Figures 3.6 and 3.7 give the fundamental periods of both motions of test structures. As mentioned previously (Section 3.4.1), the periods shown for the complete structure have been adjusted to reflect only the variations in periods due to variations in the overall structural stiffness. The period variations, caused by the addition of partition masses, have been removed from the data by scaling the measured period squared by the ratio of generalized bare frame mass to generalized mass of the structure with partitions.

$$T^2 = \left(\frac{M_{\text{bare frame}}}{M_{\text{frame + partition}}} \right) T^2_{\text{Mean}} \qquad (3.22)$$

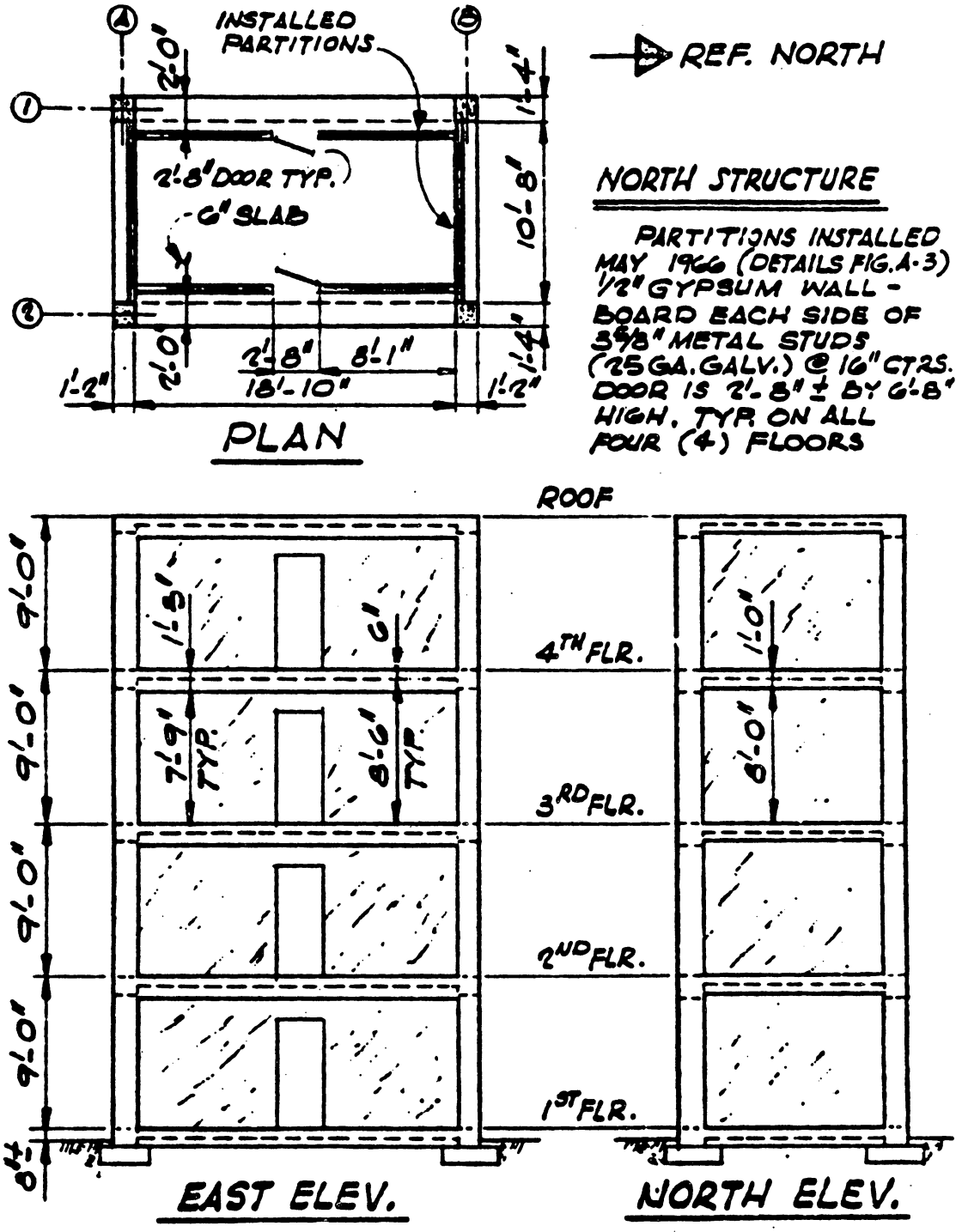

FIGURE 3.2 NORTH STRUCTURE WITH GYPSUM WALLBOARD PARTITIONS [Ref. No. 29].

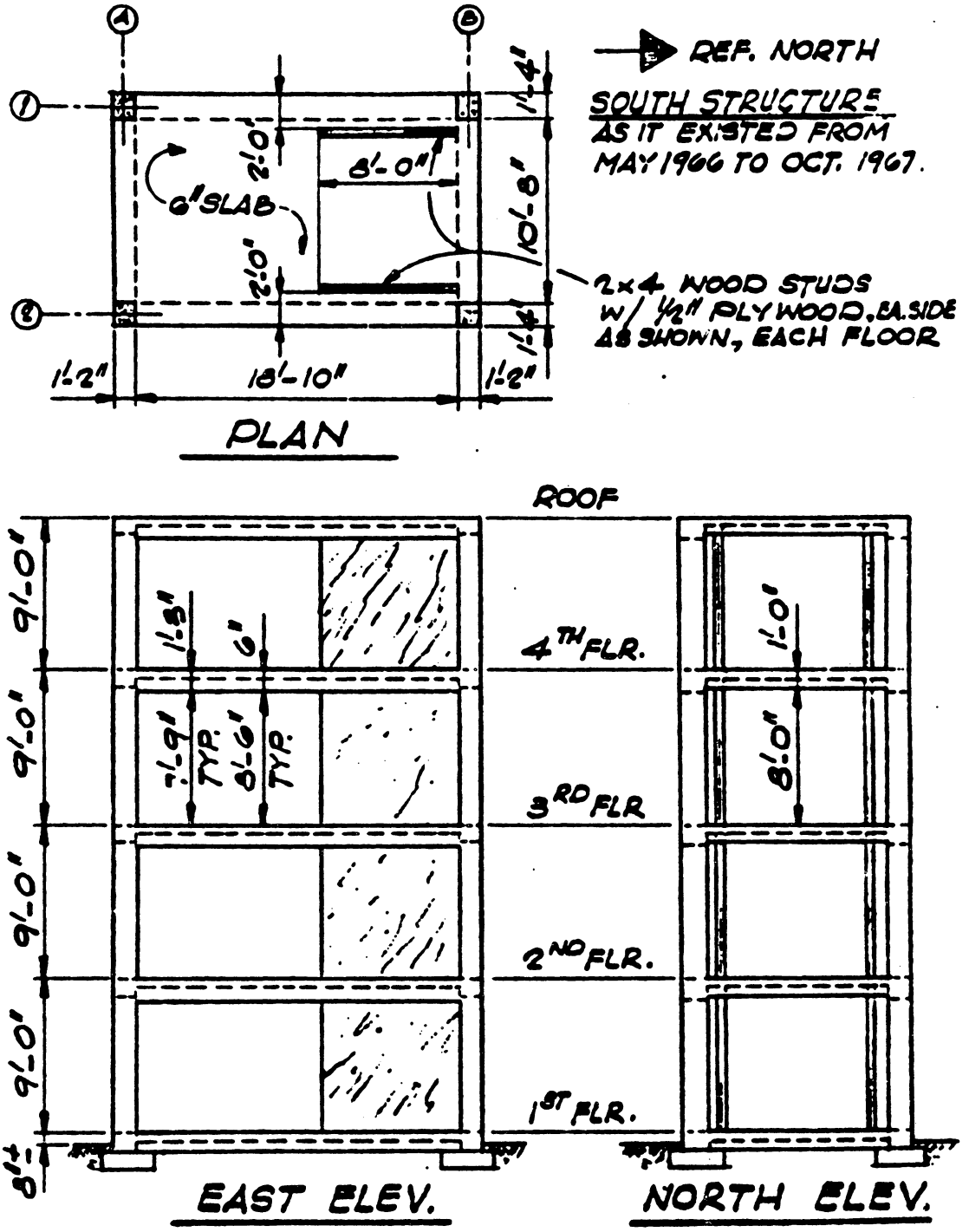

FIGURE 3.3 SOUTH STRUCTURE WITH PLYWOOD PARTITIONS [Ref. No. 29]

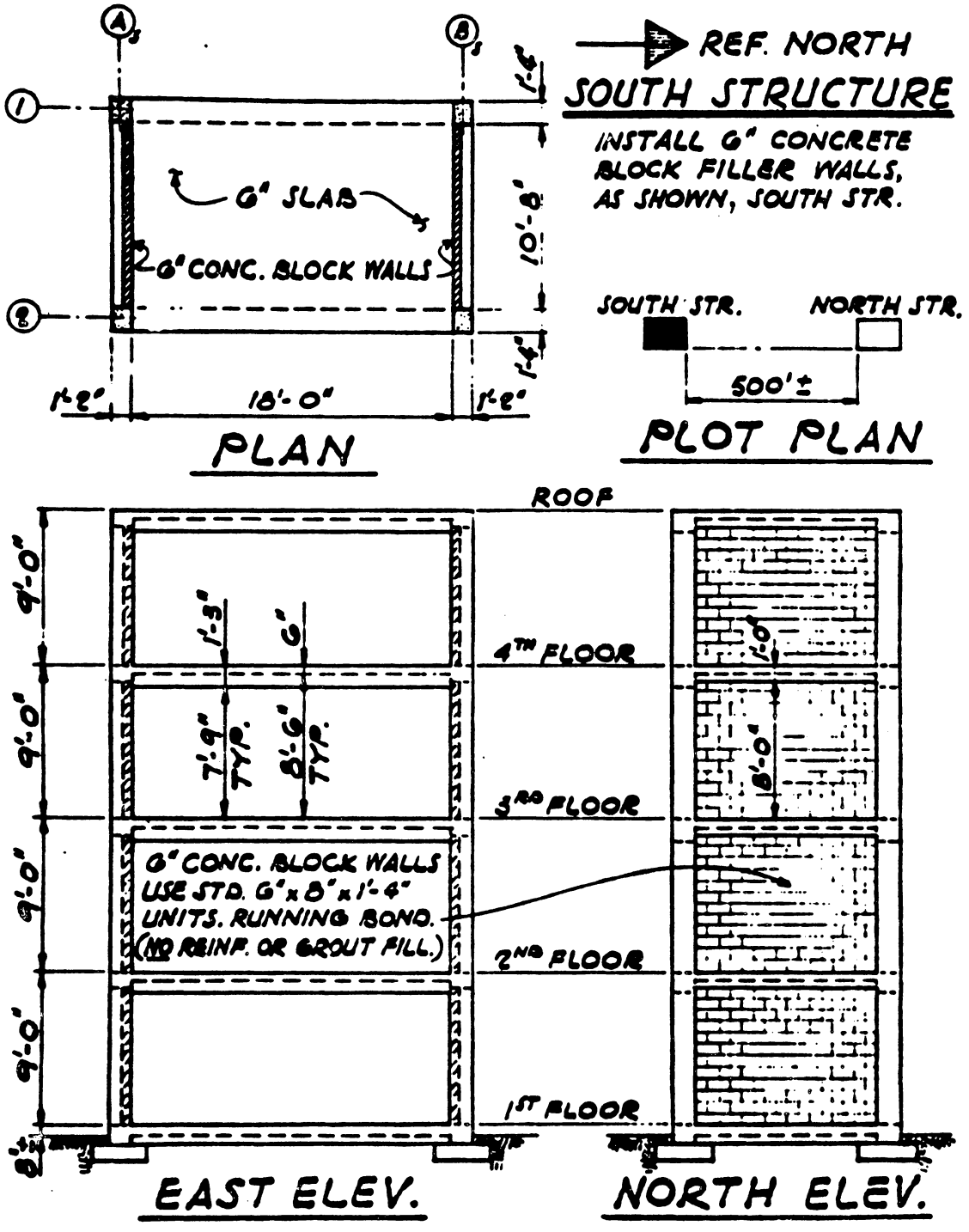

FIGURE 3.4 SOUTH STRUCTURE WITH CONCRETE BLOCK WALLS [Ref. No. 29]

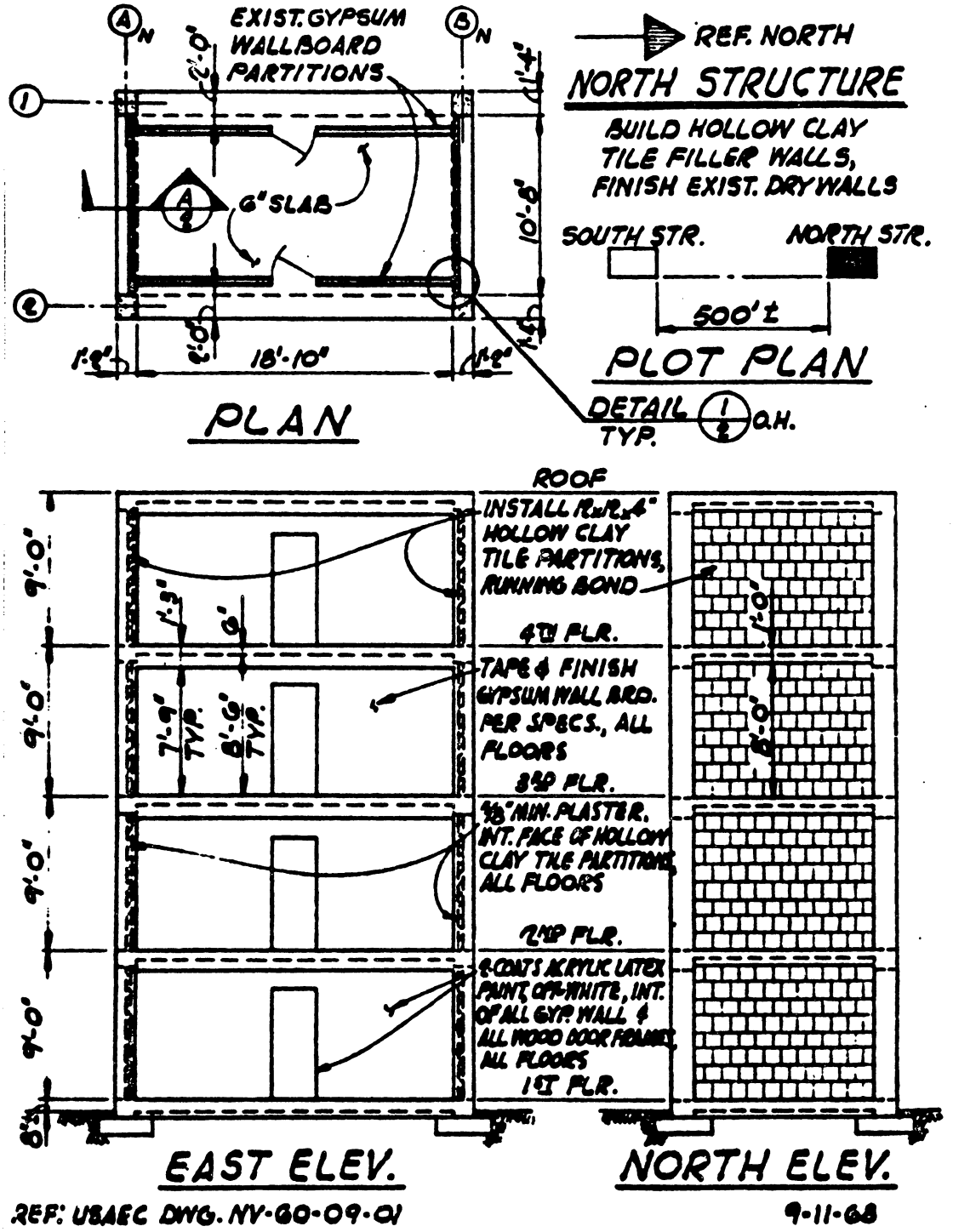

FIGURE 5.5 NORTH STRUCTURE WITH HOLLOW CLAY TILE WALLS [Ref. No. 29]

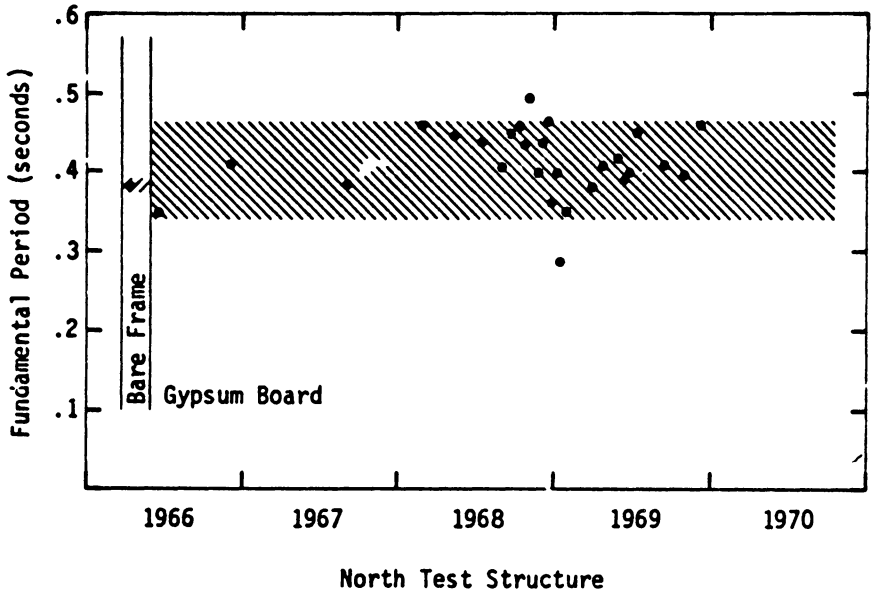

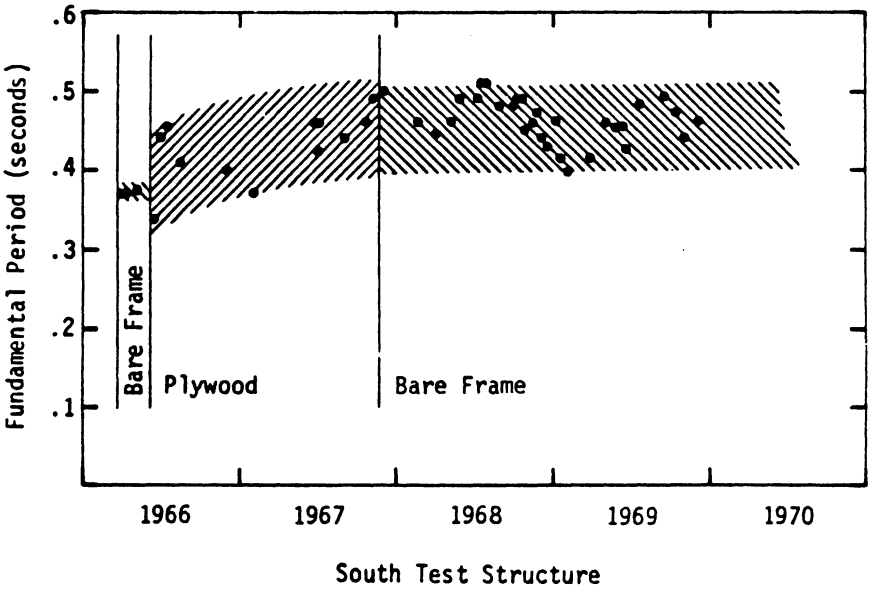

FIGURE 3.6 EXPERIMENTALLY OBTAINED FUNDAMENTAL MODE PERIODS FOR LONGITUDINAL MOTIONS [Ref. No. 29]

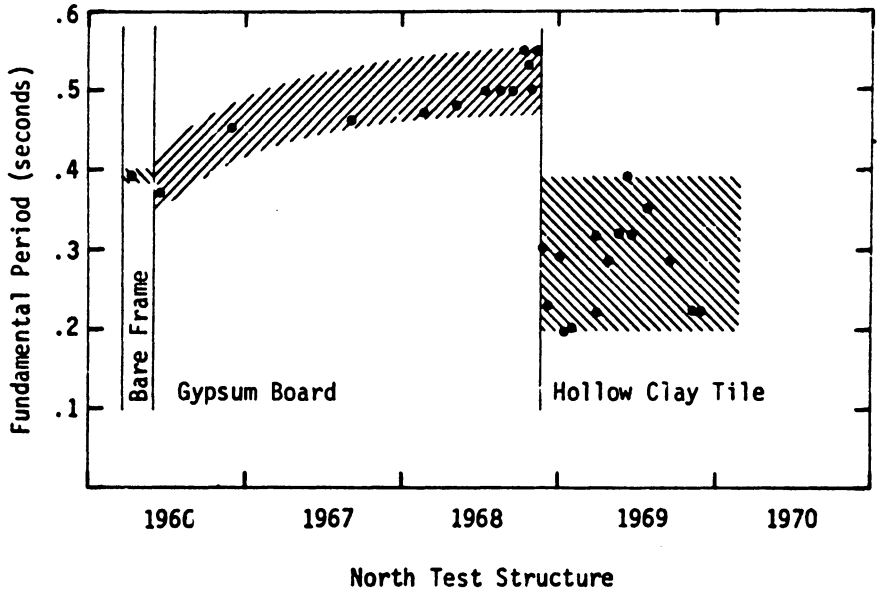

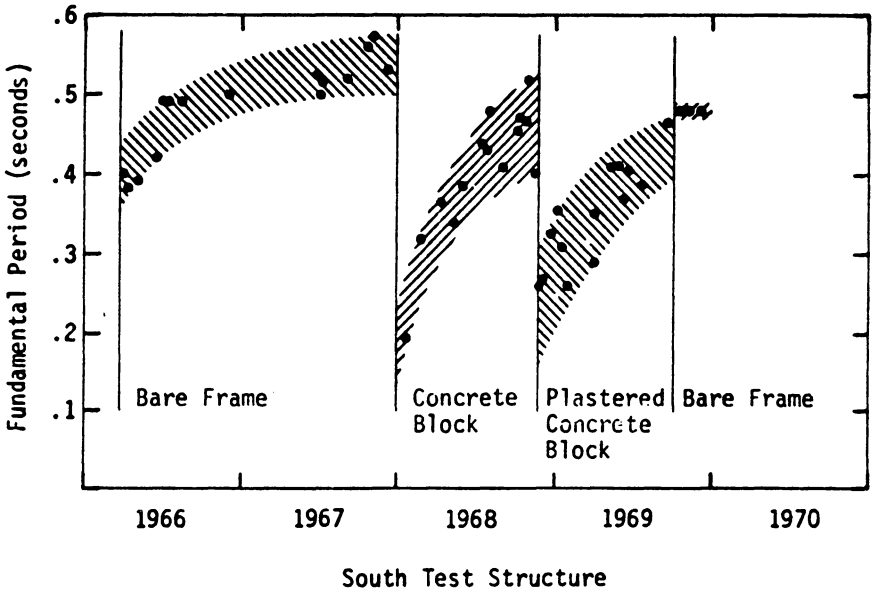

FIGURE 3.7 EXPERIMENTALLY OBTAINED FUNDAMENTAL MODE PERIODS FOR TRANSVERSE MOTIONS [Ref. No. 29]

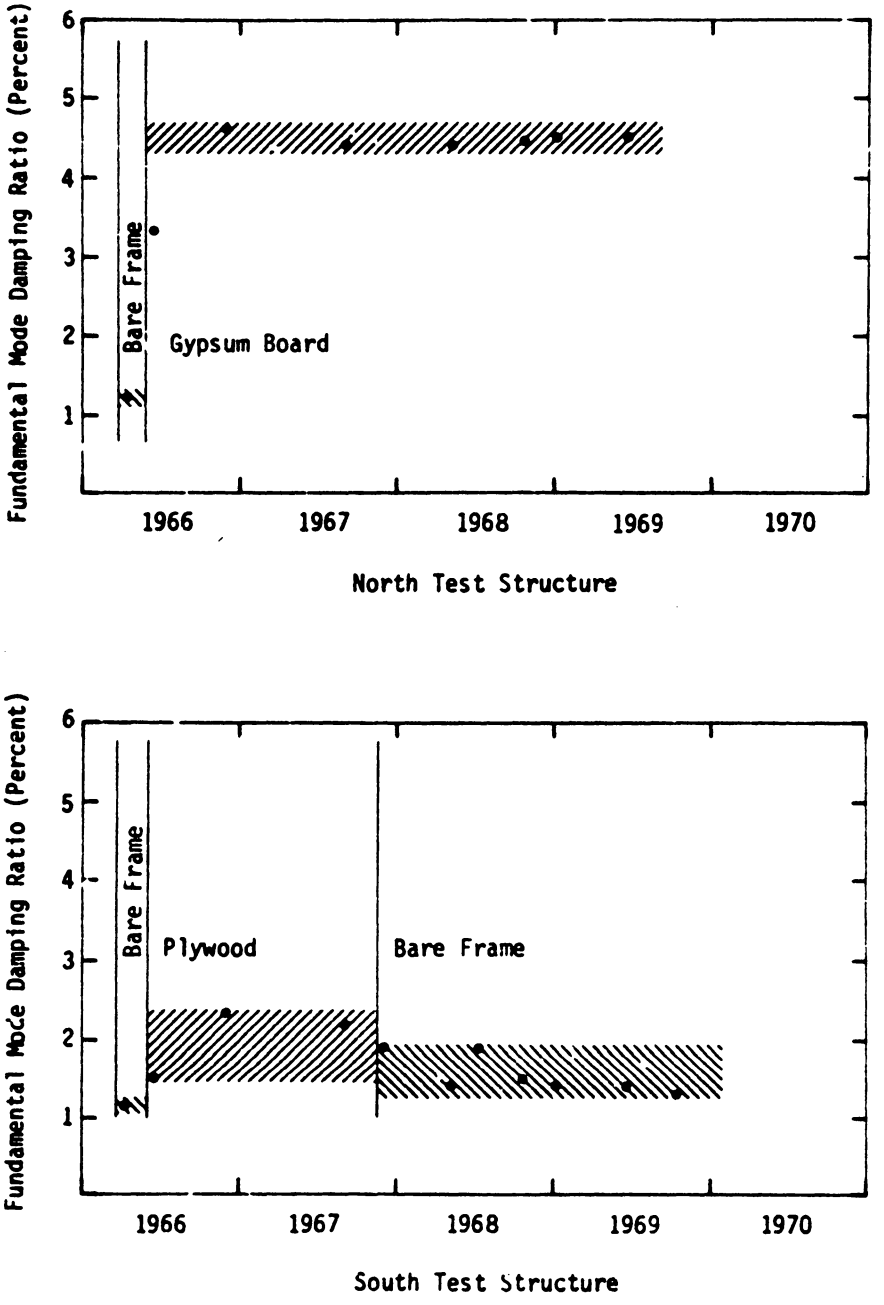

FIGURE 3.8 EXPERIMENTALLY OBTAINED FUNDAMENTAL MODE DAMPING RATIOS FOR LONGITUDINAL MOTIONS [Ref. No. 29]

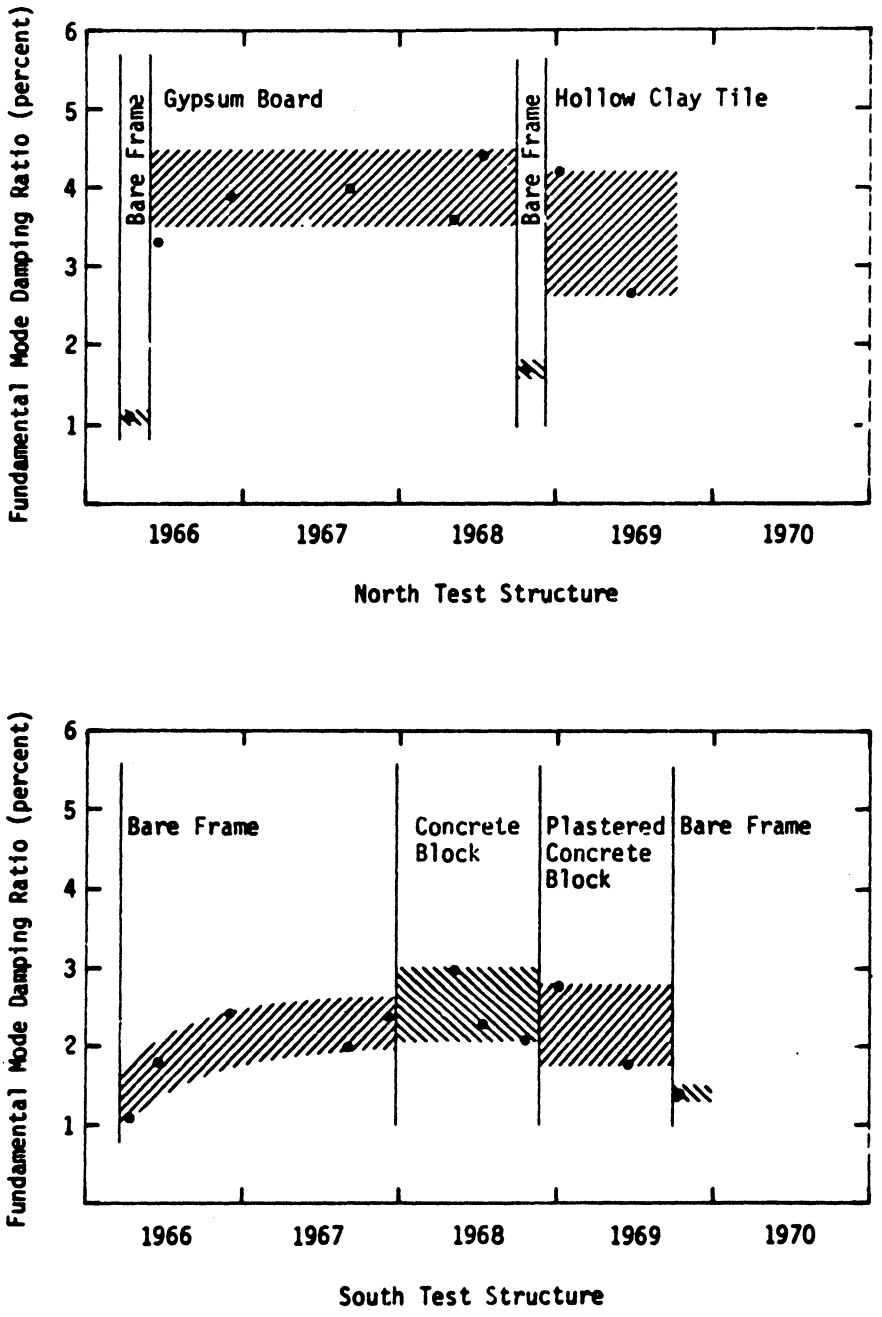

FIGURE 3.9 **EXPERIMENTALLY OBTAINED FUNDAMENTAL MODE DAMPING RATIOS FOR TRANSVERSE MOTIONS** [Ref. No. 29]

Table 3.4 Information for Using Fig. 3.10 and Fig. 3.11

Model No.	1L	2L	3L	1T	2T	3T
Beam and column condition	UNCR	CR	CR	UNCR	CR	CR
Slab condition	UNCR	UNCR	CR	UNCR	UNCR	CR

Note: L = longitudinal motion
T = transverse motion
UNCR = uncracked
CR = cracked

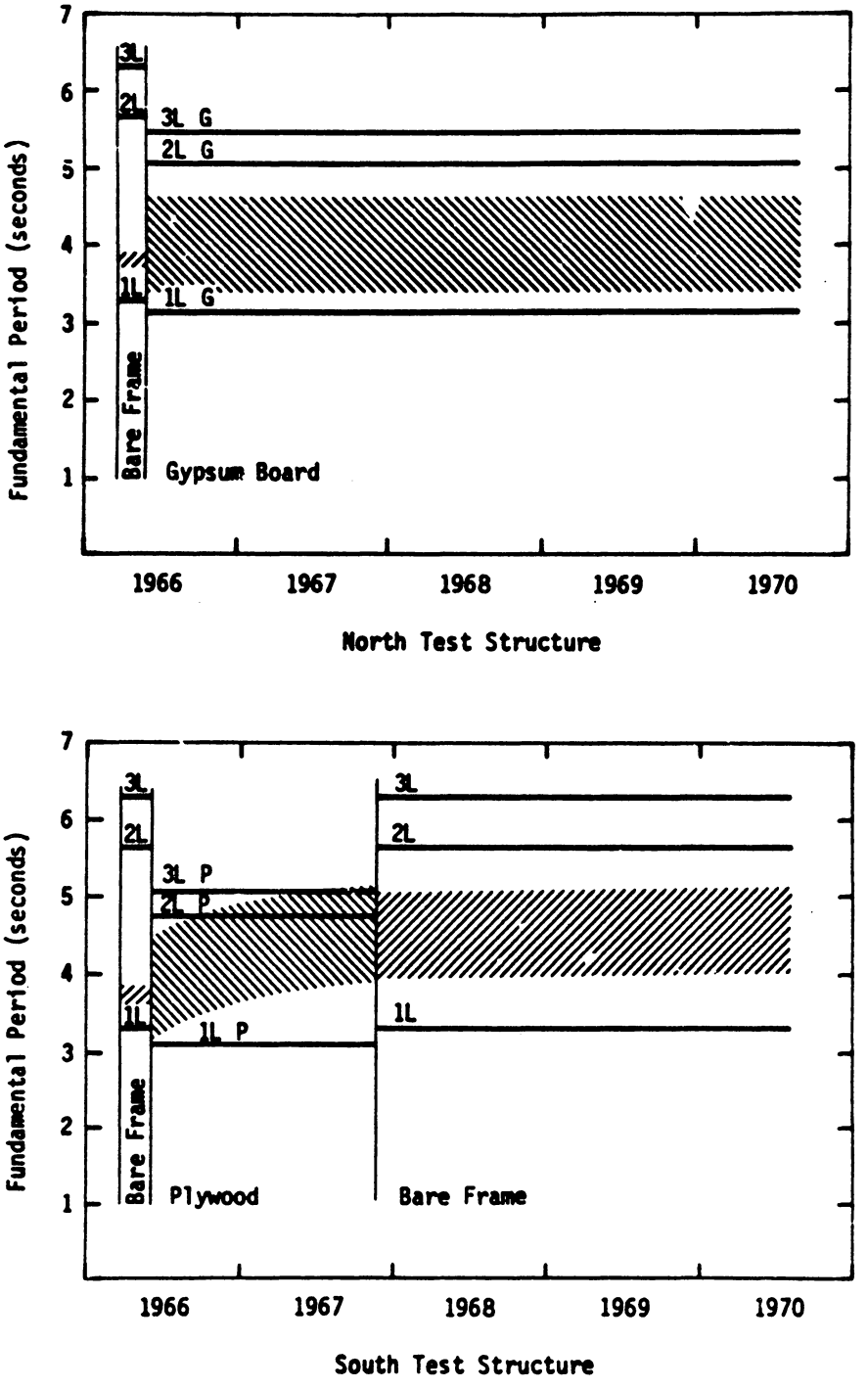

FIGURE 3.10 **COMPARISON BETWEEN THEORETICAL AND EXPERIMENTAL FUNDAMENTAL MODE PERIODS FOR LONGITUDINAL MOTIONS** [Ref. No. 29]

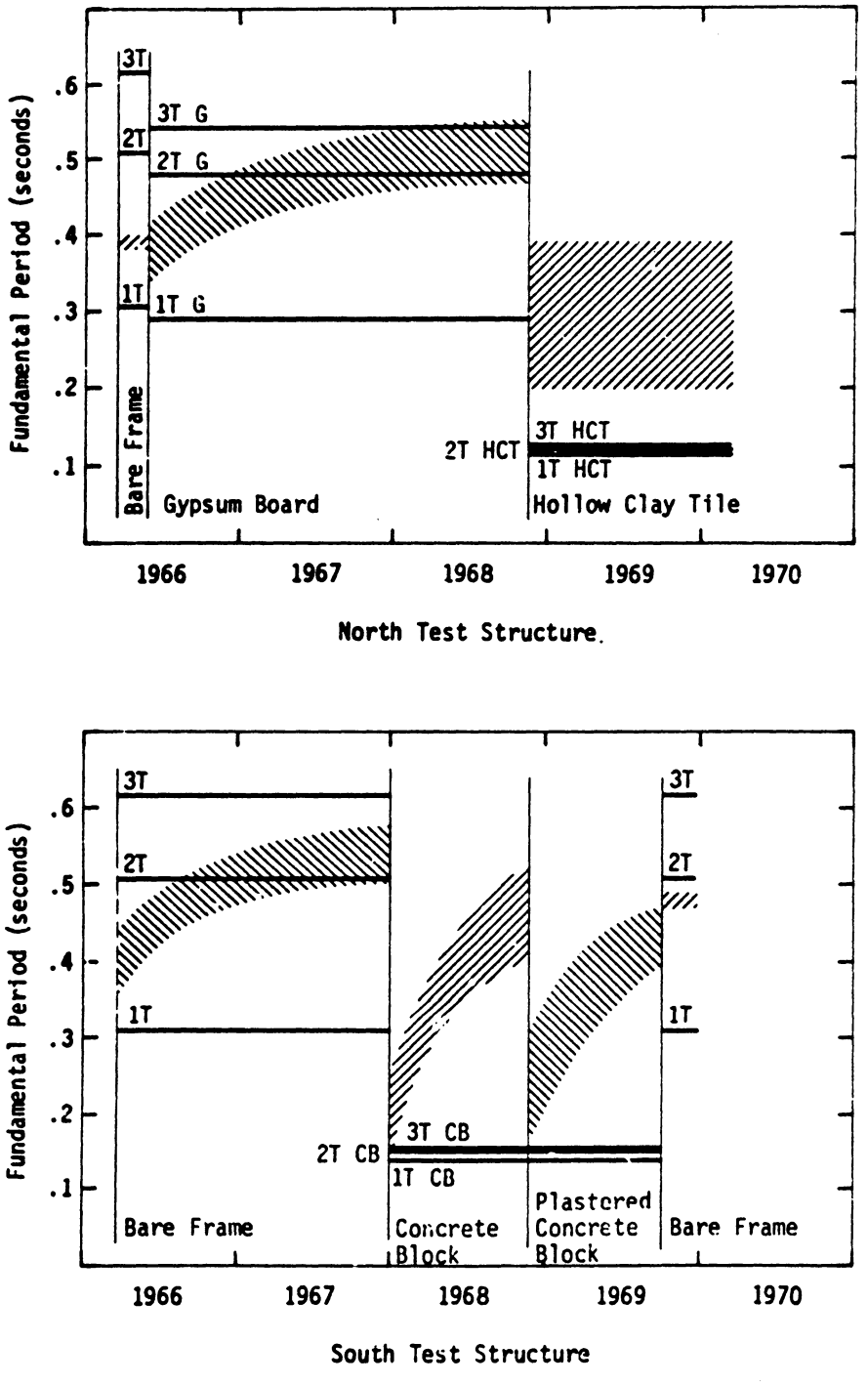

FIGURE 3.11 COMPARISON BETWEEN THEORETICAL AND EXPERIMENTAL FUNDAMENTAL MODE PERIODS FOR TRANSVERSE MOTIONS [Ref. No. 29]

3.6 Comparison of Theory to Experiment

The periods found experimentally and the theoretically predicted values are summarized in Table 3.1. Figures 3.10 and 3.11 compare the theoretical fundamental periods to the bands of data shown previously in Figures 3.6 and 3.7.

There are no figures showing the comparison between theoretical and experimental damping ratio values because the theoretical values are only partially theoretical and represent only differences and not absolute quantities. Damping ratio comparisons are made for each partition type separately.

Although the experimental data are used somewhat scattered, a number of conclusions, both qualitative and quantitative, can be drawn. It can be noted from the bare frame data in Fig. 3.6 there is great variation. To evaluate the structural effects on nonstructural partitions for a frame that has variable dynamic response characteristics, some time must be spent in discussing the bare frame behavior alone.

3.6.1 Bare Frame

Of greatest significance is the large variation in the fundamental period (and therefore stiffness) for the bare frame as a function of chronological time [Fig. 3.6 and Fig. 3.7, Ref. No. 29].

A number of physical causes may explain the observed scatter in the data. First, because hairline cracking will develop randomly, even for steady state vibration and because the ground motion is itself random, increases in the periods due to development of hairline cracking must therefore be random.

Second, the dead weight compressive stress may keep hairline cracks closed for a sufficient length of time to allow recementing across the cracks, in effect, healing and stiffening the structure.

Third, amplitude dependent nonlinearities in the actual structure behavior are undoubtedly a cause of much of the scatter.

Periods from event records have been taken from vibrations having various peak amplitudes, although all amplitudes were between 0.1 and 2.5 centimeters roof displacement. This corresponds to a rough lower limit of the more linear range of experimental data.

Finally, some scatter of course exists from errors in measurement and analysis of data. These errors, however, are not expected to exceed 5%.

Bare frame damping ratios are less scattered than the period value. Figure 3.8 [Ref. No. 29] shows a band of damping values for longitudinal motion of the south test structure. For this particular structure, the bare frame has a damping ratio 1.6% with variance of 0.4%.

3.6.2 Frame with Gypsum Board Partitions

Bands of experimentally obtained fundamental periods and theoretical periods are shown in Figures 3.10 and 3.11 [Ref. No. 29] in the regions designated gypsum board. Immediately evident is the scatter in data, greater than the scatter in the bare frame data. Therefore, conclusions are expected to be more approximate than conclusions regarding the bare frame. Comparison between the experimental bands of period data shows a reduction of 11% of bare frame value

after partitions were installed. The theoretical model shows reduction in period of 10%.

Considering the large scatter, the experimental data do not contradict the validity of the theoretical gypsum board partition stiffness model. Note that the comparison of periods for bare frame and periods for frames with gypsum board partitions were for records of motions after two years of structure life. Therefore, it is not expected that there exists a significant systematic trend in the bare frame dynamic properties over the time period used in the comparison. Damping data (see Figures 3.8 and 3.9, Ref. No. 29) are not nearly as scattered as the period data.

There may be large discrepancies between the experimentally obtained damping ratios and theoretical damping ratios, because the experimental racking test apparatus may not accurately represent the racking experienced by a partition in an elastic frame. The boundary condition between frame and partition is undoubtedly the physical difference which may cause the discrepancy. The racking test data accurately describe the amount of energy dissipated internally during racking deflections of the partition. On the other hand, in the actual structure significantly more energy is apparently dissipated by the working of the frame and partition at the partition boundary. Relative motions between the two elements and consequent rubbing or working undoubtedly causes the discrepancy. However, gypsum board partitions contribute significantly to the overall damping of the structure, but contribute little stiffness to the total structure.

3.6.3 Frame with Concrete Block Partition

The south test structure has unreinforced, hollow concrete block partitions installed for approximately two years after the bare frame had generally reached its asymptotic, cracked condition. Bands of experimental data were compared to theoretically predicted periods in Figure 3.11 (Ref. No. 29), the extreme variation in the fundamental period for the frame with concrete block partitions. Measured period variation range from a low of 0.19 sec. to approximately 0.5 second one year later. This variation in period corresponds to a reduction in generalized stiffness. During this period, no damage to the partition was observed other than the expected fine peripheral cracking of the mortar bond between the partition and the frame.

After one year, the interior surfaces of the partition were plastered. In this process most of the fine cracks around the boundary were filled. After the partition had been plastered, the period returned to a value close to that which it had when partitions were fresh. Therefore, for the amplitude of motion considered for experimental study (Ref. No. 29, 0.1 centimeter to 2.5 cm peak roof displacement) in a one year period the effect of the concrete block partitions varied from a stiffening of the bare frame by factor of almost 7 to no stiffening of the structure. This can be attributed to the working of the boundary between the frame and the partition, gradually breaking the entire peripheral mortar bond. After approximately one year of severe ground-motion, the partitions were contributing nothing to the overall structural stiffness.

Experimentally obtained values of damping ratios of the frame with concrete block partition are shown in Fig. 3.9 for transverse motion of south structure. Increases in the damping ratios, as compared to the bare frame values before and after the partition had been installed, are so small and the scatter in the data is so large that no conclusions can be made other than that damping increases caused by the installation of the partitions are slight (less than 1%).

So, unreinforced masonry infilled walls have extreme but short-lived stiffness for vibrations. Increases in the total damping ratio are less than 1%. As the partitions lose their effective stiffnesses, the increase in damping ratios also decreased.

3.6.4 Frame with Plywood Partitions

A partial plywood partition existed in plane of south test structure for a short time in the early life of the structure. Little can be said conclusively in comparing the predicted theoretical response characteristics to experimental characteristics because the plywood partition existed in the structures when the bare frame properties were varying most (in the first two years of the life of the structure). Thus, no quantitative comparisons can be drawn.

Qualitatively speaking, the only conclusion which can be made about the plywood partition stiffness is that the predicted partition stiffness is not contradicted by data. Similarly, the theoretically predicted damping ratios for the frame with partitions is also not contradicted by the data because for both periods and damping ratios the predicted variations from equivalent bare frame values are lower

than the scatter in the bare frame data. Further experimental study is needed to verify conclusively any structural plywood partition model.

Considering the small amplitude of motion corresponding to the lower limit of the more linear range, the stiffness and damping ratios may be confidently predicted using linear elastic analysis.

Chapter 4

STATIC ANALYSIS OF NONLINEAR STRUCTURES

4.1 Introduction

In this chapter the nonlinear analysis of frames with filler walls are discussed. In the real structures, there are numerous factors that play an important part in aggravating the nonlinearity of structures. A few of those that are easily conceived are the effects of axial loads in the members, plasticity of the material, the effect of shape factor not being unity, the strain hardening effect, and the foundation effect. Reinforced concrete structures exhibit more of the nonlinear properties, particularly in the construction of tall buildings. The stress-strain or moment curvature relationships of this material are highly nonlinear, including discontinuities. An important case of nonlinearity in reinforced concrete structures is due to the cracking of concrete. In statically indeterminate structures, the local reduction of stiffness due to cracking and the plastic behavior of concrete can result in considerable redistribution of moments with respect to elastic distribution [10].

Earlier, engineers only took partial account of the nonlinearity in structural design, using their own judgment, which resulted in conservative designs. For example, the computed elastic response of a structure due to earthquake ground motion is considerably greater than code design response, and yet buildings designed for code forces have withstood rather severe earthquakes [35]. However, nonlinear

analysis techniques are involving knowledge of elasto-plastic, bi-linear, or Ramberg-Osgood moment curvature functions for beams and columns of structures, and the performance of step by step analyses determine the response of the structure. A considerable portion of the effort in the development of the analyses has been concentrated in better modeling of members stressed beyond their elastic limits [10].

4.2 Frames with Filler Walls

There has been a considerable amount of research, both analytical and experimental, done on the behavior of frames with filler walls. Holmes [18] presented a method for determining the strength and stiffness of frame wall composites based on the concept of the wall acting as a diagonal brace. In this method, the wall was replaced by an equivalent diagonal strut. Holmes derived formulas to predict the stiffness and strength of single infilled panels.

Smith [32] also interpreted the stiffness of the frame wall composite on the basis of the equivalent strut concept. Extensive theoretical and experimental studies were made concerning the properties of equivalent struts. The equivalent strut can be determined based on the relative frame-wall stiffness; the frame wall system was considered as a pin-jointed diagonally braced frame. The objection to Smith's behavioral model is its inherent lack of generality in reproducing actual behavior of multi-story structures. This model cannot explain the actual failure mechanism of frame-wall system. It is summarized in this study because it provides explicit evidence of nonlinear behavior in the actual structure.

Fiorato, Sozen, and Gamble [12] presented results of tests for reinforced concrete frame with filler walls. These authors also presented the knee-braced frame model. This nonlinear model provides a means for estimating quantitatively the load capacity of the system after initial cracking. Details of this model will be discussed further in the next sections.

4.3 Development of Cracking

An important case of nonlinearity in structures is due to development of cracking. The development of cracking in a frame-wall system depends on the properties of the frame and wall, the dimensions of the frame and wall, and magnitudes of the shear, moment, and axial loads on the structure. The relationship between these factors determines the nature of the cracking which can occur in the frame-wall composite. When cracks form, the integrity of the joints along the interface of the wall and frame affects the compatability and shear transfer (shear flow) between the wall and frame.

The cracks which may develop in the basic frame-wall structure can be idealized as shown in Fig. 4.1. The crack in the tension column of the reinforced concrete frame, labeled (1), results from axial and bending tensile stresses in the column. The horizontal crack which extends across the base of the structure, labeled (2), results primarily from bending (normal) stresses acting on the cross section. This type of cracking will be referred to as flexural cracking. The diagonal-horizontal crack, labeled (3), results primarily from shearing stresses acting in the wall. This mode of cracking

1) Column Cracking

2) Flexural Cracking

3) Shear Cracking

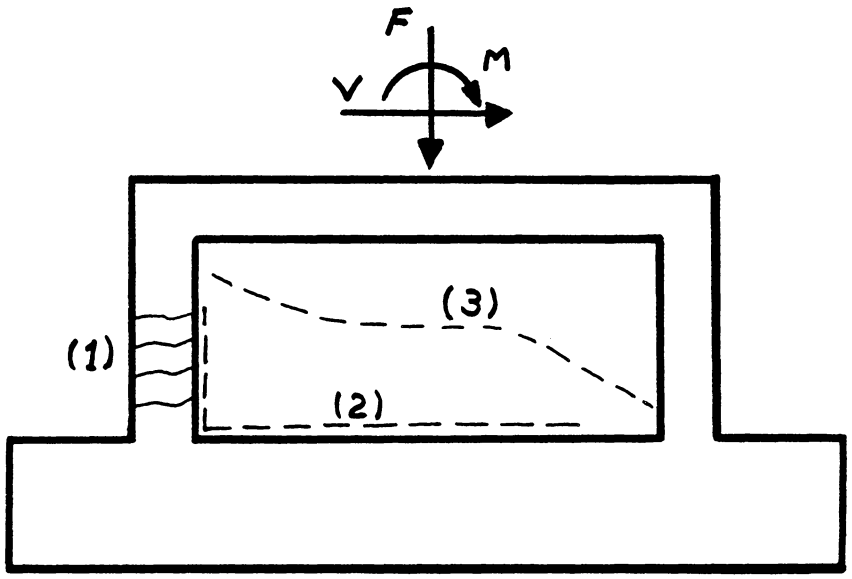

Figure 4.1 Modes of Cracking--Idealized

will be referred to as shear cracking.

The formation of cracks decreases in the stiffness of the structure which is reflected in a decreased slope of the load-deflection property for the structure. After the formation of flexural cracks in a wall of the structure, the wall can be replaced by a diagonal strut. Equivalent strut can be determined based on the relative frame-wall stiffness. The frame-wall system is considered as a pin-jointed diagonally braced frame [32].

At the latter stage of loading with the formation of shearing cracks in the walls (failure of the compression strut), a system of braced columns develop which governs the response of the system. The column in the lower story of the frames are being braced by segments of the cracked wall. The braces reduce the effective height of the column, allowing the frame to carry higher loads. The braced columns carry most of the applied load, while some of the load is transmitted through the wall segments by frictional forces. This model is referred to as knee-braced frame model [12].

The load causing flexural cracking can be calculated based on the elastic flexure formula for a linear distribution of strain throughout the cross section. Fiorato [12] suggested the following expression for flexural cracking load:

$$V_{crf} = K \frac{I f_t}{x_{tw}} \tag{4.1}$$

V_{crf} = critical shear that produces flexural cracking

K = coefficient depending on the moment-shear ratio

f_t = tensile stress at cracking

I = moment of inertia of the frame wall composite

x_{tw} = distance from the neutral axis to the extreme fiber of wall

Flexural gaps may also occur because of poor construction, or prior motion of the building. After formation of flexural gaps, the wall is replaced by a diagonal strut in the frame.

4.4.1 Equivalent Strut Model for Lateral Stiffness of Infilled Frames

Figure 4.2 shows schematically a deflected frame with a partition and the idealization for mathematical modeling. The schematic of the deflected frame and partition immediately suggest the idealized model shown of an equivalent compressive strut. B. S. Smith [32] has performed extensive theoretical and experimental studies concerning the properties of equivalent struts. His study is summarized here because it is one of the simpler methods to predict the partition stiffnesses for nonlinear classification.

The equivalent strut properties can be determined based on the relative frame-wall stiffness. Theoretical frame-wall stiffness can be expressed as,

$$\lambda \ell = \ell \sqrt[4]{\frac{E_c\, t}{4EI\, \ell'}} \tag{4.2}$$

in which E_c, t, and ℓ' are the Young's modulus, thickness, and length of side, respectively, of the infill; and E, I, and ℓ are the Young's modulus, second moment of area, and length of side, respectively, of the frame. The parameter $\lambda\ell$ is similar to that used in beam on elastic foundation theory, where it expresses the relative stiffness

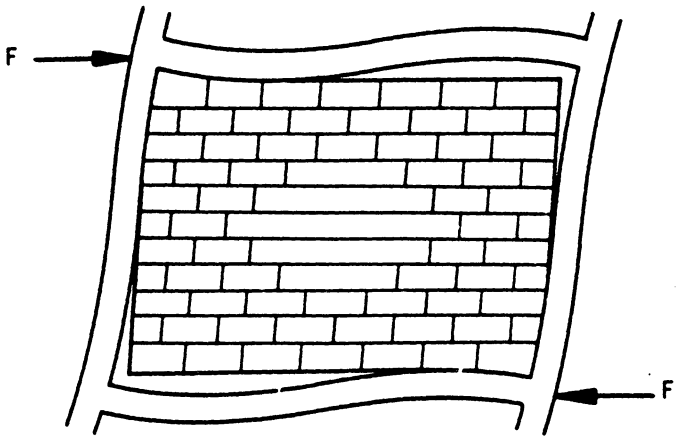

Schematic of Deflected Frame with Partition

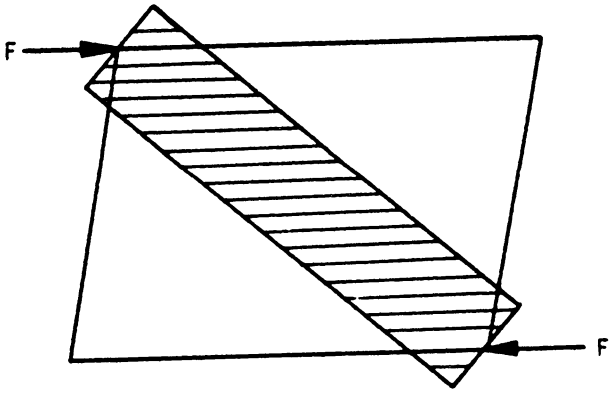

Equivalent Strut

Figure 4.2 [Ref. No. 29]

of a foundation to an interacting beam. These correspond to the infill and frame, respectively. The smaller the value of $\lambda\ell$, the stiffer the frame relative to the infill.

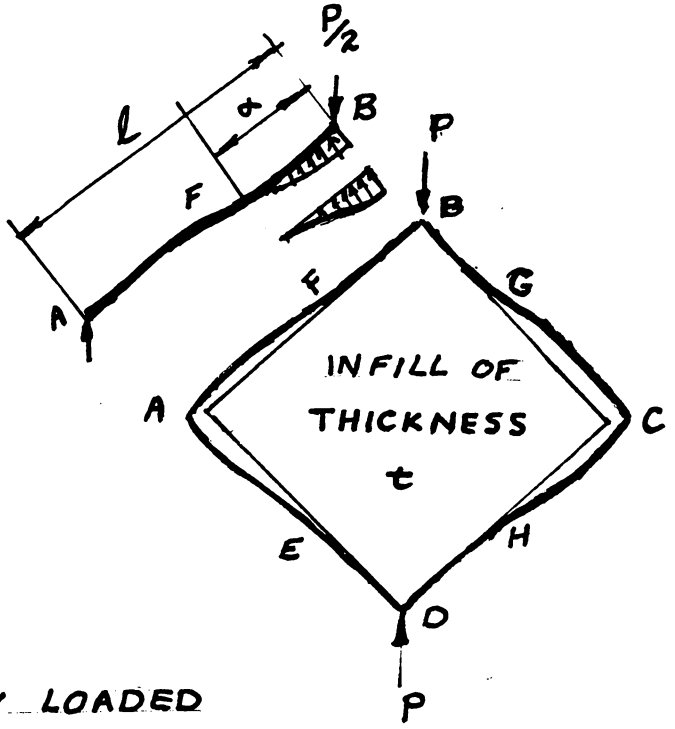

FIG. 4.3 DIAGONALLY LOADED INFILLED FRAME

4.4.2 Diagonal Stiffness

In earlier investigations by Holmes [18] and Smith [31], it was assumed for convenience that the infill behaved as a diagonal strut acting directly between the corners of the frame. This assumption was known to be a simplification because the infill, although acting as a diagonal strut, clearly reacts against each side of the frame over finite lengths extending from the loaded corners, as illustrated in Fig. 4.3. By including the effects of these lengths of contact, it is possible to explain the large increase in overall diagonal stiffness

resulting from a relatively small increase in the frame stiffness. The following approximate theoretical examination provides a rational solution to this interaction problem. The stages of the analysis may be briefly summarized as follows:

1) A relation is derived between $\lambda\ell$ and length of interaction, i.e., length of contact.
2) The length of contact is related to the diagonal stiffness of the separate infill.
3) The results of steps 1 and 2 are combined to give relationship between $\lambda\ell$ and diagonal stiffness of the infill.

Steps 1 to 3 are explained in more detail:

1. Consider Fig. 4.3 and in particular the side AFB, of which FB remains in contact with the infill. Assuming a triangularly distributed reaction along FB, the bending and equilibrium equation may be written for separate lengths AF and FB. These may then be related by the continuity condition at F. A further equation for the energy of AB and infill allows the whole set to be reduced to a single transcendental equation in terms of $\lambda\ell$ and α/ℓ, the parameter used for the length of contact. A similar analysis can be made, using a parabolic distribution of the reaction along FB, to produce an alternative equation relating α/ℓ and $\lambda\ell$. The solution of these equations yield the two curves given in Fig. 4.4 [Ref. 32] which shows, also, the experimental results for the length of contact.

The close alignment of the two curves, and the satisfactory agreement of the experimental results, could lead to the adoption of either curve. However, the third curve shown in Fig. 4.4 also agrees

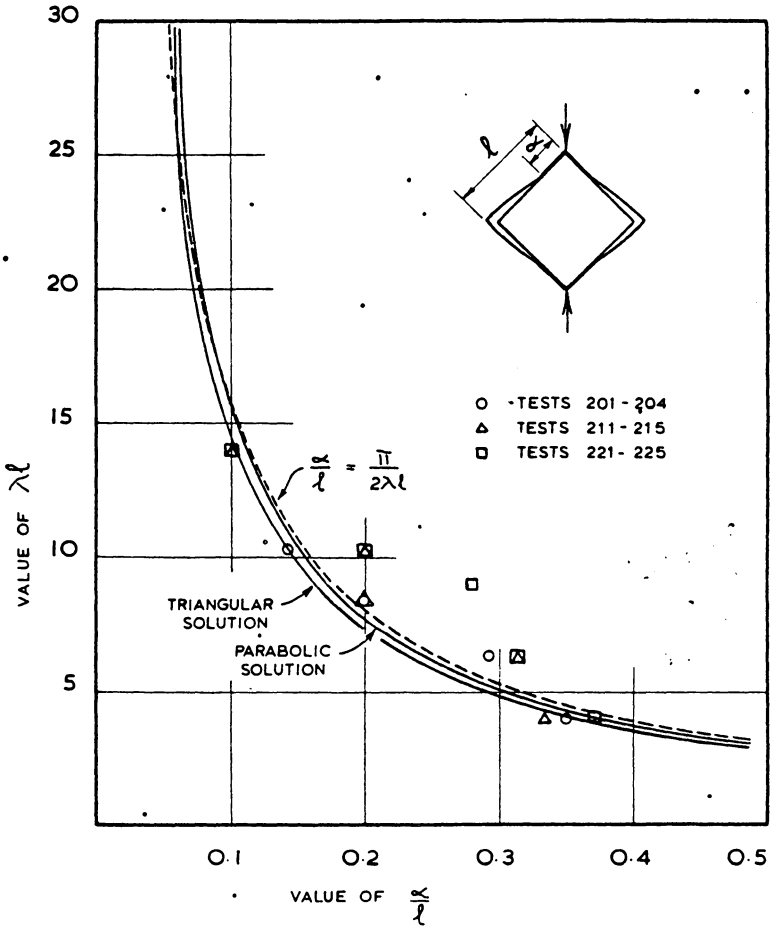

FIGURE 4.4 LENGTH OF CONTACT AS FUNCTION OF $\lambda\ell$ [Ref. No. 32]

closely with the experimental results and other curves; the additional curve is given by

$$\frac{\alpha}{L} = \frac{\pi}{2\lambda\ell} \tag{4.3}$$

which has been adapted from the equation of the length of contact of a free beam on an elastic foundation, subject to a concentrated load.

2. To relate the diagonal stiffness of infill to its length of contact with the frame, a triangularly distributed force is assumed to act over each length of contact, BF, BG, DH and DE, with maximum values at the loaded corners B and D (Fig. 2). A finite difference method may then be used to analyze the stress distribution over the assumed two dimensional infill, and from this, the diagonal strains along the loaded diagonal may be derived. Figure 4.5 shows the result of this calculation for five difference lengths of contact from α/ℓ = 1/8 to 5/8 [Ref. No. 32]. This analysis gives the curves of diagonal strain. The total semi-diagonal strain, measured from the area under each curve, may be used to determine the effective width of the infill for each length of contact. These theoretical results are shown in Fig. 4.6 [Ref. No. 32] where the w/d (i.e., effect width/diagonal length of infill) is plotted as a function of α/ℓ. The experimental values for the effective width of the mortar infills are shown in Fig. 4.6. The discrepancy between experimental and theoretical values was at first attributed to the nonlinear behavior of the mortar which, in the more highly stressed regions near the loaded corners, might have given a sufficient increase in the diagonal strain to account for the reduced stiffness. However, a further series of

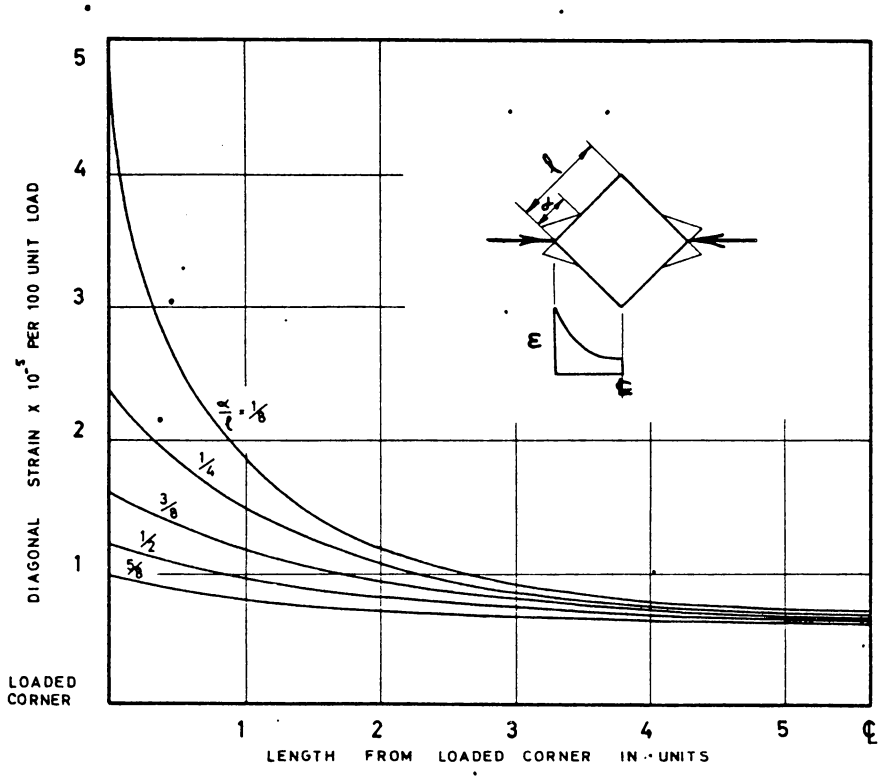

FIGURE 4.5 VARIATION OF DIAGONAL STRAIN FOR DIFFERENT LENGTHS OF CONTACT [Ref. No. 32]

diagonal loading tests on a steel frame with relatively linear material infills, gave results relating w/d and α/ℓ (in Fig. 4.6).

It seems probable that the excessive theoretical predictions are due partly to assuming a triangular interaction distribution which, perhaps, should have been more heavily loaded towards the corner, and partly due to the inexactness of the finite difference method, especially in the region near the application of the load.

3. The effective width may be expressed as a function of $\lambda\ell$, by combining Figs. 4.4 and 4.6, to give the curve in Fig. 4.7 [Ref. No. 32].

Returning to the original problem, it would be reasonable to attempt to predict the stiffness of a laterally loaded frame by assuming each infill to be replaced by an equivalent strut of a width depending on the relative stiffness of the frame and infill. The observed and calculated load deflection relationships for one story and four story reinforced concrete structures with masonry partitions are shown in the next sections.

The disadvantage of the strut model is that it cannot explain the actual failure mechanism of frame-wall system. Details of tests of eighth-scale models of reinforced concrete frames with filler walls were presented by Fiorato, Sozen, and Gamble [12]. These authors also presented their knee-braced frame model for the analyses of these frames. In this model, the wall, after initial cracking, is assumed to act as knee braced on the frame. This study is summarized in the next section because this nonlinear model provides a means for estimating the load capacity of the system after initial shear cracking.

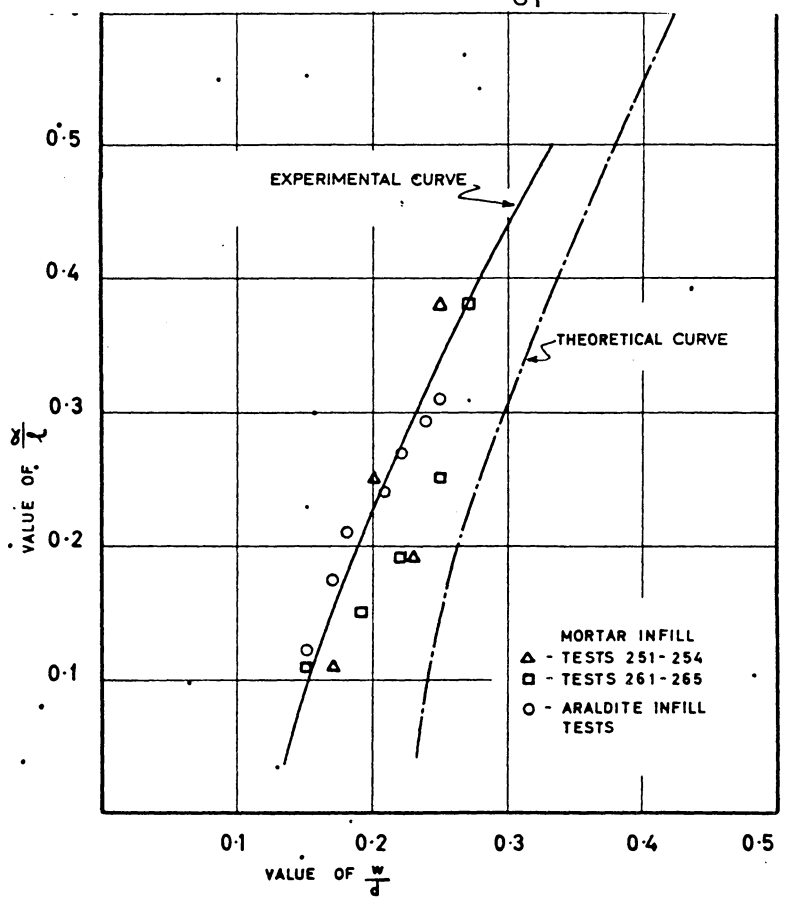

FIGURE 4.6 EFFECTIVE WIDTH AS FUNCTION OF LENGTH OF CONTACT [Ref. No. 32]

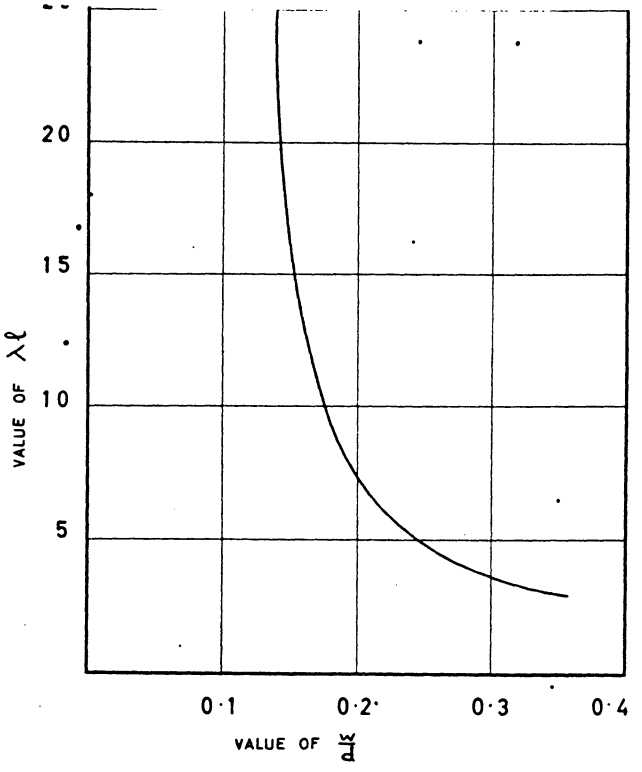

FIGURE 4.7 EFFECTIVE WIDTH AS FUNCTION OF $\lambda\ell$ [Ref. No. 32]

4.5.1 Response of Frames Containing a Cracked Wall

Once shear cracks form in the wall (failure of the compression strut), the rigidity of the frame-wall system is reduced considerably. The behavior of system becomes more dependent upon the material and geometric properties of the frame, which is braced by the segments of wall between the cracks, as described below.

The pattern shown in Fig. 4.8 [12] represents the cracks which are observed at advanced stages of loading. The crack pattern indicates that, after shearing cracks form in the wall, the lower portion of the tension column is braced by the bottom segment of the wall. The upper segment of the wall forms a haunch at the intersection of the compression column with the top beam. Also, in the crack patterns of the columns there is the tendency of unbraced portions of the columns to bend about wall segments. This structural system is referred to as a "knee-braced-frame" system.

The braces are essential in reducing the effective height of the column, allowing higher loads to be carried. In addition, some load is transmitted through the wall segment by friction. The capacity of the braced columns and the force developed through friction of the wall panels represents the major load-carrying mechanism of knee-braced-frame system.

In the following sections a hypothetical model for the braced frame behavior, as described above, is explained, although the model is not strictly representative of the behavior of frame wall systems. Following shear cracking, it does provide a means for estimating quantitatively the load capacity and corresponding deflection of the

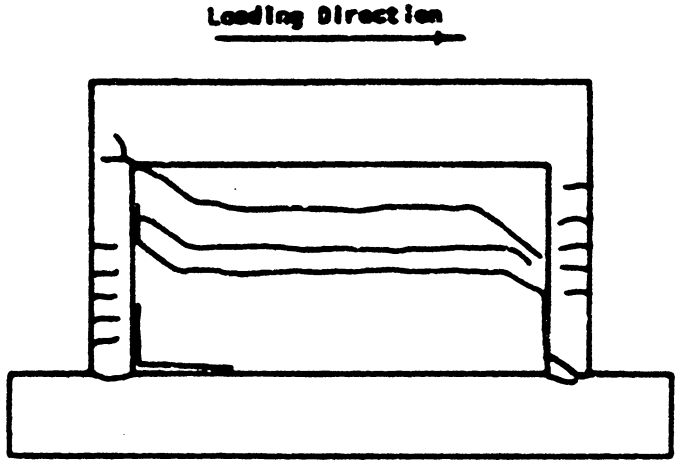

FIGURE 4.8 CHARACTERISTIC CRACK PATTERN FOR ONE-STORY SPECIMENS [Ref. No. 12]

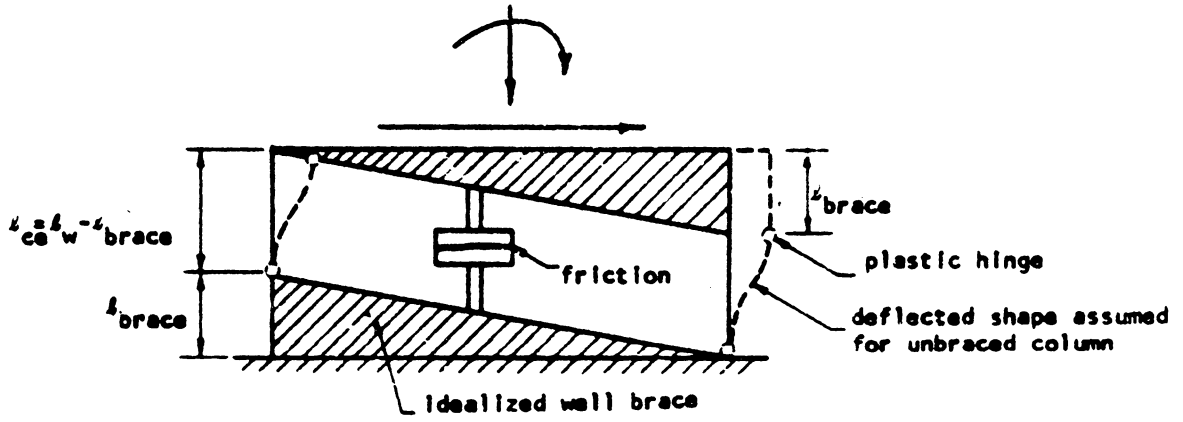

FIGURE 4.9 HYPOTHETICAL MODEL FOR DESCRIBING THE RESPONSE OF THE FRAME-WALL SYSTEM SUBSEQUENT TO CRACKING OF THE WALL [Ref. No. 12]

system. The results obtained using the knee-braced-frame model are presented and discussed in relation to the observed response of test specimens.

4.5.2 A Hypothetical Model for the Frame-Wall System Subsequent to Cracking of the Wall

Based on phenomena observed during tests, the concept of the frame being partially braced by the wall is developed. The effective lengths of the tension and compression columns are reduced by the braces formed from the wall segments.

In calculating the strength of the system, it is assumed that the capacity of the braced columns are developed by yielding of the sections at the ends of clear span of the column. The clear span of the columns is defined in this case as the effective height of the column, ℓ_{ce}, which is the height of the wall panel, ℓ_w, less the height of the wall brace, ℓ_{brace}.

It is difficult to evaluate the amount of load transmitted through the wall by frictional forces. Frictional forces can develop along the interfaces of segments of the cracked wall because of normal forces carried by the wall. No general criteria have been developed for incorporating these effects quantitatively into the framework of the hypothetical model for the system. By not accounting for frictional forces, the capacity of the frame-wall system, as calculated by the knee-braced-frame model, should be underestimated.

Deflections are calculated by assuming that the unbraced portions of the columns are free to distort (Fig. 4.9). This assumption implies

that a significant portion of the wall does not contribute to the stiffness of the system. In the actual structure, only the compression column is free to deflect. However, the restraint of the wall on the upper portion of the tension column is ignored since the segments of cracked wall in the upper portion of the panel may translate.

4.5.3.1 Calculation of the Load Capacity Using the Knee-Braced-Frame Model

This procedure used to calculate the ultimate capacity of the system, based on the assumption of the knee-braced-frame model, is described. Since frictional forces are not included, the calculation of the load capacity of the knee-braced-frame system is reduced to the determination of the load necessary to develop the yield capacity of the braced columns. The following expression is used:

$$V_{max} = \Sigma_1^2 \frac{M_y}{\frac{\ell_{ce}}{2}} = \Sigma^2 \frac{M_y}{\ell_{ce}} \qquad (4.4)$$

V_{max} = total load capacity of structure

M_y = yield capacity of section considered

ℓ_{ce} = effective height of column

V = number of columns

The effects of axial loads, which develop in the columns due to the overturning moment, are not included in calculating the capacity. The increase in the moment capacity of compression column is offset by the decrease in the capacity of the tension column. The yield capacity of the sections should be modified to account for the effect of the

applied vertical load. Two modifications are made to the procedure described to account for constant vertical load: (1) the yield moment used in Eq. (4.4) should be adjusted for the axial column force, and (2) the total shear force is increased to include the frictional force caused by the normal compressive force applied to the wall.

The vertical load on the columns is assumed to be uniformly distributed over the frame-wall cross section in order to calculate the force in the columns and in the wall. Once the force in each column is obtained, the yield capacity is determined from the axial load-moment interaction diagram for the critical section. Equation (4.4) is then used to calculate the capacity of the specimen.

Vertical load also induces a normal force in the wall. From the normal force a horizontal frictional component of force is calculated. The coefficient of friction can be determined on the basis of panel tests. This frictional component is added to the shear force calculated from Eq. (4.4) to give value for load capacity of the structure.

4.5.3.2 Calculation of the Load Capacity Using the Knee-Braced-Frame Model for a One Story Reinforced Concrete Frame with Masonry Partitions

For a one story reinforced concrete structure with masonry partition (Fig. 2.1), the brace height is taken at mid-height of the wall panel in the first story. Thus, the effective height of the columns is equal to half the height of the wall.

It is reasonable to expect that initial shear cracking is developed at the center of the panel. With the formation of a

horizontal shearing crack, the tension column is braced at the mid-height of the panel by the lower wall segment. If shear forces sufficient to crack the lower segment of the wall cannot be carried through the unbraced upper portion of the column, the braced height remains at the mid-height of the panels.

Table 4.1 (reproduced from Fiorato's report [12]) shows the comparison of the observed and calculated results for reinforced concrete frame with masonry partitions (the coefficient of friction is taken to be 0.46 on the basis of masonry panel tests). In almost every case the observed capacity is in excess of the calculated value. As mentioned above, one of the reasons for the underestimation of the observed response is the presence of frictional forces which can develop because of normal forces induced in the wall by the overturning moment on the structure.

4.5.4 Calculation of the Deflection Corresponding to the Load Capacity of the Knee-Braced-Frame Model

The total lateral deflection of an idealized frame-wall system (knee-braced-frame) consists of several components of distortion. These are: (1) the distortion of unbraced portion of the columns, (2) the rotation of the columns resulting from slip of the anchored reinforcement, (3) the bending distortion of the system caused by the applied moment, and (4) the shearing distortion of the intact segments of the walls.

In calculating the deflection of the knee-braced-frame system caused by the distortion of unbraced partitions of the columns, the end

Table 4.1 Observed and Calculated Capacities of Specimens Without Openings [Ref. No. 12]

Mark	Reinforcement Ratio (ρ_g)	Vertical Load		Max. Load Observed (kips)	Calculated[b] (kips)	Observed / Calculated
		kips/column	psi[a]			
S2B	0.022	0	0	9.2	5.1	1.80
S2H	0.022	0	0	5.0	5.1	0.98
S2I	0.022	0	0	6.4	5.1	1.25
F2B	0.022	0	0	5.9	5.1	1.16
F2C	0.022	0	0	5.7	5.1	1.12
F3B	0.034	0	0	6.1	6.0	1.02
F3C	0.034	0	0	7.2	6.0	1.20
P2B	0.022	5.0	210	8.4	9.2	0.91
P2C	0.022	5.0	210	8.5	9.2	0.92
P2D	0.022	2.5	105	7.7	7.2	1.07
P2E	0.022	2.5	105	7.3	7.2	1.01
M2B	0.022	0	0	17.9	10.2	1.75
M2C	0.022	0	0	17.0	10.2	1.67
M2D	0.022	2.5	80	20.2	15.1	1.34
M2E	0.022	5.0	160	25.9	19.3	1.34

[a]Vertical load uniformly distributed over frame-wall cross section (transformed area)

[b]Based on knee-braced-frame hypothesis

conditions of the columns are idealized as shown in Fig. 4.10. It is assumed that the columns are connected by a rigid beam at the top. At the point where the columns are bending about the wall brace, a joint is assumed with the rotational stiffness indicated in Fig. 4.10. With this system the deflection is calculated at the load corresponding to the formation of the mechanism at which the columns are considered to be fully cracked.

Slip of the reinforcement at the points of plastic hinging contributes a significant portion of the total column deflection. The deflection caused by slip can be calculated as

$$a = \frac{a_b \, \ell_{ce}}{0.9 \, d} \tag{4.5}$$

a = deflection due to slip

a_b = slip $= \frac{\ell_b \, f_y}{2E_s}$, and $\ell_b = \frac{d_b \, f_y}{4f_b}$

ℓ_{ce} = effective height of column

d = effective depth of column

d_b = diameter of bar

f_y = yield strength of reinforcement

f_b = unit bound stress

ℓ_b = development length

E_s = Young's modulus of elasticity for steel bar

Equation (4.5) assumes that the rotation due to slip occurs about a point on the cross section located 0.9 d from the level of reinforcement.

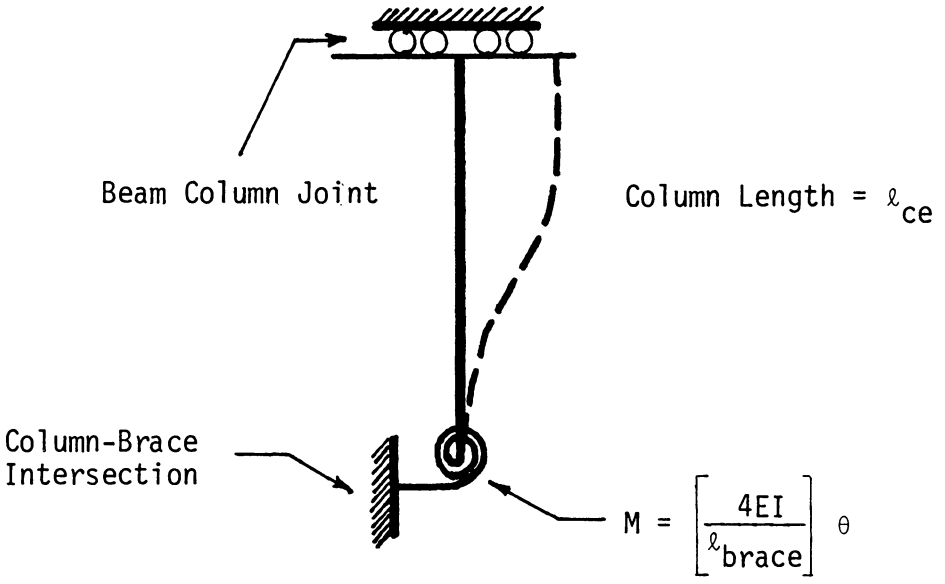

Figure 4.10 Idealization of Column End Condition Used in Calculating Deflections

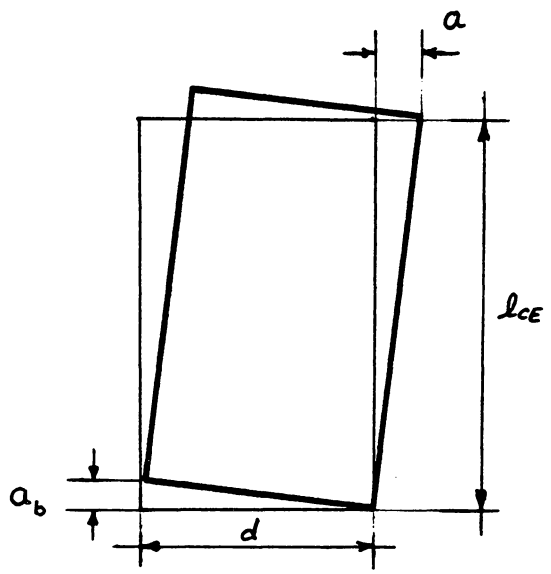

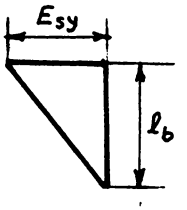

$$\epsilon_{sy} = \frac{f_y}{E_s}$$

$$a_b = \ell_b \frac{\epsilon_{sy}}{2} = \ell_b \frac{f_y}{2E_s}$$

Figure 4.11 Slip of the Reinforced Concrete in the Tension Column.

The final two components of the deflection are the bending distortion of entire system and shearing distortion of the intact segments of the walls. The calculation of these quantities was explained in Chapter 2. Only modifications should be made because of cracking. For calculating the bending distortion, the moment of inertia of the fully cracked frame-wall structures should be used in the equations derived in Chapter 2.

4.5.6 Comparison of Calculated and Observed Response for a One Story Reinforced Concrete Frame with Masonry Partitions

The observed and calculated load-deflection relationships for a one story structure reinforced with masonry partitions are shown in Fig. 4.12 [12]. The calculation is based on the strut model before shearing cracks, then knee-braced-frame model provides a fair estimate of the response after shear cracks. The deflection calculation at the point of maximum load is somewhat lower than the observed values; however, the calculation of deflection is very sensitive to the value of the effective length of columns.

In calculating the capacity of the structure, it is assumed that plastic hinges form at the ends of unbraced column segments. The formation of these hinges in the compression column was observed. In the tension column, hinging was less obvious. However, strains measured on the reinforcement at the top of the tension column indicated that the yield capacity of the section was developed prior to failure.

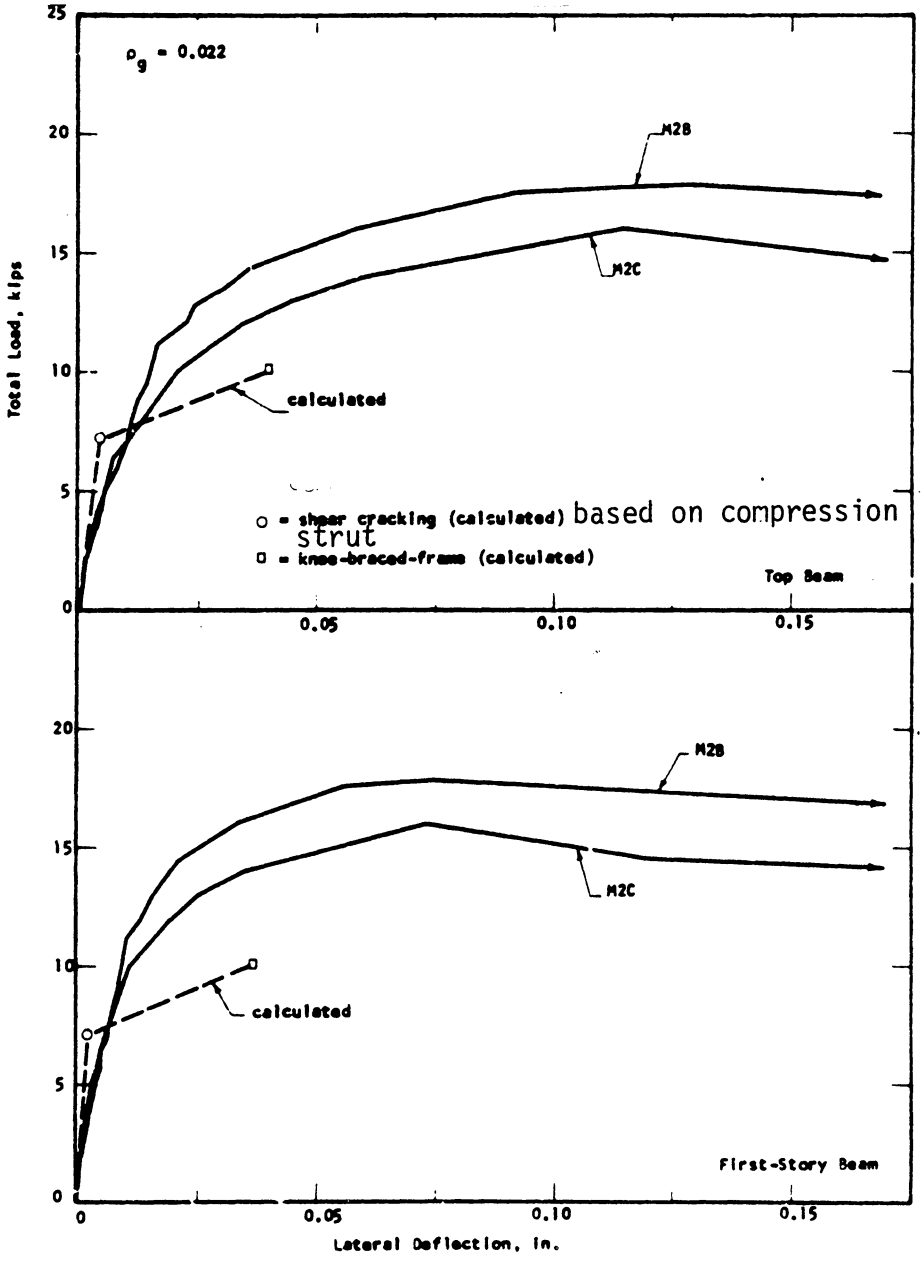

FIGURE 4.12 LOAD-DEFLECTION RELATIONSHIPS FOR SPECIMENS M2B AND M2C [Ref. No. 12]

4.5.7.1 Observed Response for a Five Story Reinforced Concrete Frame with Masonry Partitions

The additional overturning moment acting on the first story of five-story specimens causes axial column forces which decreases the stiffness of the tension column and increases the stiffness of the compression column. Because of these effects, the behavior of the five-story structures differ somewhat from that of the one-story structures.

Flexural cracking is observed prior to shear cracking in the five-story specimens. At later stages of loading, shearing cracks extend through the wall, partitioning the wall into segments. The lower segment of the cracked wall serves to brace the tension column near the mid-height of the wall. A knee brace also formed between the compression column and first story beam, thereby completing the braced-column system. Although the braced system which formed is similar to that observed in the one-story specimens, the failure mechanism which formed in the one-story specimens is not developed completely in the five-story structures.

The presence of the axial forces in the columns leads to a different response. At loads nearing ultimate, the reinforcement in the tension column has yielded, as determined from the measured strains. Therefore, the moment and shear capacity of the tension column are reduced considerably. Ideally, the tension column is acting as a flexible element which is being pulled against the segments of the wall panel by a force applied at the top of the column. On the other hand, the capacity of the compression column is increased by an axial compressive force. Within the range of axial forces which could have

been developed, the moment-thrust relationship for the column cross sections can be practically linear. Thus, it is reasonable to assume that the decrease in moment capacity of the tension column is offset by the increase in capacity of the compression column. It is difficult to evaluate quantitatively exactly how much axial thrust is developed in the compression column because it is possible that normal forces in the wall participated in resisting the overturning moment.

4.5.7.2 Comparison of Calculated and Observed Response for a Five Story Reinforced Concrete Frame with Masonry Partitions

The calculated and measured load-deflection curves are shown in Fig. 4.13 [12] for the deflection of the first story top beam. The calculation is based on the strut model before shearing cracks, then the knee-braced frame model provides a fair estimate of the response after shear cracking. Also, the capacity of the specimen based on linear analysis (Eq. (2.4)) is included in Fig. 4.13. However, the linear analysis does not adequately describe the deformation of the structures. Comparison of the calculated and observed deflections at the first story indicates a fairly good agreement, considering the sensitivity of the results to the effective length of the columns.

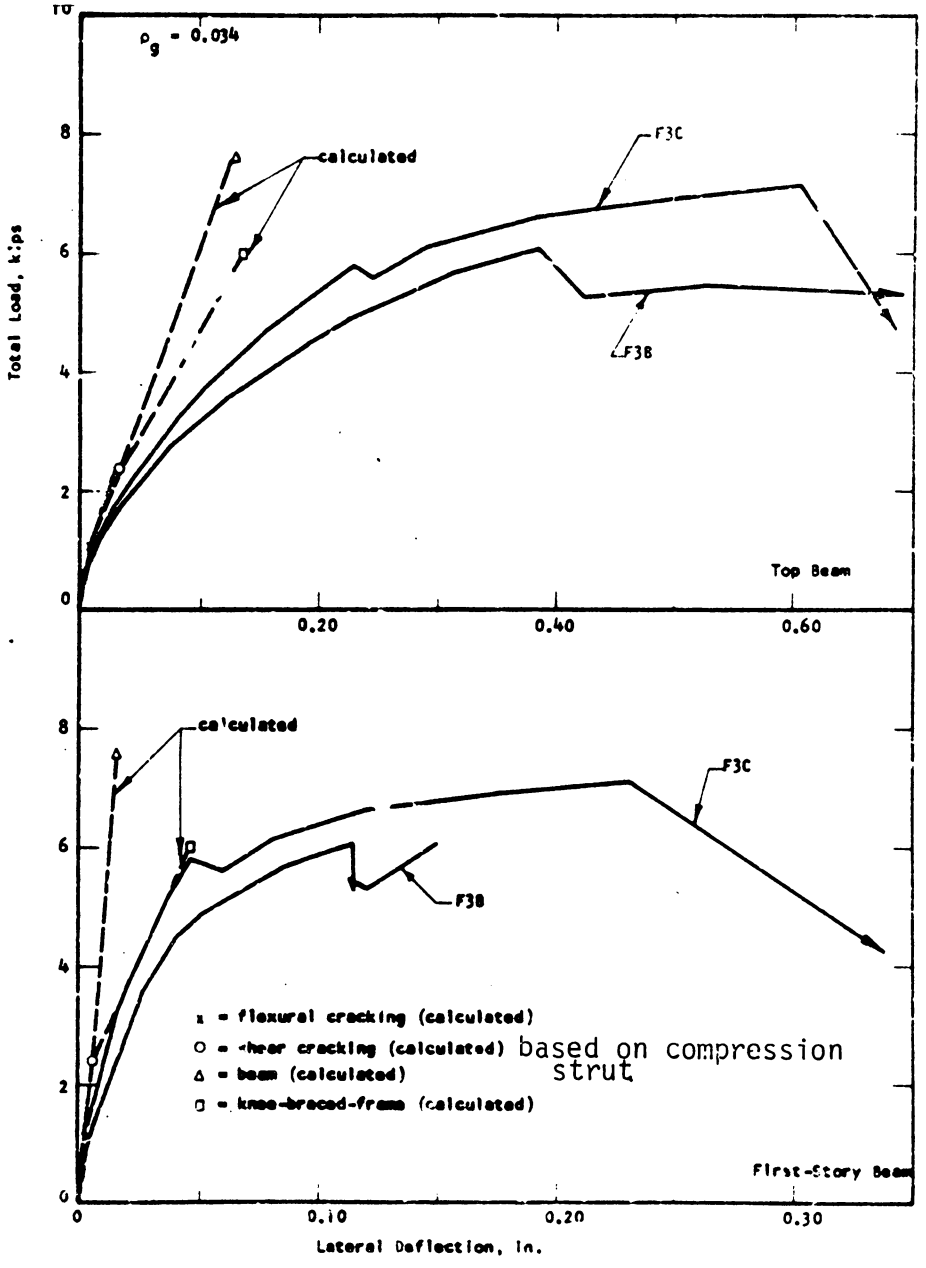

FIGURE 4.13 LOAD-DEFLECTION RELATIONSHIPS FOR SPECIMENS F3B AND F3C [Ref. No. 12]

Chapter 5

DYNAMIC ANALYSIS OF NONLINEAR STRUCTURES

5.1 Introduction

This chapter deals with the dynamic analysis of nonlinearly structures, that is, frame with filler panels with gaps. The method of solution of the equilibrium equations for dynamic analysis is presented. The computer programs that can perform nonlinear dynamic analyses of a plane frame with filler panels are discussed. Several examples are summarized to illustrate the application of the techniques that are explained, and to illustrate the effects of varying certain parameters in the analyses.

5.2 The Methods of Solution

Numerous methods have been suggested for the nonlinear dynamic analysis of a structural system. The method that has received considerable attention in the literature recently is the linear acceleration method [7,35,36]. This method involves, as the name implies, the assumption of a linear variation in acceleration over a time interval. This method is summarized below [7,36].

The matrix equation of motion for the structural system at time $t - \Delta t$ can be written as follows [7]. (Note that it has been assumed that there is no change in mass matrix over the time step Δt. In addition, as discussed later in this chapter, it is also assumed that there is no change in the damping matrix C.)

$$\underset{\sim}{M}\,\ddot{\underset{\sim}{D}}_{t-\Delta t} + \underset{\sim}{C}\,\dot{\underset{\sim}{D}}_{t-\Delta t} + \underset{\sim}{S}_{t-\Delta t}\,\underset{\sim}{D}_{t-\Delta t} = \underset{\sim}{A}_{t-\Delta t} \tag{5.1}$$

$\underset{\sim}{M}$ = mass matrix

$\underset{\sim}{C}$ = damping matrix

$\underset{\sim}{S}_{t-\Delta t}$ = stiffness matrix

$\underset{\sim}{A}_{t-\Delta t}$ = vector of applied nodal actions

$\ddot{\underset{\sim}{D}}_{t-\Delta t}$ = vector of nodal accelerations

$\dot{\underset{\sim}{D}}_{t-\Delta t}$ = vector of nodal velocities

$\underset{\sim}{D}_{t-\Delta t}$ = vector of nodal displacements

Similarly, the matrix equation of motion for time t can be written as:

$$\underset{\sim}{M}(\ddot{\underset{\sim}{D}}_{t-\Delta t} + \Delta\ddot{\underset{\sim}{D}}_{t}) + \underset{\sim}{C}(\dot{\underset{\sim}{D}}_{t-\Delta t} + \Delta\dot{\underset{\sim}{D}}_{t})$$

$$+ \underset{\sim}{S}_{t}(\underset{\sim}{D}_{t-\Delta t} + \Delta\underset{\sim}{D}_{t}) = \underset{\sim}{A}_{t-\Delta t} + \Delta\underset{\sim}{A}_{t} \tag{5.2}$$

where

$\underset{\sim}{S}_{t}$ = stiffness matrix

$\Delta\underset{\sim}{A}_{t}$ = vector of changes in applied nodal action

$\Delta\ddot{\underset{\sim}{D}}_{t}$ = vector of changes in nodal accelerations

$\Delta\dot{\underset{\sim}{D}}_{t}$ = vector of changes in nodal velocities

$\Delta\underset{\sim}{D}_{t}$ = vector of changes in nodal displacements

The changes in the above vector quantities are over the time interval Δt.

If Equation (5.1) is subtracted from Equation (5.2), and the assumption is made that the structures behave linearly in the small time interval Δt, that is, $\lim_{\Delta t \to 0} S_t = S_{t-\Delta t}$, then the resulting incremental equation of motion becomes:

$$\underset{\sim}{M}\,\Delta\ddot{\underset{\sim}{D}}_t + \underset{\sim}{C}\,\Delta\dot{\underset{\sim}{D}}_t + \underset{\sim}{S}_{t-\,t}\,\Delta\underset{\sim}{D}_t = \Delta\underset{\sim}{A}_t \tag{5.3}$$

Since the acceleration is assumed to vary linearly over the time step t, the incremental velocity and displacement at time t can be found by integration. These values are:

$$\Delta\dot{\underset{\sim}{D}}_t = \Delta t\;\ddot{\underset{\sim}{D}}_{t-\Delta t} + \frac{\Delta t}{2}\,\Delta\ddot{D}_t \tag{5.4}$$

$$\Delta\underset{\sim}{D}_t = \Delta t\;\dot{\underset{\sim}{D}}_{t-\Delta t} + \frac{(\Delta t)^2}{2}\,\ddot{\underset{\sim}{D}}_{t-\Delta t} + \frac{(\Delta t)^2}{6}\,\Delta\ddot{\underset{\sim}{D}}_t \tag{5.5}$$

If the above equations are solved for incremental acceleration and velocity, one obtains:

$$\Delta\ddot{\underset{\sim}{D}}_t = \frac{6}{(\Delta t)^2}\,\Delta\underset{\sim}{D}_t + \underset{\sim}{P}_{t-\Delta t} \tag{5.6}$$

where

$$\underset{\sim}{P}_{t-\Delta t} = -\frac{6}{\Delta t}\,\dot{\underset{\sim}{D}}_{t-\Delta t} - 3\ddot{\underset{\sim}{D}}_{t-\Delta t}$$

$$\Delta\dot{\underset{\sim}{D}}_t = \frac{3}{\Delta t}\,\Delta\underset{\sim}{D}_t + Q_{t-\Delta t} \tag{5.7}$$

where

$$Q_{t-\Delta t} = -3\dot{\underset{\sim}{D}}_{t-\Delta t} - \frac{\Delta t}{2}\,\ddot{\underset{\sim}{D}}_{t-\Delta t}$$

Equations (5.6) and (5.7) can be substituted into the incremental equation of motion (5.3) to obtain the following algebraic equations:

$$\underset{\sim}{S}^*_{t-\Delta t}\,\Delta\underset{\sim}{D}_t = \Delta\underset{\sim}{A}^*_t \tag{5.8}$$

in which the pseudo stiffness matrix is given by

$$\underset{\sim}{S}^*_{t-\Delta t} = \frac{6}{(\Delta t)^2}\,\underset{\sim}{M} + \frac{3}{\Delta t}\,\underset{\sim}{e} + \underset{\sim}{S}_{t-\Delta t} \tag{5.9}$$

and the pseudo action vector is given by

$$\Delta \underset{\sim}{A}^{*}_{t} = \Delta \underset{\sim}{A}_{t} - M\, P_{t-\Delta t} - C\, Q_{t-\Delta t} \tag{5.10}$$

The primary case of this study is a structure excited by ground motions. The equations of motion for a structural system subjected to ground acceleration are given as:

$$\Delta A_{t} = - M\, \Delta \ddot{\underset{\sim}{D}}_{Gt} \tag{5.11}$$

Substituting Eq. (5.11) into Eq. (5.10) yields

$$\Delta \underset{\sim}{A}^{*}_{t} = - M[\Delta \ddot{\underset{\sim}{D}}_{Gt} + \underset{\sim}{P}_{t-\Delta t}] - \underset{\sim}{C}\, Q_{t-\Delta t} \tag{5.12}$$

In Equations (5.11) and (5.12), $\Delta \ddot{\underset{\sim}{D}}_{Gt}$ represents the change in ground accelerations over the time interval Δt.

5.3 Nonlinear Dynamic Analyses of a Plane Frame with Filler Panel

5.3.1 The Summary of the Computer Program for Nonlinear Dynamic Analyses of a Plane Frame with Filler Panels

As mentioned in section 1.4.1, Kost [22] developed a computer program to perform nonlinear dynamic analyses of a plane frame with filler panels. The source of nonlinearity was the presence of gaps between the side and tops of the panels and the frame. He also developed a program for the analysis of a plane frame with monolithic panels, that is, no gaps.

For both linear and nonlinear cases, the analytical model of the frame members of the structure consisted of conventional plane-frame elements. The filler panel was represented by finite element meshes using the 16 degrees of freedom Oakberg-Weaver rectangular plane stress element (Fig. 5.1). Special elements were developed for panel corners

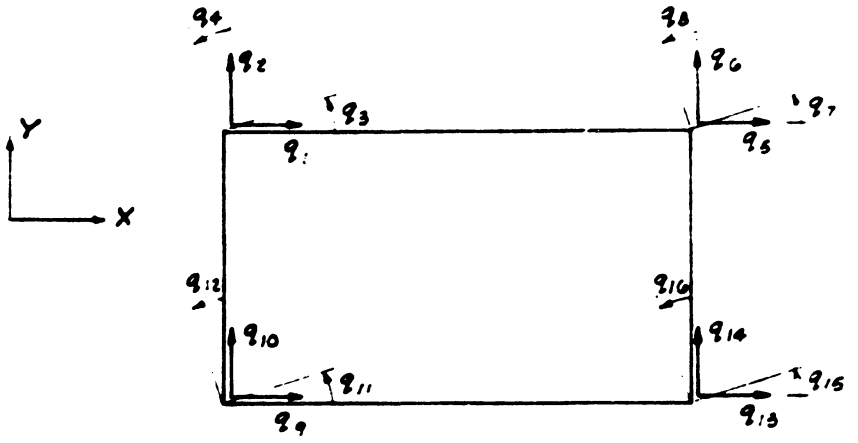

FIGURE 5.1 16 DEGREE OF FREEDOM OAKBERG-WEAVER ELEMENT
[Ref. No. 22]

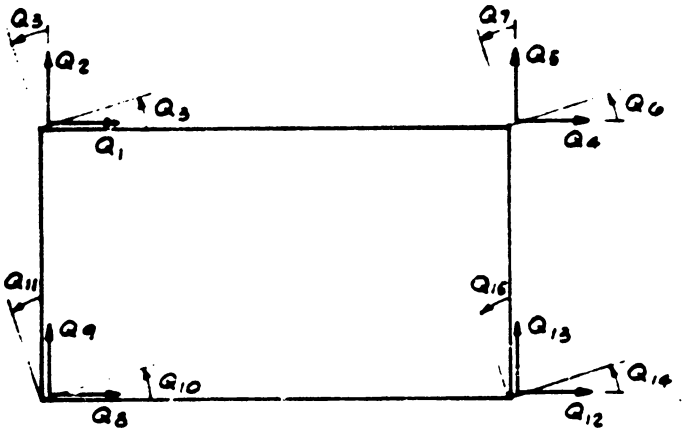

FIGURE 5.2 MODIFIED 15 DEGREE OF FREEDOM UPPER LEFT-HAND CORNER ELEMENT
[Ref. No. 22]

by performing coordinate transformation (Fig. 5.2). In addition, to reduce the number of degrees of freedom and the problem size (Fig. 5.3), a static condensation procedure was employed for the filler panels. By the use of this procedure, all filler panel interior degrees of freedom and certain edge degrees of freedom were eliminated. This resulted in a filler panel composed of one or more elements with three degrees of freedom per edge node. These degrees of freedom are an x-translation, y-translation, and a rotation about z-axis, which are compatible with the frame degrees of freedom (Fig. 5.4).

A computer program was developed for the dynamic analysis of the structure with gaps between the filler panels and the frames. The equations of motion were solved by the incremental linear acceleration method. Criteria were developed for the monitoring of gap closing and opening, and the stiffness matrix was modified upon gap closing and opening by the insertion and removal, respectively, of imaginary links between contacting nodes. Provisions were also included for specifying the coefficients of the damping matrix on the basis of a linear analysis. This choice was made because most experience in the field of structural engineering has been in this form of damping. For the same reason, it is desirable to relate the amount of damping in the nonlinear case to that of modal damping in the linear case.

If it is assumed for the nonlinear case that damping is constant, does not change with time, the damping can be computed on the basis of performing the analysis for frequencies and mode shapes corresponding to a frame and panel with gaps. The details were discussed in Chapter 3.

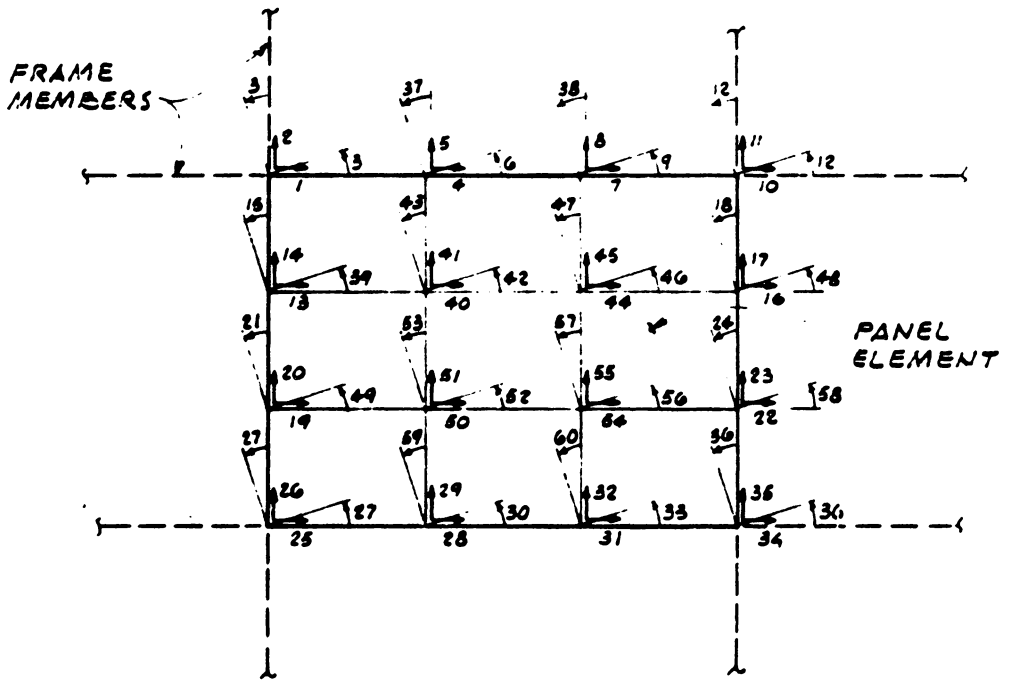

FIGURE 5.3 FILLER PANEL SHOWING DEGREES OF FREEDOM

[Ref. No. 22]

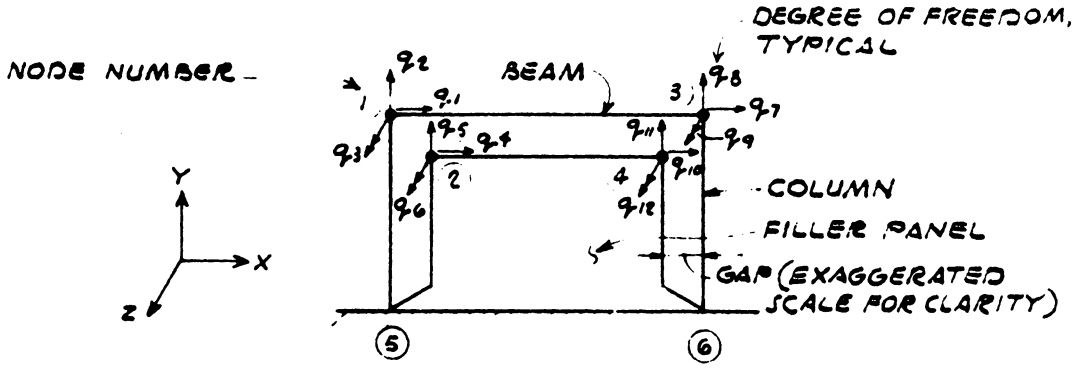

a. STRUCTURE BEFORE LOADING

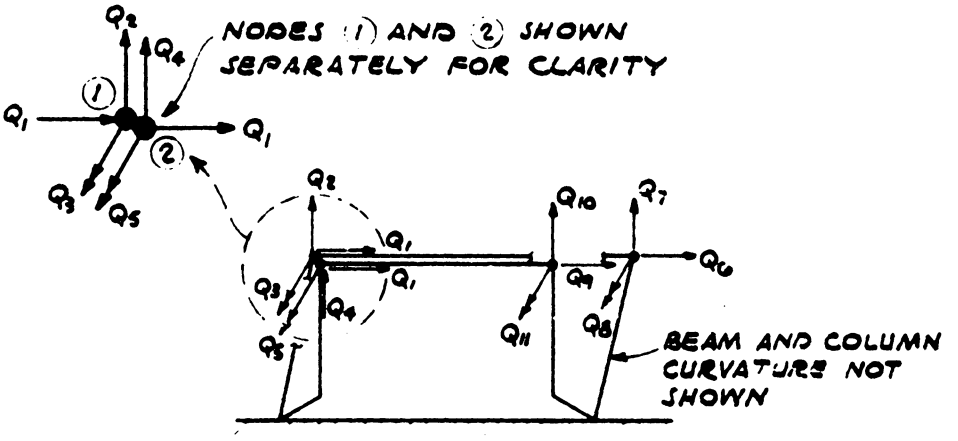

b. STRUCTURE DURING RESPONSE AT INSTANT OF GAP CLOSURE

FIGURE 5.4 EXAMPLE STRUCTURE SHOWING GAP CLOSURE
[Ref. No. 22]

A series of analyses were performed on a four-story single bay structure to illustrate the application of the nonlinear program and compared to linear analysis. Three different cases were analyzed. In the first case (structure A), the structure was assumed to have no filler panels; that is, the frame alone was analyzed. In the second case (structure B), the structure was assumed to consist of a frame and monolithic filler panels. In the third case (structure C), the structure was assumed to consist of frame and filler panels with large gaps between the sides and tops of the panels and frames. The properties of the panel and frame are summarized in Table 5.1.

Based on results of investigations summarized in Table 5.2, it was concluded that it is not necessary to use more than six elements per panel to compute the response of structure with good accuracy. Periods from the frequency analyses are shown in Table 5.3. The result for two elements per panel were quite close to the higher number of elements per panel. For example, the first mode period using two elements per panel was only 0.7% less than for 15-element case; and fourth mode period was only 2.4% less than that for the 15-element case.

The periods of vibration for the structures are presented in Table 5.4 and the mode shapes for the horizontal displacements of left nodes at each story level listed in Table 5.5. Note the period of vibration of the first mode of structure with filler wall panels and large gaps (structure C) is 0.3505 seconds, the period of the first mode of the frame only (structure A) is 0.4494 seconds, and the period of first mode of structure with monolithic filler panels (structure B) is 0.08418 seconds. As expected, because of the rigid nature of

Table 5.1 Properties of Frame and Filler Panels
[Ref. No. 22]

Beams:	Length (total)	20.0 ft
	Axial area	2.451 ft^2
	Shear area	1.389 ft^2
	Moment of inertia	0.308 ft^4
	Modulus of elasticity	0.432 x 10^6 k/ft^2
	Poisson's ratio	0.28
Columns:	Lenth (total)	9.0 ft
	Axial area	1.556 ft^2
	Shear area	1.296 ft^2
	Moment of inertia	0.176 ft^4
	Modulus of elasticity	0.432 x 10^6 k/ft^2
	Poisson's ratio	0.28
Walls:	Length (total)	20.0 ft
	Height (total)	9.0 ft
	Thickness (equivalent)[a]	0.267 ft
	Modulus of elasticity	0.216 x 10^6 k/ft^2
	Poisson's ratio	0.250
Mass at roof (frame only)[b,c]		0.510 $k\text{-}sec^2/ft$
Mass at floors (frame only)[c]		0.570 $k\text{-}sec^2/ft$
Mass at roof (frame and walls)[b,c]		0.580 $k\text{-}sec^2/ft$
Mass at floors (frame and walls)[c]		0.710 $k\text{-}sec^2/ft$

[a]The equivalent wall thickness was assumed to be equal to the average cross-sectional width of the hollow blocks.

[b]Used in one-story example.

[c]Used in four-story example.

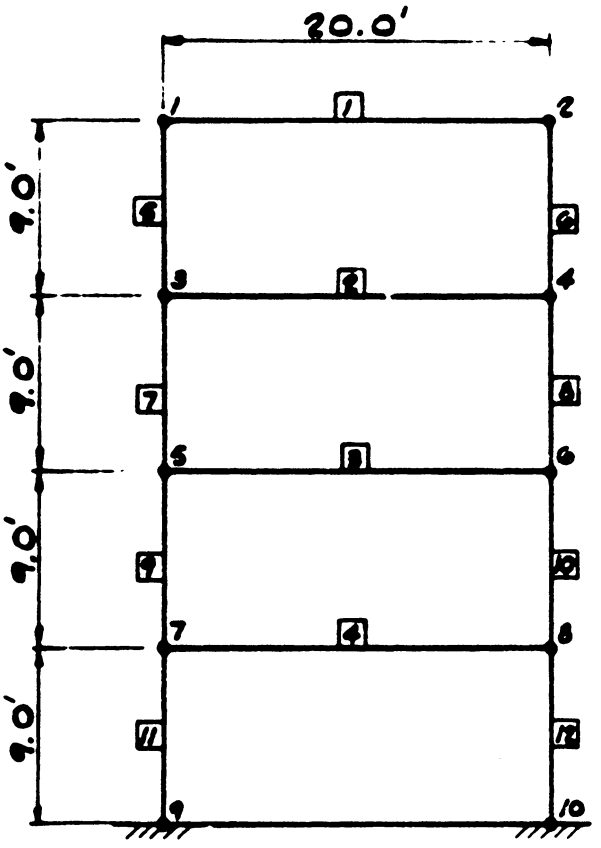

FIGURE 5.5 STRUCTURE A (FRAME ONLY)

[Ref. No. 22]

Table 5.2 Mode Shapes for Four-Story Structure [Ref. No. 22]

Mode	Number of Panel Elements	Story R	Story 3	Story 2	Story 1
1	0	1.0000	0.8422	0.5707	0.2347
	1	1.0000	0.7545	0.4731	0.2001
	2	1.0000	0.7595	0.4813	0.2092
	3	1.0000	0.7600	0.4822	0.2102
	6	1.0000	0.7618	0.4845	0.2120
	10	1.0000	0.7621	0.4849	0.2124
	15	1.0000	0.7625	0.4856	0.2130
2	0	-0.9609	0.1379	1.0000	0.7370
	1	-0.9480	0.1692	1.0000	0.8678
	2	-0.9620	0.1482	1.0000	0.8928
	3	-0.9628	0.1455	0.9983	0.8937
	6	-0.9634	0.1409	1.0000	0.8998
	10	-0.9627	0.1392	0.9980	0.8992
	15	-0.9637	0.1380	0.9991	0.9019
3	0	0.6422	-0.9218	-0.0578	1.0000
	1	0.6568	-0.8404	-0.2170	1.0000
	2	0.6772	-0.8348	-0.2454	1.0000
	3	0.6801	-0.8324	-0.2482	1.0000
	6	0.6774	-0.8308	-0.2561	1.0000
	10	0.6788	-0.8289	-0.2580	1.0000
	15	0.6782	-0.8282	-0.2604	1.0000
4	0	0.3163	-0.7790	1.0000	-0.8421
	1	0.3550	-0.8327	1.0000	-0.6732
	2	0.3731	-0.8444	1.0000	-0.6585
	3	0.3770	-0.8462	1.0000	-0.6569
	6	0.3767	-0.8509	1.0000	-0.6532
	10	0.3792	-0.8525	1.0000	-0.6519
	15	0.3792	-0.8538	1.0000	-0.6509

Table 5.3 Periods for Four-Story Structure (seconds) [Ref. No. 22]

Number of Panel Elements	Mode			
	1	2	3	4
0	0.44909	0.14009	0.077310	0.054606
1	0.083054	0.025362	0.014333	0.011275
2	0.084220	0.026105	0.014947	0.011897
3	0.0084297	0.026173	0.014986	0.011930
6	0.084776	0.026443	0.015188	0.012123
10	0.084818	0.026481	0.015205	0.012135
15	0.084841	0.026547	0.015256	0.012187

Table 5.4 Periods for Structures A, B, and C (seconds) [Ref. No. 22]

Mode	Structure A	Structure B	Structure C
1	0.4494	0.08418	0.3505
2	0.1401	0.02610	0.1245
3	0.07731	0.01495	0.07869
4	0.05461	0.01190	0.05977

Table 5.5 Mode Shapes for Structures A, B, and C [Ref. No. 22]

Mode	Story	Structure A	Structure B	Structure C
1	R	1.0000	1.0000	0.9997
	3	0.8422	0.7595	0.8379
	2	0.5706	0.4814	0.6029
	1	0.2346	0.2092	0.2936
2	R	-0.9608	-0.9620	0.9977
	3	0.1380	0.1482	-0.1148
	2	1.0000	1.0000	-0.8414
	1	0.7369	0.8928	-0.7224
3	R	0.6422	0.6772	0.6788
	3	-0.9217	-0.8348	-0.9604
	2	-0.0576	-0.2454	-0.6636
	1	1.0000	1.0000	0.9933
4	R	0.3163	0.3732	0.2577
	3	-0.7790	-0.8444	-0.6976
	2	1.0000	1.0000	0.9885
	1	-0.8422	-0.6585	-0.7513

structure with partitions as compared to a frame structure, there is a considerable decrease in the period for the case of the frame with monolithic panels.

In the calculation of the dynamic response, two cases of ground acceleration were used: an approximation of a step function (Fig. 5.6a) and a cyclic function (Fig. 5.6b). The cyclic input approximates a sine wave digitized at a time interval of 0.025 seconds. For both cases of input, responses were calculated at time intervals of 0.01 seconds, and a damping ratio of 0.03 was assumed in all modes.

The maximum values of the displacements of three structures due to the step function are summarized in Table 5.6. As expected when the fundamental period of structure is closer to period of input motion, then the displacements are greater than the displacements of the other two structures.

A series of analyses were performed to illustrate the effects of various gap widths on the response of the structure. The gap widths selected for the four analyses were 0.005, 0.01, .015, and 0.020 feet. These widths were selected as a fraction of the interstory displacement at the time of maximum response of the structure subjected to the cyclic input.

Selected results of these analyses are presented in Table 5.8, listing the maximum displacements at each level for each analysis. Note that as the gap widths become smaller, the limiting case is that of the monolithic frame and panel (structure B). As the gap widths become larger, the limiting case is that of a frame and panel with large gaps (structure C). Displacements of the structure with frame

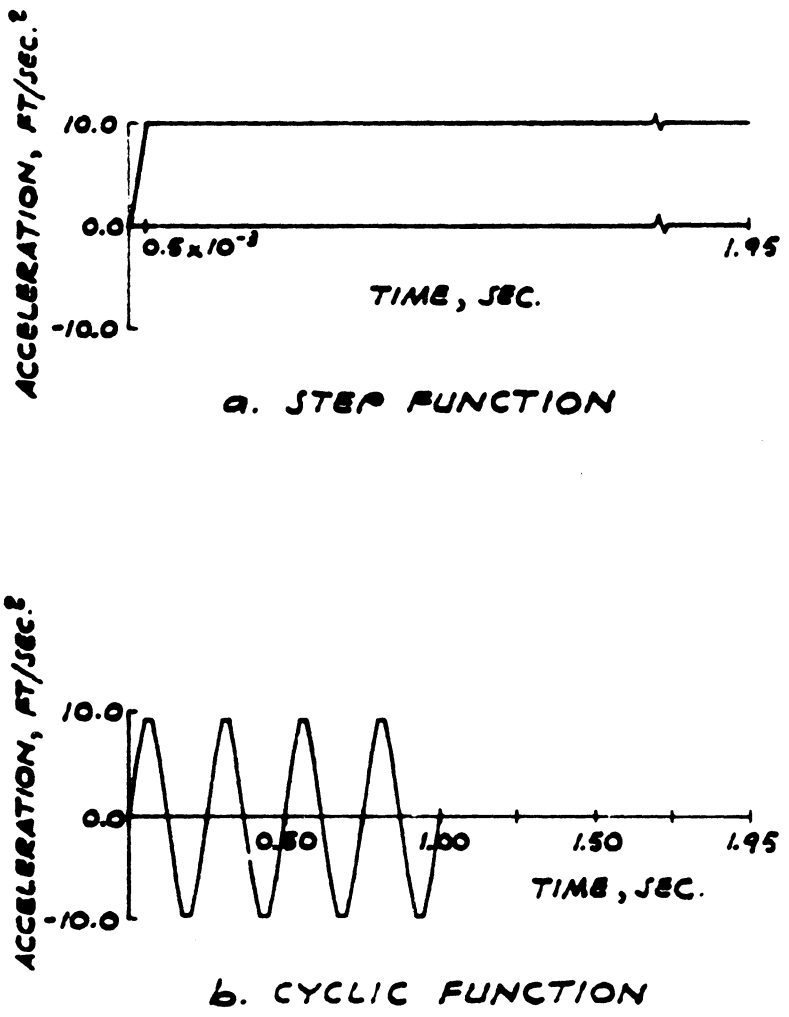

FIGURE 5.6 GROUND ACCELERATIONS FOR FOUR-STORY EXAMPLE [Ref. No. 22]

Table 5.6 Maximum Story Displacements for Step Function (feet) [Ref. No. 22]

Story	Structure		
	A	B	C
R	-0.122	-0.00449	-0.0745
3	-0.106	-0.00352	-0.0645
2	-0.0748	-0.00237	-0.0486
1	-0.0323	-0.00112	-0.0250

Table 5.7 Maximum Story Displacements for Cyclic Function (feet) [Ref. No. 22]

Story	Structure		
	A	B	C
R	-0.0723	-0.00334	-0.0862
3	-0.0596	-0.00259	-0.0706
2	-0.0387	-0.00172	-0.0490
1	-0.0147	-0.000799	-0.0226

Table 5.8 Displacements for Varying Gap Widths (feet) [Ref. No. 22]

Structure	Level 1	2	3	R
Monolithic frame and panel (Structure B)	-0.0008	-0.0017	-0.0026	-0.0033
0.005 ft gap width	-0.0138	-0.0270	-0.0410	-0.0481
0.010 ft gap width	-0.0237	-0.0465	-0.0706	0.0917
0.015 ft gap width	0.0317	0.0660	0.0966	0.1236
0.020 ft gap width	-0.0259	-0.0493	0.0702	-0.0880
Large gap width (Structure C)	-0.0226	-0.0490	-0.0706	-0.0862
Frame only (Structure A)	-0.0147	-0.0387	-0.0596	-0.0723

only (structure A) have also been included.

From the above analyses it can be seen that different gap widths can have a significant effect on the dynamic response of a structure. For the same structure with different width gaps, the results are likely to be different; that is, a different width might produce maximum response. It is not possible to determine in advance what the critical widths will be for a given structure [22].

Chapter 6

SUMMARY AND CONCLUSIONS OF FRAMES WITH FILLER WALLS

6.1 Observed Response

The stages of response observed in the frames with filler walls are summarized in this section.

The initial response of the specimens is primarily dependent on the shearing rigidity of the filler walls. As indicated by the load-deflection relationships, the initial response is practically linear. It is possible to calculate the initial load-deflection relationship using a standard elastic analysis for the bending and shearing components of the total deflection. Linear response is terminated by cracking of the filler wall. Flexural or shear cracking of the wall causes the first significant changes in the initial response of the structures. The rigidity of the frame wall system is reduced considerably, with the behavior of the structures becoming more dependent on the physical properties of the frame and the wall.

For relative high moment-to-shear ratio of the applied load, flexural cracks form prior to shearing cracks. For five story reinforced concrete structures with masonry partitions, flexural cracks developed prior to shearing cracks, while shearing cracks developed first in the one story structures.

With the formation of flexural cracks in a wall of the structure, the wall can be replaced by a diagonal strut. Equivalent strut can be determined based on the relative frame-wall stiffness. The frame

wall system is considered as a pin-jointed diagonally braced frame.

With the formation of shearing cracks in the walls, a system of braced columns develop which governs the response of the system. The column in the lower story of the frames are being braced by segments of the cracked wall. The braces reduce the effective height of the column, allowing the frame to carry higher loads than it could without the braces. The braced columns carry most of the applied load, while some of the load is transmitted through the wall segments by frictional forces.

The influence of openings in the filler walls is to decrease the strength and stiffness of the structure. However, it is significant that the strength of the structures are not decreased in proportion to the reduction in the area of the wall. The primary influence of the opening is that it affects the location of brace height and equivalent strut. Further analytical work and research are needed to evaluate the effect of openings.

6.2 Conclusions

A number of conclusions can be made regarding the structural affects of nonstructural partitions. These conclusions are based on experimental data obtained from five story, four story, and one story test structures. The conclusions regarding frame properties follow.

For reinforced concrete structures, the stiffness and period of the bare frame are remarkably variable. The stiffness can assume a number of values between well defined limiting values. The limiting values are based upon the condition of the frame, whether the frame

is fresh and uncracked or old, having fully developed hairline cracks throughout the tensile areas in the concrete. On the basis of these assumptions, the limiting cases may be predicted with confidence using accepted structural theories. The condition of the actual structure between these two limiting cases can presently only be estimated, but it is obviously a function of age and vibration history.

In the light of experimental data and the normal condition of most reinforced concrete structures, a reasonable damping ratio for the reinforced concrete frame near design level stresses might be 1.5%. For low amplitude ratios, a value of 0.7% might be more appropriate.

The bare steel frame has an extremely low value of damping. The damping ratio of a steel frame depends to some extent on its structural configuration and perhaps to a greater extent on its connection details. It is also evident that for any configuration, the steel frame damping ratio will be less than 1%. A reasonable average frame damping ratio, considering standard construction details would seem to be 0.5%.

The presence of filler walls has effects on the strength and response of the frame subject to lateral loads. In general, the frame-wall combination is considerably stronger than the frame alone. The load-resisting mechanism of the frame-wall combination varies depending on the properties of the individual structural element and on the level of loading. The conclusions regarding partition properties follow.

Gypsum board partitions contribute little stiffness to the total structure, but what exists may be predicted with acceptable accuracy

using a simple shear element model an effective modulus of rigidity of 29,000 psi.

Gypsum board partitions contribute significantly to the overall damping of the structure. Using the formulae presented in this study, the fundamental mode damping ratio was 3.8% with partition and 1.5% without partitions.

Plywood partitions contribute little stiffness to the total structure, but what exists may be predicted with acceptable accuracy using a simple shear element model an effective modulus of rigidity of 30,000 psi. Further experimental study is needed to verify the damping of the structural plywood partition model.

Unreinforced masonry partition walls have variable stiffnesses. Limiting partition stiffness may be confidently predicted using the masonry material properties and the equivalent compressive strut approximation. After a history of extensive vibration, it can be expected that the partition stiffness will be reduced and the knee-braced frame model may be used to predict the stiffness of structure. At present, the actual structural stiffness between these two limiting conditions can be estimated. This estimate can be made quite accurately if some knowledge of the age of the structure and the history of prior vibration exists.

Increases in the total viscous damping ratio due to infill masonry wall are less than 1%. As the partitions lose their effective stiffness, the increases in damping ratio also decrease.

REFERENCES

1. American Concrete Institute Committee 442, "Response of Buildings to Lateral Forces," Journal, ACI, No. 2, Proc. Vol. 68, February 1971, pp. 81-106.

2. Benjamin, J. R., and Williams, H. A., "Behavior of One-Story Reinforced Concrete Shear Walls Containing Openings," Journal, ACI, Vol. 30, No. 5, November 1958.

3. Blume, John A., & Associates Research Division, Concrete Test Structures: First Progress Report on Structural Response, March 1968.

4. Blume, John A., & Associates Research Division, First Progress Report on Racking Tests of Wall Panels, August 1966.

5. Blume, John A., & Associates Research Division, Second Progress Report on Racking Tests of Wall Panels, July 1968.

6. Cloud, W., "Period Measurements of Structures in Chile," Bulletin of the Seismological Society of America, Vol. 53, No. 2, Feb., 1963.

7. Clough, R. W., and Benuska, K. L., and Wilson, E. L., "Inelastic Earthquake Response of Tall Buildings," Proceedings, Third World Conference on Earthquake Engineering, Wellington, New Zealand, 1965.

8. Clough, R. W., King, I. P., and Wilson, E. L., "Structural Analysis of Multi-Story Buildings," Journal Structural Division, ASCE, Vol. 90, No. ST3, Proc. Paper 3925, June 1964, pp. 19-34.

9. Cole, D. G., "The Damping Capacity of Hardened Cement Paste, Mortar, and Concrete Specimen," Vibration in Civil Engineering, B. O. Skipp, ed., Butterworths, London, England, 1966.

10. Council of Tall Buildings, Chapter CB-6, Nonlinear Behavior and Analysis, 1978, pp. 171-276.

11. Fedorkiw, J. P. and M. A. Sozen, "A Lumped-Parameter Model to Simulate the Response of Reinforced Concrete Frames with Filler Walls," University of Illinois, Civil Engineering Studies, Structural Research Series No. 338, Urbana, June 1968.

12. Fiorato, A. E., Sozen, M. A., and Gamble, W. L., An Investigation of the Interaction of Reinforced Concrete Frames with Masonry Filler Walls, Report to the Department of Defense, Office of Civil Defense, University of Illinois Civil Engineering Studies Report No. UILU-ENG.-70-100, November 1970.

13. Freeman, S. A., Concrete Test Structures: Second Progress Report on Structural Response, John A. Blume & Associates Research Division, July 1971.

14. Freeman, S. A., Third Progress Report on Racking Tests of Wall Panels, John A. Blume & Associates Research Division, November 1971.

15. Freeman, S. A., "Racking Tests of High-Rise Building Partitions," Journal Structural Division, ASCE, Proc. Paper 13136, No. ST8, August 1977.

16. Gere, J. M., and Weaver, W., Jr., Analysis of Framed Structures, D. Van Nostrand Co. Inc., Princeton, New Jersey, 1965.

17. Hogan, M., "The Influence of Wind on Tall Building Design," BLWT-4-71, thesis presented to the University of Western Ontario, at London, Canada, in March, 1971, in partial fulfillment of the requirements for the degree of Doctor of Philosophy.

18. Holmes, M., "Steel Frames with Brickwork and Concrete Infilling," Proceedings of the Institution of Civil Engineers, Vol. 19, August 1961, pp. 473-478

19. Hurty, W. C., and Rubenstein, M. F., Dynamics of Structures, Prentice-Hall, Inc., Englewood Cliffs, New Jersey, 1964.

20. Jacobsen, L. S., "Frictional Effects in Composite Structures Subjected to Earthquake Vibrations," Department of Mechanical Engineering, Stanford University, Stanford, March 1959.

21. Karamanski, T., "Calculating Infilled Frames by the Method of Finite Elements," Tall Buildings, Pergamon Press, Oxford, England, 1967, pp. 455-461.

22. Kost, G. E., "Nonlinear Dynamic Analysis of Frames with Filler Panels," John A. Blume & Associates, Research Division, San Francisco, California, Nov. 1972.

23. Lamar, S., and Fortoul, C., "Brick Masonry Effect in Vibrations of Frames," Proceedings, Fourth World Conference on Earthquake Engineering, Santiago, Chile, 1969.

24. Lazan, B. J., and Goodman, L. E., "Material and Interface Damping," Shock and Vibration Handbook, Vol. 11, C. M. Harris and C. E. Crede, eds., McGraw-Hill Book Co., Inc., New York, N.Y., 1961.

25. Lionberger, S. R., Statics and Dynamics of Building Frames with Non-Rigid Connections, Doctoral Dissertation, Dept. of Civil Engr., Stanford University, March 1967.

26. Natarajan, P. S., and Wen, R. K., "Effect of Walls on Structural Response to Earthquakes," ASCE National Structural Engineering Meeting, Portland, Oregon, April 6-10, 1970.

27. Newmark, N. M., "A Method of Computation for Structural Dynamics," Journal Engineering Mechanics Division, ASCE, Vol. 85, No. EM3, Proc. Paper 2094, July 1959, pp. 67-94.

28. Penzien, J., "Damping Characteristics of Prestressed Concrete," Journal of the American Concrete Institute, Sept., 1964.

29. Raggett, J. D., "Influence on Nonstructural Partitions on the Dynamic Response Characteristics of Structures," John A. Blume & Associates, San Francisco, CA, July 1972.

30. Raggett, J. D., "Estimating Damping of Real Structures," Journal of the Structural Division, ASCE, Proc. Paper 11554, No. ST9, Sep. 1975.

31. Smith, B. S., "Behavior of Square Infilled Frames," Journal Structural Division, ASCE, Vol. 92, No. ST1, Proc. Paper 4690, February 1966, pp. 381-403.

32. Smith, B. S., "Lateral Stiffness of Infilled Frames," Journal Structural Division, ASCE, Vol. 88, No. ST6, December 1962, pp. 183-199.

33. Thomas, F. G., "The Strength of Brickwork," The Structural Engineer, Vol. 33, No. 2, February 1953, pp. 35-46.

34. Weaver, W. Jr., Nelson, M. F., and Manning, T. A., "Dynamics of Tier Buildings," Journal Engineering Mechanics Division, ASCE, Vol. 94, No. EM6, Proc. Paper 6293, December 1968, pp. 1455-1474.

35. Wiegel, R. L., Earthquake Engineering, Prentice-Hall, Inc., N.J., 1970.

36. Wilson, E. L., A Computer Program for the Dynamic Stress Analyses of Underground Structures, University of California at Berkeley, Report No. 68.1, January 1968.

37. Wilson, E. L., and Clough, R. W., "Dynamic Response by Step-by-Step Matrix Analysis," Symposium on the Use of Computers in Civil Engineering, Lisbon, Portugal, Paper No. 45, October 1962.

The vita has been removed from the scanned document